INVERSE METHODOLOGY FOR MULTI-POINT AERODYNAMIC ROTOR BLADE DESIGN

A THESIS
PRESENTED TO
THE ACADEMIC FACULTY
BY

FIDENCIO TAPIA

IN PARTIAL FULFILLMENT OF THE REQUIREMENTS FOR THE DEGREE
DOCTOR OF PHILOSOPHY IN AEROSPACE ENGINEERING

SCHOOL OF AEROSPACE ENGINEERING
GEORGIA INSTITUTE OF TECHNOLOGY
MAY 1996

INVERSE METHODOLOGY FOR MULTI-POINT AERODYNAMIC ROTOR BLADE DESIGN

Approved:

Daniel P. Schrage, Chairman

Lakshmi N. Sankar

Stephen Ruffin

Date Approved: May 23, 1996

ACKNOWLEDGEMENTS

I wish to thank my advisor, Dr. Daniel P. Schrage, for his continuous encouragement in pursuing my degree and for the freedom that I was granted in my research topic. I am specially indebted to Dr. Lakshmi N. Sankar for a myriad reasons, ranging from technical guidance, proofreading many of my works, pleasant class sessions, making computational codes available for me, and most of all for the example he set for me. I am very grateful to Dr. Stephen Ruffin and Dr. Robin Gray for their valuable comments and suggestions throughout this work. In addition, I want to express my appreciation to Dr. Shi Jin for his comments and for being part of my reading committee.

This would not be possible without the financial support and encouragement of the *Consejo Nacional de Ciencia y Tecnología (CONACYT)*, where I specially thank Ing. Javier Meléndez for his help with all the required paperwork along these years. Financial support was also provided by the Institute of International Education, Fulbright Commission, with special recognition to Mrs. Jenifer Chambers in the Mexico City office for all her help, guidance and friendship.

Dr. Dimitri Mavris, at the Aerospace Systems Design Lab, deserves special recognition for keeping us at the top level by guiding us in a friendly atmosphere. I also thank all the members at the lab for their support and motivational discussions. A special thank you is owed to Mr. Sergio Velazquez for the most interesting critiques which kept the dream alive and to Mr. Mario Quattlebaum for his help throughout this work.

My father Roberto Tapia for his endless moral support and wise advice.

Nothing could be done without the help and support received from my wife Maria Luisa and my daughter Daniela. We did it!

Last, but not least, I would not be what I am without the love and encouragement of my big family and friends.

I thank you all!

TABLE OF CONTENTS

LIST OF TABLES

LIST OF FIGURES

NOMENCLATURE

A	MGM coefficient, coefficient matrix
a	Lift curve slope, speed of sound
$\bar{a}$	Normalized speed of sound
B	MGM coefficient, coefficient matrix
b	Number of blades
C	MGM coefficient, coefficient matrix
c	Chord
CC	Convergence Criteria

$$CC = \frac{\sum_{k=1}^{l}\sum_{j=1}^{m}\alpha_k \sqrt{\frac{\sum_{i=1}^{n}\left(C_{p_{i,j,k}}^{\ actual} - C_{p_{i,j,k}}^{\ target}\right)^2}{n}}}{lm}$$

C_d	Drag coefficient
C_{do}	Profile drag coefficient
C_l	Lift coefficient
C_m	Moment coefficient
C_{mo}	Moment coefficient at zero lift
C_p	Pressure coefficient

C_T	Thrust coefficient
D	Coefficient matrix
H_{12}	Shape factor (Momentum thickness/displacement thickness)
J	Jacobian of the transformation
L	Lift
l	Number of azimuthal stations
l. e.	Leading edge
M	Mach number
M_{dd}	Drag divergence Mach number
M_{tip}	Tip Mach number
m	Number of radial stations
n	Number of points on airfoil surface
p	Pressure
Q_i	Induced torque
r	Local radius
R	Rotor radius
Re	Reynolds number
s	Airfoil surface length
T	Thrust
t	time
$\bar{t}$	Normalized time

t. e.	Trailing edge
U	Air speed, Contravariant velocity
U_P	Velocity component along control axis
U_T	Velocity component perpendicular to control axis
u	Velocity component in the x-direction
V	Contravariant velocity
$\overline{V}$	Normalized velocity
v	Velocity component in the y-direction
v_i	Induced velocity
W	Contravariant velocity
w	Velocity component in the z-direction
x	Chordwise coordinate, nondimensional radial station (r/R)
y	Spanwise coordinate
z	Spatial coordinate
MGM	Modified McFadden Garabedian
α	Weight factor, effective angle of attack
α_{tpp}	Tip path plane angle
δ_2	Displacement thickness

φ	Perturbation velocity potential
ϕ	Inflow angle, Velocity potential
$\bar{\phi}$	Normalized velocity potential
Γ	Bound circulation
γ	Specific heat ratio
η	Coordinate in computational domain
μ	Inflow ratio
Ω	Angular speed
θ	Collective pitch angle
ρ	Density
$\bar{\rho}$	Normalized density
τ	Time
ξ	Coordinate in computational domain
Ψ	Azimuth angle
ζ	Coordinate in computational domain

Fluid Airfoil	Airfoil designed using potential theory.
Solid Airfoil	Airfoil obtained after subtraction of displacement thickness from the fluid airfoil.

SUMMARY

The capabilities demonstrated by the current generation of helicopters make them such versatile machines that they have expanded the possible flight envelopes available to man. Even though there are certain missions that only helicopters will be able to undertake, almost any flight plan which remains in the subsonic regime can easily be performed by rotorcraft (helicopters, tilt rotor aircraft, etc.). The heart of the machine, identified as the main rotor, is one of the most important components in determining the final performance limits for the whole machine.

Traditional design techniques use the 'cut and try' method, in which a rotor is analyzed for several flight conditions; modifications to the original geometry were done based mainly on the designer's experience and then the whole process was repeated again. The main disadvantage of this method is the time involved in designing the rotor. Airfoils used in building the rotor blade were selected from well known airfoils whose performance data was already available, consequently limiting the designer to select only from what is available.

The present work discusses several techniques which had been used for airfoil design and optimization, particular to rotor blade airfoils. Nonetheless, this work focuses

on the inverse design methodologies in which target performance parameters are specified from the beginning of the design process. This method in turn solves for the geometry that will match these performance variables as closely as possible.

Common performance objectives are the reduction of profile and induced power, which mean the redistribution of lift in the rotor disc and the modification of the blade shape to induce less drag. Target lift distributions which require less induced power are developed. The required lift can be then translated into different pressure distributions meeting this lift requirement while inducing less drag and consequently requiring less profile power.

After having translated the lift requirements into specific target pressure distributions at certain locations, the inverse design methodology will produce a new geometry which will more closely match the target distributions. The procedure is then repeated several times until some convergence criteria is satisfied.

The full range of flight conditions can be studied with these methods: hover, forward flight and even combinations of both; so for every new design a custom made rotor can be designed as opposed to the selection of airfoils which will better fit the application.

CHAPTER I

INTRODUCTION

1.1 Motivation

The flying capabilities of the helicopter make it such a versatile, unique machine that a major market is often assured for this type of aircraft. It is a well known fact that customers are always eager for more capable machines and that new technologies can provide a competitive edge to helicopter manufacturers. Thus the helicopter companies are always developing and promoting these new technologies, in order to have a more capable concept, and thus a machine capable of a better performance. However, affordability is also a strong consideration and new design optimization techniques are also sought which will reduce the design cycle time in developing new rotor systems.

This improved performance can be interpreted in several ways; as a greater payload capacity, higher forward speed, more stable hover, or as a power reduction in certain flight conditions, among others. Although some of these improvements could be achieved with a higher performance engine, the common factor to all of them is that this

higher performance will not be achieved unless some optimization is performed on the rotor system design.

Rotor aerodynamics dictate how a specific rotor will perform, but most importantly this discipline provides insight into how the rotor should be modified in order to achieve the performance goal.

1.2 Objectives

The main objective of this research is to develop a robust design procedure applicable for helicopter rotor blades that will take advantage of the potential improvements that inverse design methodologies offer. Design for performance will be the most important concept throughout this work since the methodology will focus on matching specific performance objectives set forth from the beginning of the design process. Typical objectives for rotor design studies are the reduction in profile and induced power requirements. Creating a robust method which can develop the new rotor blade for a variety of flight conditions as fast as possible are also objectives in the present work. One of the main disadvantages of the traditional approaches for rotor design is the

time involved, so minimizing the design cycle time, which will reduce cost, is another objective.

1.3 Scope Of Work

Any aerodynamic goal that the design team will target for the rotor performance is necessarily related to the lift distribution present over the rotor disc. Tailoring this distribution can lead to a more capable rotor; thrust can be maximized or power can be minimized. Tailoring the lift distribution is only the first step in the process of achieving performance targets.

Lift distribution optimization is considered as a necessary step in the design process. This is done for every flight condition for which the helicopter is being designed. Both hover and forward flight conditions are considered.

The present work attempted, among other things, to attack the problem of forward flight inverse design for the first time. Although the airfoil experiences many different flight conditions during one blade revolution, the objective of the design is to develop a rotor that will match pre-specified pressure distributions at different azimuth stations,

thereby matching a specific lift distribution. Since no single airfoil will match all the pre-determined pressure distributions at the azimuth stations and/or flight conditions (hover or forward flight), some way of combining them becomes necessary. This means that the designer is dealing with an over-specified problem, and consequently is looking for a single airfoil that will match several pre-specified pressure distributions. The strategy used in this work is to avoid the over-specified limitation by solving the problem in a least squares sense.

Unlike many previous rotor design efforts the present study includes viscous effects in the design stage. Using these means, new objective functions can be considered earlier in the design stage, such as drag, or lift to drag ratios. Earlier design efforts considered only a 'fluid' airfoil, which is any airfoil geometry designed by using solely potential theory. Actual 'solid' airfoil shapes are considered in the present study. 'Solid' airfoil geometries are those generated by subtracting the displacement thickness from the 'fluid' airfoil.

After the design team has optimized the lift distribution, an attempt is made to modify the pressure distributions over the blade. This step can lead to more significant power savings, by means of drag minimization, which in turn will imply a reduction in profile power required. Thus, modifying these pressure distributions can lead to

machines which perform better, achieve the design goal and earn a higher ranking from the final customers.

Once these pressure distributions are tailored by the aerodynamicist, the inverse design tool is used to specify the rotor geometry that will be required to produce the target pressure distributions. Optimization of the pressure distribution can be considered as a design process in itself. It has the constraint of matching the required lift and moment coefficients, as well as minimizing the drag produced. This distribution should also be built to achieve good boundary layer characteristics such as no separation of the flow field or weakening of any shock waves that may be present.

Separation prediction models were studied in order to include this aspect in the pressure distribution definition. Pressure distribution optimizers were evaluated as means to find the best possible pressure distribution. Different families of pressure distribution were then analyzed as means to generate different airfoils for different targets.

Special attention was dedicated to laminar pressure distribution due to the low viscous drag that could be achieved if they were obtained. However, this flow regime is unlikely to be found in helicopters, due to the many different sources which cause the flow to become turbulent. Laminar target pressure distributions were analyzed studying the feasibility of a laminar airfoil.

CHAPTER II

PREVIOUS RESEARCH AND BACKGROUND METHODOLOGIES

The performance of a new helicopter will mainly be affected by the main rotor characteristics, geometry and operational conditions. Variables such as rotor radius, tip speed and chord length, among many others, will play a significant role in the final behavior of the whole machine. Specification of these values is not a trivial task and has to be done considering the many flight conditions in which the new machine will operate. Methods for the selection of disk loading, rotor solidity and tip Mach number have been developed and are widely used in the design process[1,2].

Taper and twist distributions will also play key roles in rotor performance. They are usually selected after values for the disk loading, rotor solidity and tip Mach number have been assigned. Taper and twist distributions were greatly studied in the past and the optimum distributions for these two variables are now available[3], although it may not be practical to build a rotor using them. Bingham[4] reviewed the effects of all these variables and showed that if these variables are selected the required airfoil performance can be

determined at each airfoil location. After radius, tip speed, chord, twist and taper are optimized, the designer needs to select airfoils to completely specify the rotor aerodynamically.

Three generic flow conditions can be distinguished for helicopters[5]. Region 1, in Figure 1, shows the forward flight condition for the advancing blade. This means high Mach numbers (close to 1) and thus low C_l coefficients. Region 2 also shows the forward flight condition but for the retreating blade. In this condition, Mach numbers will be lower thus requiring a higher C_l. Region 3 shows the hovering condition, in which moderate Mach numbers and C_l coefficients are to be found. In general the designed airfoil should have good drag-rise characteristics for region 2 and high lift to drag ratios for region 3. For all three regions the airfoil should have a low moment coefficient to minimize rotor loads.

When the helicopter is hovering, the only difference in flow field for a specific airfoil will be due to its radial location along the blade. This implies that the flow field will be the same along one revolution, thus specifying the design condition and facilitating the design process. This can be translated into specific objectives for the airfoil in this region, these being: $C_l / C_{d\,max} \approx 100$ at $M=0.6$ and $C_l \approx 0.65$.

However, in forward flight condition the specific design objectives are quite different. The blade is at a peak velocity at $\Psi=90°$ where the tip Mach number is close to 1 and the lift required is almost zero. At $\Psi=90°$, the drag might be very high due to the drag divergence phenomena. At $\Psi=180°$, tip Mach number is the lowest and thus required lift is high. In between these two stations the conditions change gradually with the blade rotation. Performance objectives can be specified at these two stations, thus enforcing conditions between these two for every other azimuth station.

A general list of design objectives[5-9] that a helicopter airfoil should to satisfy can be expressed as follows:

-$C_m \approx 0$ with respect to the aerodynamic center for all flight conditions.

-High C_l at $M \approx 0.4$.

-Low C_d at high subsonic Mach number.

-Low C_d at moderate C_l and Mach numbers.

An example of a whole subdivision of these objectives by hierarchy is given as follows:

<u>1st Priority:</u>

1st Design Objective: $|C_{mo}| \leq 0.01$ at $M=0.3$ to minimize rotor loads.

2nd Design Objective: $C_{l\,max} \geq 1.5$ at M=0.4 to delay retreating blade stall.

3rd Design Objective: $M_{dd} \geq 0.81$ for usefulness of the airfoil at the blade tip.

4th Design Objective: $|C_{mo}| \leq 0.015$ for $M \leq 0.7$. C_m does not grow with compressibility effects.

2nd Priority:

5th Design Objective: $C_d \leq 0.008$ at $C_l = 0.6$ and M=0.6 for hover.

6th Design Objective: $C_l \geq 1.655$ at M=0.5. For avoidance of retreating blade stall.

7th Design Objective: $|C_{mo}| \leq 0.02$ at M=0.3 for C_l between 0 and 1. Limits growth of nose-down C_m on airfoils with aerodynamic center behind quarter chord.

8th Design Objective: $C_{do} \leq 0.01$ at $M = M_{dd} + 0.02$. Low drag rise beyond drag divergence is desirable because a portion of the advancing blade generally operates beyond M_{dd}.

3rd Priority:

9th Design Objective: $M_t > M_{dd}$. Where M_t is the M at $dC_m/dM = -0.25$. By delaying the onset of pitching moment break until after drag divergence, it is possible to improve the probability that a rotor will be power limited rather than structurally limited.

10th Design Objective: $0.01 > M^2 C_m > -0.04$. Restore loads into the coefficient based limit by means of the M^2 factor.

11th Design Objective: Gradual stall at M between 0.3 and 0.4. Aimed at the reduction in low excursion associated with stall.

12th Design Objective: $C_{do} \leq 0.007$ for $M \leq M_{dd}-0.1$. Elimination of drag creep and other sources of drag degradation.

The objectives shown above represent the most important goals that the helicopter airfoil designer must target. In the present study the general guidelines given previously are used to select a target pressure distribution although all of the specific objectives may not be satisfied. In fact some of the specific objectives are conflicting. For example, the second objective requires a $C_{l\ max}$ greater than 1.5 and objective 11 targets for a gradual stall about the same Mach numbers. Airfoils producing generous amounts of lift tend to stall with little warning. Examples of their usage range from their original presentation[5-9] in the 1970's to the very recent work presented by Nakadate and Obukata[10] in 1994 in which airfoils were designed using the Navier-Stokes equation for a specific set of these objectives.

As progress has been made along these lines, designers have already identified some key trends in helicopter airfoil design[11,12]. These trends must be taken as design guidelines for future efforts. They are divided as general trends and region-specific trends. Region-specific trends pertain to the three regions shown in Figure 1.

General trends:

1) As camber increases, $C_{l\,max}$ increases, but the zero lift M_{dd} decreases.
2) With a constant mean line, as thickness decreases M_{dd} improves.
3) Thickness variation of 11-15% causes small variations in $C_{l\,max}$ at $M < 0.4$; if thickness decreases beyond 11%, high deterioration in $C_{l\,max}$ is encountered.
4) For small $|\Delta C_{m\,o}| \leq 0.005$, pitching moment adjustments can be achieved with negligible lift and drag penalties by means of trailing edge contour changes. Even small trailing edge changes can cause premature turbulent separation if applied to trailing edge configurations already possessing significant curvature.
5) Within the same family of airfoils and for a constant low speed C_{mo}, camber and thickness variations will improve either $C_{l\,max}$ or M_{dd}, but will not improve both; in order to do so, the airfoil loading would have to be redistributed more efficiently along the chord, at the cost of increasing nose-down C_m.
6) To have a high M_{dd} at low lift, the airfoil must be peaky and/or have a surface with very large curvature at its maximum thickness location.
7) Trailing edge cusp and reflexed (nose-up) mean lines move the aerodynamic center back, closer to the trailing edge at a possible cost of premature turbulent separation.
8) On airfoils with low trailing edge loading breaks in lift, drag and moment will occur within a small M excursion ($\Delta M \approx 0.05$).

The region-specific key trends suggest some criteria on how to achieve the 12 design objectives for helicopter airfoils:

For Region 1 (High M, low C_l, advancing side):

1) In order to achieve good drag rise characteristics, a rapid change in curvature must occur near the airfoil leading edge on both the upper and lower airfoil surfaces.
2) The surface Mach number preceding the shock waves on the upper and lower airfoil surfaces must be less than 1.16 at the design point.
3) The pressure recovery following the shocks on the airfoil should be mild.
4) The flow must remain attached over the entire airfoil surface.
5) To achieve well behaved boundary layer characteristics at the trailing edge, the trailing edge C_p should be minimized as much as possible (more negative).
6) The airfoil trailing edge bluntness should be less than one-half the boundary layer thickness at the trailing edge.
7) In order to achieve a low drag level at Mach numbers below the onset of drag-rise, the upper and lower surface boundary-layer must remain laminar back to approximately 30% of the chord, although this might be nearly impossible in helicopters.

For Region 2 (Low M, high C_l, retreating side):

1) Mach number ahead of leading edge shock should be less than 1.4 at conditions corresponding to maximum lift at M=0.4.

2) The pressure distribution ahead of the leading edge shock should be shaped to promote isentropic recompression.
3) Pressure recovery following the shock should be designed to maintain attached flow up to 90% of the chord for the condition corresponding to maximum lift.
4) In order to achieve the first aerodynamic performance objective, $|\Delta C_{m\,o}|<0.01$, the design pressure distribution must be constrained so that the pitching moment coefficient is minimized.

For Region 3 (Moderate M and C_l, hover conditions):

1) In order to meet the target drag of $C_d=0.008$ at M=0.6 and $C_l=0.6$, wave drag must be virtually zero.
2) The lower surface pressure distribution should be shaped to promote laminar flow and hence reduce the airfoil profile drag.
3) The flow must remain attached to the trailing edge. From this we can infer that the analysis tools must be able to treat transonic flow.

Some authors[12] believe that the most important region is Region 1, high M and low C_l, so in case of conflicting objectives selected for the design, Region 1 should outweight the other conditions since it will affect the largest portion of the airfoil shape.

Since the early days of helicopter design, the fact that the airfoil pitching moment would impose heavy loads on the hub was realized; this is why symmetrical airfoils were sought, since they would reduce these loads. The popular NACA 0012 was developed in the 1930's by experimental means and became the standard airfoil for helicopters[11,12] well until the 1970's, mainly due to the low loads transmitted to the hub and to the fairly good performance that different rotors built around this airfoil could achieve. In addition, symmetrical airfoils on uniform blade planforms were the easiest to manufacture. An extensive compilation of helicopter airfoils available at the time is presented in ref. 13.

Various other airfoils were also developed by experimental techniques; specially cambered versions of the NACA 0012. Gradual variation in geometric parameters led to the famous Clark Y, Raf and Gottingen 398 airfoils, circa 1915. One of the first airfoils designed specially for helicopters was the 9-H-12, still using the same empirical methods[14].

Several approaches became available over time; one of the earliest ones was the conformal mapping of the airfoil onto a circle, then singularity methods were used to calculate the airfoil shape from a target pressure distribution. This type of methods had limited success due to its usage being constrained to low Mach numbers[15].

Davis[16] presented rules and guidelines on how to develop design tools. Specifically, his work presents a certain approach on how to convert an analysis code into a design tool by building iterations around it and posing some rules on how to alter the geometry. This work heavily impacted further research since most of the following design methodologies employed this approach.

Inverse methods computed the pressure distribution on the surface of an arbitrary airfoil and modified its geometry in a systematic manner until the specified pressure distribution was obtained. The airfoil surface was replaced by a vortex sheet with the tangency condition satisfied by requiring the total stream function to be a constant along the airfoil surface. The method was inherently coupled to a panel solver which became the major disadvantage because of the obsolescence of the flow model[17].

The FX 69-H-098 (H for helicopter) airfoil was designed for helicopters around 1973. It was designed to satisfy two transonic requirements. Its design included several theories, such as the hodograph method, transonic potential flow theory, boundary layer calculations as well as blade element-momentum theory; this later theory using non-uniform inflow for hover and axial flight, and uniform inflow for other flight conditions[14]. This work proved the feasibility of designing airfoils that fulfill requirements for specific design points.

Inverse design techniques were preferred by some designers because of the implicit advantage of designing to match a specified performance. In this method, the pressure distribution is specified a priori and then the airfoil required to produce it is computed iteratively. The airfoil geometry is changed in a systematic way so that successive pressure distributions will be closer to the target than the previous one. The main advantages of these methods stem from the fact that they allow the designer to specify the pressure distribution and thereby the lift, pitching moment and boundary layer characteristics of the configuration. Obviously the use of this method requires the feasibility of the specified pressure distribution; this feasibility assured by satisfying certain criteria[18].

One of the earliest versions of inverse methods first calculated the thickness distributions and initial mean line shape. Determination of the vorticity on the mean line which will cancel the difference between the specified and the calculated pressures on the upper surface was the next step; finally, normal and tangential induced velocity matrices must be calculated for the mean line and upper surface of the airfoil[19].

The modified Garabedian McFadden (MGM) method became the standard among the different inverse design methods. In this procedure the airfoil coordinates are varied in such a systematic way that every new airfoil will more closely match a target pressure distribution as specified in the first step of the process[20]. The procedure became widely

used for airfoils and was even extended for a complete wing[21]. Target pressure distributions were specified at spanwise control stations. Then, the MGM method was applied to modify the airfoil at that station. The wing was then redefined by interpolating airfoils between the two control stations.

Whyte[22] presented an extensive compilation on how computer models were used in the Canadian research establishments. This work shed some light on how Computational Fluid Dynamics could be used for design much as the work by Davis[16] had suggested some years before.

Optimization of the pressure distribution naturally became the next step in inverse design research. Maximization of lift[23] became one the most popular objective functions; however, in the case of helicopters this was not the case because of the whole different set of conditions to which the airfoil would be submitted. Some other approaches made skin friction minimization the target; in any case, careful tailoring of the target pressure distribution became one of the most important problems to be tackled by the airfoil designer, since this step would drive the design process.

A pressure distribution optimization procedure was developed in order to tailor pressure distributions inexpensively and in an automated manner. Families of pressure distributions are characterized by generalized equations for the velocity distribution along

the airfoil surface. The main advantages are that there exist a series of variables that may be varied to determine the velocity distribution that will best satisfy the lift, drag and pitching moment requirements at the design point conditions. The pressure distributions in both surfaces can be defined by a few parameters using this method[24,25].

Several researchers undertook the task of optimizing the target pressure distribution. One of the most important works in this area was done by Stratford[26]; he developed a recovery pressure profile that will minimize drag by keeping the flow on the verge of separation. Liebeck[23] used this pressure profile and studied the acceleration portion of the pressure distribution in order to get the maximum lift possible while keeping the flow subsonic and not separated. This area of research has provided continuous improvements until recent times, specially in the work done by Narramore et. al.[27]. In this work, a full Navier-Stokes methodology is implemented to design airfoils for maximum lift using the same Stratford recovery pressure profile. Included is the work done by Lyrintzis[28] which focuses on the variational problem of maximum lift in a certain pressure distribution and offers proof of feasibility for the distribution, as well as presenting a method for the prediction of the transition point.

Owen[29] approached the inverse design problem by coupling an Euler solver and a boundary layer code; he imposed constraints on the moment coefficient -a valuable

objective for helicopters- and added the concept of multi-point design, i. e. designing an airfoil for several flow conditions.

An alternative to inverse design methods is the concept of direct numerical optimization. These methods need to select one or two design objectives which have the highest priority and can be predicted with confidence. These objectives are to be minimized or maximized by changing the airfoil geometry, in such a systematic way that every airfoil will be better than the previous one. Computational resources required by the implementation usually limit this approach, although an optimized airfoil can greatly reduce the wind tunnel time and cost[30].

Vanderplaats[31] introduced the idea of employing airfoil libraries as a means for airfoil modification. He performed an airfoil optimization based on a sequential application of a second order Taylor series approximation to airfoil characteristics. One of the most complete optimization efforts involved a two dimensional unsteady full potential solver and an unsteady integral laminar/turbulent boundary layer. The viscous interaction was considered by means of unsteady transpiration velocities normal to the airfoil surface. The velocities, once calculated from the boundary layer integral thickness parameters, are input into the inviscid flow boundary conditions. Airfoils were generated starting with an NACA 0012 airfoil. This airfoil was then modified with the NACA 66012, NACA 0009 and NACA 66009 as library airfoils, whose coordinates are chosen

as the one which best satisfies the optimization process at the moment. In some cases, instead of library airfoils camber shape functions are used. The airfoil was designed for a specific advance ratio and blade station taking the average C_l or C_d as two different objective functions[32]. Vuillet[33] presented an comprehensive course on rotor design and an extensive report on the history of European developments for helicopter airfoils focusing on the optimization scheme.

Special cases also drew some attention from researchers, specially the tilt rotor configuration that has been under development in recent times. Airfoils required for such special cases are within the scope of the presented methodologies. Narramore[34] and Liu et. al.[35] presented excellent examples on how these methods could be adapted for special design cases.

Some attempts to couple the inverse design techniques with optimization methods have been performed[36]. In these, the inverse equation is solved in an alternative way, introducing a guess of the solution and iteratively attempting to minimize the error, so the equation is presented as an optimization problem, finding a solution that minimizes the error. In the specific case of helicopters, different airfoils are designed for different flow conditions. Some cases studied the retreating and advancing sides, after two different airfoils had been designed the final airfoil must be chosen. Linear combination with weighting factors can be used to generate the final airfoil.

Hassan[37] et. al. presented one of the first design efforts using a rotor flow solver, as opposed to a two dimensional flow solver used by most of the previous researchers. Several cases are presented in which new rotors are developed for the hover case using inverse methodologies. The whole blade geometry is specified in this way and performance objectives, rather than pure pressure distributions are matched.

Multi-point approaches were successfully incorporated into the design process by solving the problem in a least squares fashion. Tapia[38] et. al. solved the inverse design problem for several flow conditions present at one control station along the blade revolution by using the least squares method. The work provided useful results, such as matching a specific target lift distribution that will reduce the induced power while keeping the thrust constant. A three dimensional flow solver was used so that the whole blade could be specified in this fashion.

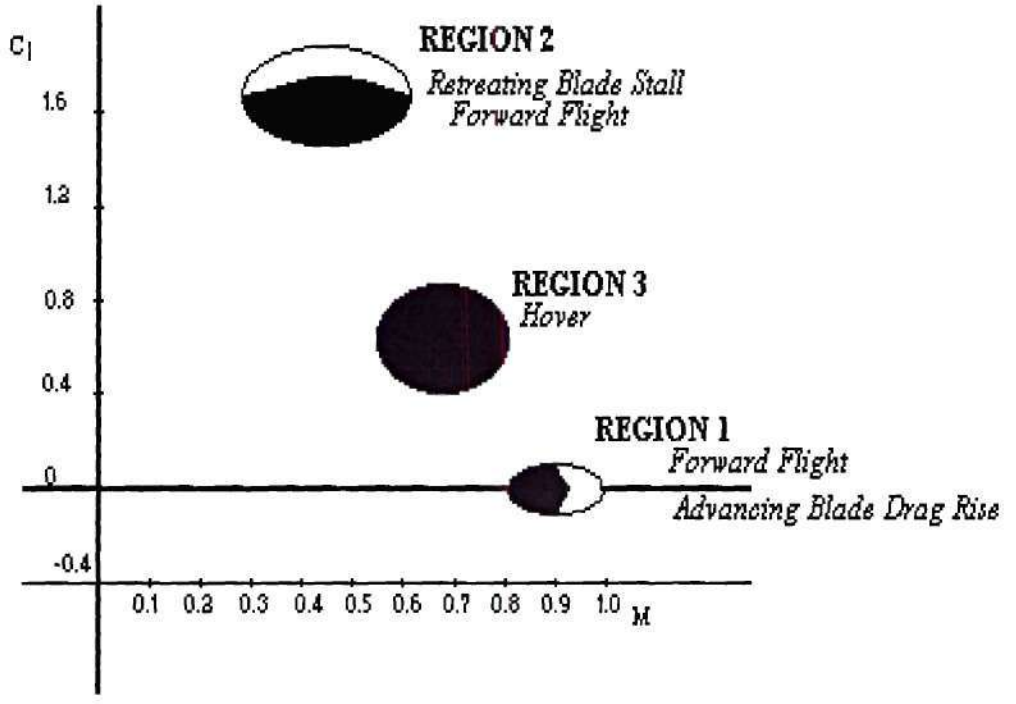

Figure 1. Typical regions for helicopter blade operation. Shaded regions show desired operating conditions. Open regions give unreasonable performance.

CHAPTER III

A NEW ROTOR DESIGN METHODOLOGY

Rotor design has always been of great interest to the helicopter designer. An efficient helicopter is by far most dependent on the rotor capabilities; however, since helicopters spend their flying time under different flight conditions (i.e. hover or forward flight at different flight speeds), the problem of designing the rotor system becomes a very challenging one.

Until a decade ago, rotor design was carried out by selecting a set of candidate airfoils that would have characteristics that matched the ones required. Computational Fluid Dynamics (CFD) methodologies were used to evaluate static and dynamics loads of these airfoils. Finally, the hover and forward flight characteristics of the constructed rotor were evaluated with the aid of performance codes. Effects such as aeroelastic deformation, inflow, etc., were accounted for only during this third stage with the performance codes.

Typically, the set of candidate airfoils was comprised by choosing some of the well known airfoils, for which 2-D data was already available. In such a case, the job left to the aerodynamicist was to find a specific combination of airfoils, chord and twist distributions that would match or improve over the requirements. Optimization of chord and twist distributions has been common practice almost since helicopters appeared in the market, but the airfoil distribution was limited to the selection of well known airfoils which would best fit into the application.

Until approximately a decade ago, this situation began to change based on a work pioneered in the fixed wing community: specifying the loads over the wing and then customizing a geometry that would produce these specified loads[25,39]. In the case of helicopters, the same procedure could be applied; loads could be specified along the blade and the required geometry would be found. However, the completely different aerodynamic environment between hover and forward flight requires a more comprehensive airfoil design process[38].

Specifying a 3-D body for a certain pressure distribution is a challenging task; early attempts focused on specifying only the airfoil shape (i.e. the 2-D geometry). Along these lines, the first recorded works looking for an airfoil useful for helicopters dated back to the 1930's, when the famous NACA 0012 airfoil was invented by experimental means. Over the next 40 years, the same experimental procedures were used to produce a larger

set of different airfoils until airfoil shape optimization and inverse design concepts were introduced[11,17].

A vast set of airfoils were developed using these techniques. Some designers began using combinations of these concepts[36], optimization and inverse design, in an attempt to completely specify the airfoil geometry. The optimization methodologies have the disadvantage of huge computational requirements, but the advantage of generating an improved airfoil after each design step. Research has been continuous and will continue to be in the foreseeable future using this optimization strategy.

Inverse design techniques had comprised another strong line of research. In these methods, a geometry that will satisfy the requirements exactly is sought. This approach has the potential disadvantage of leading the design to unusual shapes. It may even be unable to find a specific shape since there is no guarantee that there will be an airfoil shape which will generate the specified pressure distribution. On the other hand, it has the advantage of requiring less computer resources and having a promising rate of convergence.

During the last 10 or 15 years, the inverse design technique has been used to generate airfoils for different flight conditions, especially for fixed wings for a large variety of performance goals, such as maximizing lift, minimizing drag, etc. The fixed wing community has already made some attempts to specify 3-D bodies, such as the whole wing

using this technique[21]. The inverse design methodologies are applied at specific spanwise control stations. Airfoils are then interpolated between two neighboring control stations.

Helicopter blades can also be designed using this same strategy; after selection of control stations, the inverse design technique is carried out at these control stations, and airfoils are interpolated in between them. In order to do a 3-D design, it is obvious that a 3-D flow solver will be required. Only a few recent attempts can be found using this methodology, and in these few cases the blades had been designed only for the hover condition, which is the simplest, since the airfoil at a specific flight condition is always under the same flow conditions. Furthermore, viscous effects have never been considered in any of these cases[37].

3.1 Overview of the Proposed Design Methodology

The present work attempted to propose a method to design a rotor blade in a full 3-D fashion. In order to do that, a 3-D flow solver for rotors is required. The full potential flow code developed by Sankar and Prichard[40] satisfies this requirement by solving the full potential equation for unsteady flow in a 3-D space. This code was selected for use throughout this work. The details of this code are presented in section 3.3.1.

Other codes required are those which compare the pressure distribution obtained from a specific rotor with the targets specified for the design. After the comparison is done, the inverse design code is run to obtain a new rotor that will more closely match target pressure distributions.

In the case of any inverse design methodology, the selection of the target pressure distribution will have a very strong impact on the final design. The target pressure distribution can be considered as the driver of the design process. Any aerodynamic goal selected for the design case will have to be translated into target pressure distributions. Pressure distributions can be optimized for each design case in order to meet lift and moment requirements as well as minimizing the drag, which will be computed by the inclusion of a boundary layer code.

Viscous effects are included in the design process by using strip theory aided by a two dimensional compressible boundary layer code. Once the pressure distribution obtained over the final blade is known, the boundary layer code uses this information to compute the displacement thickness. The displacement thickness is subtracted from the 'fluid' airfoil developed thereby producing a 'solid' airfoil which is the one that should be evaluated for manufacture.

The present methodology differs from traditional blade design by considering inflow, viscous effects and elastic deformation influences from the beginning of the design process. The procedure starts with a target load distribution over the rotor, for all azimuth angles in a specific flight condition. This load distribution specifies the allowable blade deformation in torsion and bending. It is not necessary to have the blade geometry before specifying the inflow distribution because the load distribution is a function of the wake vorticity, which in turn is a function of the bound circulation which again depends only on the load distribution. The designer will attempt to satisfy the target load distribution while keeping the torque required as low as possible. The proposed methodology is perfectly capable of defining the whole blade surface, but this approach will certainly produce a surface which will be hard to manufacture. So, in order to relax this limitation, the proposed method will only design the airfoil shape at selected 'control' stations, and the rotor will be completely defined by linearly interpolating the rest of the airfoils in the radial direction.

The present approach for the design of rotor blades attempts to define a geometry that will operate at optimum performance in hover and forward flight, and it requires the following steps:

1) The designer selects an advance ratio (μ) and rotor angle of attack (α_{tpp}) combination for forward flight, and a C_T to be achieved in hover. The advance ratio and rotor angle of attack combination might be chosen from the mission specifications, usually the flight

speed, as well as the weight of the aircraft, are functions of the mission definition, so the rotor designer will probably have the advance ratio and the rotor angle of attack specified from preliminary design. The rotor angle of attack is related to the drag that the aircraft is expected to induce; since choosing it arbitrarily will impose a target drag for the aircraft, the designer should be careful to enforce a realistic drag value.

2) A disc load distribution $L(r, \Psi)$ is developed next by modification of the load distribution produced by the baseline rotor at the specific flight conditions considered in the design process. This modified load distribution will satisfy the thrust requirements specified before while reducing the induced power required and must produce zero pitching and rolling moment for the rotor. The load distribution will determine structural and dynamic requirements for the blade, since it determines the bending and torsion loads that will be present in the rotor. The target load distribution can be specified concurrently with the structure and dynamic groups so the design can incorporate structural and dynamic requirements. The target load distribution will be responsible for the induced power required by the rotor; the objective is to tailor it so it will minimize the induced power required. These factors must be combined in order to specify an achievable and efficient load distribution.

3) Using this load distribution, the blade deformation characteristics and the inflow angles are computed using some performance code. Different performance codes can be introduced here, such as CAMRAD[41], the classical Drees'[42] model, Scully's wake[43] or

some other available wake model that can be used to compute the effective angles of attack. Obviously, the more effects considered by the selected model the better, however this will usually impose time constraints on the design methodology. Note that the inflow angles depend only on the wake vorticity, which in turn depends on the variation of bound circulation $\Gamma(r, \Psi)$, which depends only on the load distribution $L(r,\Psi)$ and consequently does not require any knowledge of the airfoil shapes.

4) At a number of radial 'control' stations selected by the designer, target C_p distributions are developed at a number of azimuth locations. In a multi-point design, for example, the designer may seek several C_p distributions at a typical control station. These C_p distributions must meet the load specifications chosen in step 2. They can also be chosen to achieve good boundary layer characteristics, such as low adverse pressure gradients on the suction side and postponement of transition to the aft portion of the airfoil.

Since separation is an undesired phenomenon for this application, the target pressure distributions must be specified in such a way that separation is avoided, or at least postponed to the aft portion of the airfoil. Stratford's separation criteria[26,44] can be used here as a design tool. The designer can easily check if the candidate pressure distribution will separate or not by use of the following simple equation:

$$C_{pm}\sqrt{s\frac{dC_{pm}}{ds}} = 0.396(10^{-6}\,\mathrm{Re}_s)^{0.1}$$

where s is the airfoil surface length from the stagnation point and

$$C_{p_m} = \frac{C_p - C_{p_{min}}}{1 - C_{p_{min}}}$$

When this equation is satisfied, separation is present at that point. With the aid of this equation separation can be checked in one non-expensive additional step. Viscous effects are considered here also to assure that the candidate C_p distribution shows a better performance as compared to the original blade. The boundary layer code will be run to compute the data needed to compute the drag by using the modified Squire-Young formula developed by Eppler and Sommers[45]:

$$C_d = 2\delta_{2_{te}} \left(\frac{U_{te}}{U_\infty} \right)^{\frac{5+H_{12_{te}}}{2}}$$

where: $H_{12\,te} = H_{12\,te}$ for $H_{12\,te} < 2.5$

$H_{12\,te} = 2.5$ for $H_{12\,te} > 2.5$

With this additional step, the designer can assure that the target C_p distribution shows an improved drag behavior when compared to the original one.

5) Obviously, a single airfoil at a given control location cannot produce the different target pressures sought by the designer. Therefore, the designer assigns a set of weight factors to these pressure distributions. If good forward flight characteristics are of interest, the designer may, for example, weigh the Ψ=90° condition more over the other stations. This set of weight factors will also be related to the mission specified for the aircraft under design, since it is the mission definition which will fix the main

characteristics required for the new aircraft (e.g. heavy lift aircraft, high speed, long time at hover, etc.). These aircraft characteristics will in turn specify the aerodynamic characteristics required for the rotor, and for the airfoil. In this way, the azimuth station that should be more heavily weighted becomes clear.

6) The rotor is analyzed and the pressure distribution over the disk is computed and compared against the target distributions at the specific controls stations. The inverse design procedure generates a new rotor that will match the target pressure distributions more closely.

7) At the end of Step 6, the actual loads achieved will differ from what was expected in Step 2, because the rotor cannot generate all the loads specified in Step 2; Steps 2 through 6 are therefore repeated with the target loads specified in Step 2 guiding the design during each subsequent iteration. It is expected that in this way every iteration will produce loads closer to the target, and the process can be stopped when some convergence criteria is satisfied, or until some maximum number of iterations is reached. Obviously, the more heavily weighted stations will converge faster to a pressure distribution closer to their targets; it is also expected that the lightly weighted stations will converge to a pressure distribution closer to their targets than the baseline rotor.

8) When the process is stopped, either because a maximum number of iterations has been reached or because the convergence criteria has been satisfied, the viscous effects analysis

is performed again in order to obtain the displacement thickness of the obtained pressure distributions. The actual airfoils can then be computed by subtracting the displacement thickness from the 'fluid' airfoils designed in step 6.

3.2 Rotor Design Process

The design methodology proposed in this work will define the rotor completely from an aerodynamic point of view. It means that several variables will have to be evaluated and optimized to achieve the best performance possible. Although the design process is comprised of several design stages, the objective is to have the rotor completely defined at the end of the proposed procedure. The process is decomposed into several stages in which the design team will have to make decisions which will impact the final performance.

3.2.1. Baseline Selection.

At the very early stages of design, when the design team is still developing the conceptual aircraft, the rotor system will go into its first optimization which will usually be done by means of a weight analysis. This optimization is responsible for setting values of

the most general variables in the rotor. Rotor radius, chord and tip speed can be found and defined in this early design stage.

A second and more detailed optimization is performed in order to minimize power required by means of blade twist and/or taper. The performance effects of twist and taper are similar and in some cases the designer had chosen to relax one of these variables by optimizing only one of them. The most popular approach has been to have a highly twisted rectangular blade; although in some rotors the opposite is true by having an untwisted tapered blade. Since the effects are basically the same, any approach can be considered as long as better performance is attained with a given distribution in these variables.

Techniques such as design of experiments or the response surface methodology may be easily adapted for a complete optimization of the different variables that are involved in the rotor design problem.

The only step required to fully define a baseline is the airfoil. Initial airfoil selection is not a crucial step since it will be modified by the process. Starting airfoils can be selected to be symmetrical, such as the NACA 0012, in order to have a negligible pitching moment, or can be chosen as high speed airfoils, such as the VR7, if high speed flight is important in the design case.

Rotor angles of attack will have to be specified if forward flight will be considered in the design case. The selected value of this angle will impose a target drag for the whole machine, therefore the designer has to select realistic values.

3.2.2. Target Lift Distribution

After completion of an initial analysis of the baseline rotor, lift distributions for the flight conditions of interest will be available to the designer. Each one of these distributions can be optimized independently from each other in order to find new lift distributions that match the overall thrust requirements while inducing less power required at the desired flight conditions. Target lift distributions are developed concurrently with the structures and dynamics groups so the distribution is optimized once and for all. If the distribution is not an optimum, the designed blade generated by this methodology will converge into this non-optimum lift distribution, consequently care must be taken in the optimization of the target lift distribution.

3.2.3. Inflow Angles.

Every lift distribution developed in the previous step will have a correspondent set of inflow angles. These inflow angles can be computed from several available wake models ranging from annular momentum to very sophisticated computer codes. The

methodology presented here is not limited by the model selected since any model can be used. Of course, as more effects are considered the more realistic the design will be, nonetheless a simple model can also be used with good results. If a more sophisticated model becomes available it can be easily brought into the design process.

As mentioned before there is no need to know the airfoil characteristics to specify the inflow since this is only an indirect function of the lift distribution. Inflow angles are required to specify the effective angles of attack of the blade, which is an input table required by the rotor flow solver. It is obvious that the effective angle at which the blade is rotating will have to be known by any rotor flow solver and therefore is not a limitation of the model used here.

3.2.4. Target Pressure Distributions.

The development of target pressure distributions might be considered as the most important step in this design process. These target distributions will be the actual design drivers since the inverse methodology will focus on matching these distributions. The first step will be the selection of control stations in which these distributions will be developed. The distributions are then compared to the actual pressure distributions in a specific rotor so that the inverse design methodology can generate a new rotor.

The most important parameters to be matched when developing these target distributions are the lift, drag and moment coefficients. The lift coefficient, for the selected control station, will be known from step 2 in which a target lift distribution was developed. The moment coefficient will be constrained by the structural aspects of the design since it will be translated into blade torsion. Drag minimization will translate into more available power due to the reduction in profile power.

Since there are an infinite number of pressure distributions that will satisfy these constraints some other aspects should be considered. Separation should be avoided or at least retarded as much as possible; this can be checked as aforementioned by the Stratford's criterion[26]. If the original distributions present shocks, the pressure distribution can be modified in order to have a weaker shock, thus producing less wave drag. Laminar distribution can also be considered by delaying the transition point. The target pressure distribution can be tailored to present the point of minimum pressure well aft in the chordwise direction so that the flow remains laminar in order to reduce the viscous drag.

Several ways to automate the pressure distribution specification can be found in the literature. Although some of them were designed specially for fixed wing aircraft, they may be easily adapted for helicopters. Stratford's recovery pressure profile[26] will minimize the drag produced by the distribution by maintaining the flow at the verge of separation, thus producing little warning when the airfoil is about to stall. This special case of

Stratford's pressure distribution for zero shear stress in the pressure recovery region is determined by integrating the separation criterion presented before:

$$C_{pm}\sqrt{s\frac{dC_{pm}}{ds}} = 0.396(10^{-6}\,\mathrm{Re}_s)^{0.1}$$

where s is the airfoil surface length from the stagnation point and

$$C_{p_m} = \frac{C_p - C_{p_{\min}}}{1 - C_{p_{\min}}}$$

The result is:

$$C_{pm} = 0.49\left\{\mathrm{Re}_{so}^{\,0.2}\left[\left(\frac{s}{s_o}\right)^{0.2} - 1\right]\right\}^{1/3}$$

for $C_{pm} \leq 4/7$ or

$$C_{pm} = 1 - \frac{a}{\left[\left(\frac{s}{s_o}\right) + b\right]^{1/2}}$$

for $C_{pm} > 4/7$; where

$$a = \frac{3}{7}\left[\left(\frac{s}{s_o}\right)_c + b\right]^{1/2}$$

$$b = \left\{6.56\mathrm{Re}_{so}^{-1/15}\left[\left(\frac{s}{s_o}\right)_c^{1/15} - 1\right]^{2/3}\left(\frac{s}{s_o}\right)_c^{4/5}\right\} - \left(\frac{s}{s_o}\right)_c$$

$$\left(\frac{s}{s_o}\right)_c = \left[\left(\frac{1.586}{\mathrm{Re}_{so}^{0.2}}\right) + 1\right]$$

The subscript o refers to values at the start of the recovery region.

The ADAM procedure[24,25] can specify a pressure distribution by varying a few parameters so that the pressure distribution can be easily optimized in an automated way. Families of pressure distributions can be specified as follows:

Accelerating region:

$$C_p = C_{ps} + (C_{po} - C_{ps})\left[1 - \left(1 - \frac{s_a}{s_o}\right)^n\right]$$

where C_{po} is the pressure coefficient at location s_o where Mach number is a maximum, s_a is the airfoil surface length measure from stagnation point and C_{ps} is the stagnation pressure coefficient.

Decelerating region:

Mach number distribution is obtained with:

$$M = M_2\left[1 + k\frac{s_a - s_o}{1 - s_o}\right]^{-\phi}$$

where M_2 is the Mach number at the starting point of the recovery region, after any shocks if they are present. This equation was developed by Wortmann[46] to produce a constant form parameter in the turbulent boundary layer. The local pressure coefficient is then computed as:

$$C_p = \frac{2}{\gamma M_\infty^{\,2}}\left[\left(\frac{1+\frac{\gamma-1}{2}M_\infty^{\,2}}{1+\frac{\gamma-1}{2}M^2}\right)^{\gamma/\gamma-1} - 1\right]$$

where M_∞ is the free stream Mach number and γ is the specific heat ratio of 1.4 for air. Note that an infinite number of pressure distributions can be obtained by varying the constants n, k and ϕ.

3.2.5. Weight Factor Assignment.

The mission definition for which the aircraft is being designed will certainly highlight the most important flight conditions applicable for the new rotorcraft, as well as the relative importance among them. The designer will use this definition to assign different weight factors to the selected control stations so that the new design will excel at the flight regimes for which it is being designed. By assigning these weight factors, the designer will force the stations with the bigger weight factors to converge faster than the other control stations.

3.2.6 Design Loop.

Pressure distributions are computed for the rotor specified at the moment using the full potential solver. These distributions are then compared against the target pressure

distributions developed in step 4. The inverse design methodology is then run to compute the new rotor geometry by solving the empirical equation used in the MGM method at the specified control stations.

At each control location, at a number of points on the airfoil, the modified Garabedian-McFadden technique is used to arrive at a system of equations for the changes in the z-coordinates of airfoil shape as shown in Figure 2. In the Garabedian-McFadden technique, the following partial differential equation is used:

$$A\Delta Z + B\frac{\partial \Delta Z}{\partial x} + C\frac{\partial^2 \Delta Z}{\partial x^2} = C_p^{\text{actual}} - C_p^{\text{target}}$$

Here ΔZ is the change in the airfoil z-coordinate. This equation may be discretized at a control station j as follows:

$$a_i \Delta Z_{i-1,j} + b_i \Delta Z_{i,j} + c_i \Delta Z_{i+1,j} = C_{p\ i,j}^{\text{actual}} - C_{p\ i,j}^{\text{target}}$$

where i is a chordwise index. One such system may be written at each control station, for each of the target C_p specifications. Note that when the computed and target C_p values became equal, ΔZ goes to zero and the airfoil no longer changes.

Once a new rotor is specified, it is fed back into the potential flow solver so that new pressure distributions can be computed. The process is then repeated iteratively until a certain convergence criteria is satisfied or a maximum number of iterations is reached.

3.2.7 Performance of the New Design.

The final rotor is then analyzed thoroughly and compared against the initial configuration. Performance comparisons can be made in terms of induced and profile power required, as well as thrust produced. This method is capable of producing improvements in every target specified at the beginning of the design process. These targets must be compared to the original variables to make sure that the improvements are indeed there.

The blade geometry is automatically changed. Thickness, camber and twist of the whole blade, and airfoil sections comprising it, will be modified from the original blade in order to match the target performance. There is no mathematical proof that this is an optimum blade, however this method produces a blade that will more closely match the specified targets of the design flight conditions.

3.3. Design Details

The present methodology relies heavily on three different, but coupled tools: the full potential flow solver, the inverse design procedure and the boundary layer code. The first of these is used as the analysis tool, which computes the actual pressure distribution

for each new rotor geometry. The inverse design code is the actual designer; it specifies the geometry for new rotors, requiring the previous geometry, its correspondent pressure distribution, as well as the target pressure distributions. The boundary layer code is responsible for the analysis of the viscous effects for the target and final C_p distributions. As a last step, it computes the displacement thickness and with it the actual 'solid' airfoil. The following sections will explain in detail each of these tools.

3.3.1. Full Potential Flow Code.

The full potential flow code was developed by Prichard[40] and Sankar in 1990. It computes the unsteady, three-dimensional transonic potential flow surrounding an isolated rotor blade. It calculates the near-field aerodynamics of arbitrarily shaped rotor blades by solving a conservative form of the unsteady full potential equation on a body-fitted grid.

The grid generation method used in this code was an algebraically generated body-fitted grid. At specified radial locations, a planar sheet of grid points was placed, with each sheet normal to the radial coordinate. Each sheet is a two dimensional grid, body-fitted to the airfoil section at that radial station. The 2-D grids were generated by transforming the airfoil surface to a flat surface in the complex plane, placing a smooth distribution of grid points in the complex plane, with coordinates ξ, η and ζ, and transforming the points of the physical plane, as shown in Figure 3.

The method used to create the grid planes at each radial station generates a 'C' grid. These grids form a set of 'C' shapes curves stacked along the blade. Each 'C' grid is generated as follows: a 'wake sheet' or 'branch cut' is connected to the trailing edge of the local airfoil. Then, a transformation is determined which will transform the airfoil and wake sheet to a surface in the complex ξ–ζ plane. Once the blade surface has been reduced to a flat sheet in the complex plane stretching transformations in the horizontal and vertical directions are applied. The grid is orthogonal in the computational domain but not in the physical plane.

The same idea is used for grid planes beyond the blade tip. A 'C' grid is generated about a fictitious airfoil of nearly zero thickness and no camber. Boundary conditions differ here since the impermeability condition is not applied having thus possible velocities crossing the imaginary airfoil.

To form the third dimension, along the blade radius, several of these 'C' grids are stacked together. Each of these grids is scaled according to local values of chord, sweep angle, dihedral and twist.

The typical grid size is 121x24x22 points in the ξ, η and ζ directions respectively. Out of the 121 points in the ξ direction, 91 are on the airfoil surface, clustering them close

to the leading edge, with 46 points on the upper surface and 46 on the lower surface. Recall that the leading edge is a common point to both surfaces. The remaining points are distributed symmetrically in the 'wake sheet'. The η direction is comprised by 24 points, 18 of which are on the blade, and the remaining 6 beyond the tip. Several of these grids are concentrated in a region close to the blade tip to capture the strong velocity gradients present there. The 22 points in the ζ direction are concentrated on the blade surface and moving out from the blade gradually increasing the distance between neighboring points. The surface k=1 is a row of 'ghost' points inside the airfoil surface to easily apply the impermeability condition at the airfoil surface.

The code models the near field aerodynamics of rotor blades using numerical solutions to the full potential equation; which, in an inertial reference frame, can be written as:

$$\rho_t + (\rho u)_x + (\rho v)_y + (\rho w)_z = 0$$

or

$$\rho_t + (\rho \phi_x)_x + (\rho \phi_y)_y + (\rho \phi_z)_z = 0$$

where ϕ is the velocity potential defined by $V = \nabla\phi$ and x, y, z are Cartesian coordinates in the physical plane, t is time, u, v, and w are the velocities in the x, y and z directions, ρ is the density, V is the velocity vector with components u, v and w, and $(x)_y$ is the partial derivative of (x) with respect to y.

To obtain closure on the full potential equation the energy equation is needed. The flow is assumed to be irrotational and inviscid. The definition of the speed of sound is given by

$$a = \sqrt{\frac{\gamma p}{\rho}}$$

which can be non-dimensionalized to

$$\frac{a}{a_\infty} = \sqrt{\frac{p}{p_\infty}}\sqrt{\frac{\rho}{\rho_\infty}}$$

Using the isentropic relation for pressure and density for a perfect gas

$$\frac{p_2}{p_1} = \left(\frac{\rho_2}{\rho_1}\right)^\gamma$$

rearranging,

$$\sqrt{\frac{p}{p_\infty}} = \left(\frac{\rho}{\rho_\infty}\right)^{\gamma/2}$$

combining the two equations;

$$\frac{a}{a_\infty} = \left(\frac{\rho}{\rho_\infty}\right)^{\lambda - 1/2}$$

or

$$\frac{\rho}{\rho_\infty} = \left(\frac{a}{a_\infty}\right)^{2/\gamma - 1}$$

non-dimensionalizing density and speed by the free stream values

$$\bar{\rho} = \frac{\rho}{\rho_\infty}$$

$$\bar{a} = \frac{a}{a_\infty}$$

the result of the above algebra is

$$\bar{\rho} = \bar{a}^{2/\gamma-1}$$

The energy equation in an inertial reference frame is written as

$$\frac{a^2}{\gamma-1} + \frac{V^2}{2} + \frac{\partial\phi}{\partial t} = \frac{a_\infty^2}{\gamma-1} + \frac{V_\infty^2}{2}$$

using the non-dimensionalizations:

$$\bar{V} = \frac{V}{a_\infty}$$

$$\bar{\phi} = \frac{\phi}{a_\infty L}$$

$$\bar{t} = \frac{t a_\infty}{L}$$

where L is the characteristic length of the flow, the energy equation can be written as

$$\bar{a}^2 = 1 - \frac{\gamma-1}{2}\bar{V}^2 + \frac{\gamma-1}{2}\bar{V}_\infty^2 - (\gamma-1)\bar{\phi}_t = 1 + \frac{\gamma-1}{2}\left(\bar{V}_\infty^2 - \bar{V}^2 - 2\bar{\phi}_t\right)$$

using the isentropic relation, the energy equation is rewritten in terms of density;

$$\bar{\rho}^{\gamma-1} = 1 + \frac{\gamma-1}{2}\left(\bar{V}_\infty^2 - \bar{V}^2 - 2\bar{\phi}_t\right)$$

For numerical accuracy, a perturbation potential φ is defined as: $V = V_\infty + \nabla\varphi$. In order to solve these equations in the computational domain, the equations must be

transformed from the x-y-z coordinate system to the ξ–η–ζ system, as shown in Figure 3. The result of this transformation yields

$$\left(\frac{\rho}{J}\right)_\tau + \left(\frac{\rho U}{J}\right)_\xi + \left(\frac{\rho V}{J}\right)_\eta + \left(\frac{\rho W}{J}\right)_\zeta = 0$$

and

$$\bar{\rho}^{\gamma-1} = 1 + \frac{\gamma-1}{2}\left[1 - 2\varphi_\tau - (U+\xi_t)\varphi_\xi - (V+\eta_\tau)\varphi_\eta - (W+\zeta_t)\varphi_\zeta\right]$$

where the contravariant velocities U, V, and W are defined by

$$U = \varphi_x\xi_x + \varphi_y\xi_y + \varphi_z\xi_z + \xi_t$$

$$V = \varphi_x\eta_x + \varphi_y\eta_y + \varphi_z\eta_z + \eta_t$$

$$W = \varphi_x\zeta_x + \varphi_y\zeta_y + \varphi_z\zeta_z + \zeta_t$$

and the Jacobian of the transformation, J, is

$$J = 1 / [\eta_y (\xi_x\zeta_z - \xi_z\zeta_x)]$$

where ξ,η,ζ,τ are in the computational domain and x,y,z,t are in the physical domain. This system allows the solution of the perturbation potential φ, and knowing it, the velocity field can be computed from $V = V_\infty + \nabla\varphi$. The set of boundary conditions to be satisfied by the present problem is now considered. There are several regions where boundary conditions will be applied, with the full potential code replaced by these explicit conditions. These regions are:

-Blade Surface: On the airfoil surface, the impermeability condition is applied, $\mathbf{V} \cdot \mathbf{n}=0$, where $\mathbf{n}$ is the outward normal vector to the airfoil surface, and $\mathbf{V}$ is the total velocity.

-Branch Cut or Wake Sheet: The governing equations solved in the present analysis do not model viscous or rotational phenomena. However, both phenomena exist on the surface of the rotor blades and the wake of each. Therefore, some means of externally modeling these features is necessary. The present method applies the vorticity at the trailing edge on the radial grid stations to all points on the branch cut which lie on the constant η line aft of that radial station. This technique crudely models the radial variation of circulation, but neglects the time variation and downstream convection of the trailing vorticity. In mathematical form, this boundary condition becomes $\varphi_{upper} = \varphi_{lower} + \Gamma'$, where φ_{upper} is the potential on the upper part of the branch cut, φ_{lower} is the potential on the lower part of the branch cut, and Γ' is the bound vorticity per unit span at that radial station.

-Off-tip Points: The region outboard of the blade tip has boundary conditions similar to those of the branch cut. The following relation is used: $\varphi_{upper} = \varphi_{lower}$. This condition is similar in concept to the branch cut conditions, the only difference between this condition and those for the branch cut is that no trailing vorticity effect is present.

-Singular Line: While the actual flow along the $i=i_{le}$ line outboard of the blade is fairly simple and well-behaved, the grid has a singularity at $i=i_{le}$. To set the values of φ along the singular line, the following conditions are used for the potentials at time level (n);

$$\varphi_{ile,j,k=1} = \varphi_{ile,j,k=3}$$

$$\varphi_{ile,j,k=2} = 1/2\,(\varphi_{ile,j,k=3} + \varphi_{ile+1,j,k=2})$$

These relations may be viewed as an averaging of the velocity potential values surrounding the singular points (ile, j, 2) for $j>j_{tip}$.

The governing equation used in the linear system for these points is

$$\varphi_{\xi\xi}^{(n+1)} + \varphi_{\zeta\zeta}^{(n+1)} = 0.$$

Outer Boundary Conditions:

-Inboard Plane: The inboard plane ($\eta=\eta_{min}$) is a particularly difficult boundary condition, because of the effects of other blades and the rest of the vortex wake. These effects cannot be minimized by extending the grid further, as can be done with other effects. The current method used to handle the inboard plane is application of a symmetry condition across the inboard plane

$$\frac{\partial}{\partial\eta}\left(\frac{\rho V}{J}\right) = 0$$

or

$$\left(\frac{\rho V}{J}\right)_{i,j-\frac{1}{2},k} = \left(\frac{\rho V}{J}\right)_{i,j+\frac{1}{2},k}$$

at the j=2 plane. While this is not physically realistic, it allows accurate calculation of the flow on the outer portion of the blade without unnecessary complications. The rotor aerodynamicist is most interested in the outer part of the blade, since most of the blade's

lift, drag, and torque are generated on the outer half of the blade; thus this assumption does not cause much error in the region of interest.

-Far-field Boundary: The exact boundary condition is V=0 at infinity. Since the grid must necessarily be finite, the far-field boundary condition must be applied at a finite distance from the blade. If the condition V=0 is applied a finite distance from the blade, an error is introduced . Waves in unsteady solutions may occur which can build up and cause a meaningless solution. Two ways to handle this are to use an artificial viscosity to damp out wave propagation far from the rotor, or to apply a wave equation as a boundary condition on the outer grid surface. Alternatively, the far-field condition may be derived from an analytic solution to a linear potential flow model. The present method used a much simpler model which, for large grids, causes minimal error while greatly simplifying the algorithm. The outboard plane ($\eta=\eta_{max}$) and out plane ($\zeta=\zeta_{max}$) have the condition $\varphi^{(n)}=0$, that is, the flow is at rest at the outer boundary.

-Downstream boundary: The downstream boundary ($\xi=\xi_{min}$ and $\xi=\xi_{max}$) has a mixed condition. For all points at a given η-plane on the downstream boundary, the boundary condition applied depends on whether the free stream flow is supersonic at that radial station. The domain of dependence for subsonic flow is in all directions, while supersonic flow has its domain of dependence in the upstream direction only. If the local flow is subsonic, then the condition $\varphi^{(n)}=0$ is applied as for the $k = k_{max}$ boundary. If the flow is supersonic at that region, then the potential upstream of the boundary cannot depend on the value of the boundary. Thus, the condition on the boundary must be derived from the

upstream flow conditions. To reflect that flow conditions are steady-state but not necessarily returned to the free stream state, the condition $\frac{\partial^2 \varphi}{\partial \xi^2} = 0$ is used.

3.3.2. Inverse Design Procedure.

Unlike the full potential flow code, which is basically an analysis tool, the inverse design procedure is the one which is actually responsible for generating a new rotor geometry. It requires the target pressure distributions and a baseline geometry, from which the procedure departs, as well as the pressure distributions at the selected control stations induced by this baseline geometry at the specific flow conditions.

After each analysis run the target and computed pressure distributions are compared and used to generate a new blade, which will generate a new pressure distribution closer to the target. This process is repeated until some convergence criteria is satisfied.

The method used as the inverse design technique is the modified McFadden-Garabedian (MGM) technique developed at Lockheed by Malone et. al[25]. This is a flow solver independent technique and attempts to modify the geometry using the following rationale:

An airfoil C_p distribution depends on: a) Z(x) coordinates of the airfoil, b) dZ/dx, slopes of the airfoil and c) d^2Z/dx^2, curvature of the airfoil.

Then it follows that $\Delta C_p = C_p^{target} - C_p^{computed}$ will be a function of ΔZ, $d\Delta Z/dx$ and $d^2\Delta Z/dx^2$, where $\Delta Z = Z^{design} - Z^{baseline}$.

Since such a function does not explicitly exists. An approximate function, such as $A\Delta Z + B\, d\Delta Z/dx + C\, d^2\Delta Z/dx^2 = \pm \Delta C_p$ may be used. No physic laws are attached here, but when the $C_p^{design} = C_p^{computed}$ the design point is matched and $\Delta Z=0$, stopping the design process. In this case, $C_p^{computed}$ will be obtained from the full potential flow code. Here ΔZ is the change in the airfoil z-coordinate. This equation may be discretized at a control station j, as follows:

$$a_i \Delta Z_{i-1,j} + b_i \Delta Z_{i,j} + c_i \Delta Z_{i+1,j} = C_p{}^{actual}{}_{i,j} - C_p{}^{target}{}_{i,j}$$

where i is a chordwise index, while j is a spanwise index. One such system may, then be written at each control station, for each of the target C_p specifications.

$Z^{new} = Z^{old} + \Delta Z$, so the question will be how to solve the empirical equation. Only one ordinary differential equation needs to be solved for ΔZ, and this ΔZ can be set to 0

at any part of the airfoil so that the original shape is preserved. A, B, and C are user-specified constants that accelerate the convergence rate.

3.3.2.1. Hover Case.

The simplest possible case for the aerodynamic design of a helicopter rotor will be the hover case, due to the symmetry of flow conditions present at every azimuth station. In practice, this means that only one azimuth station needs to be considered, since flow conditions will be the same for all azimuth stations.

One design cycle has to be performed for every radial or 'control' station where the airfoil geometry is to be specified by the methodology developed. The procedure is exactly the same as presented before; the designer specifies a lift loading over the rotor, using this loading target pressure distributions are developed at the 'control' stations, the inflow is then computed using this load distribution. The first analysis run is performed for the original rotor geometry using the full potential code; the code will compute the actual pressure distributions over this rotor, the inverse design code is run and it compares the target pressure distributions with the distributions computed by the flow solver, the program will generate a new rotor geometry that will match closer the target pressure distributions. The process is then repeated using this rotor instead of the original rotor. This design cycle is repeated until some convergence criteria is satisfied. The last step is

to compute the displacement thickness produced by the final pressure distribution so that it can be subtracted from the 'fluid' airfoil to obtain the final 'solid' airfoil.

3.3.2.2. Forward Flight Case.

When the designer is considering forward flight studies the situation becomes much more complex. This is due to the fact that the flow conditions over the rotor are getting more complicated, mainly because the flow is not symmetric anymore. Each azimuth station has different flow conditions associated with it, and a single airfoil will encounter all of them. The designer faces in this case a problem of over-specification of the design problem. He can not design an airfoil for each azimuth station, since there is no practical way to modify the airfoil geometry along one revolution.

The over-specification of the problem can be overridden by combining all the conditions to be considered in a least square sense, in this way a single airfoil can be computed, it will match closer the targets specified at the different azimuth conditions. For example, assuming that at a control station the designer has the following 4 sets of linear equations:

$$[A]\ \{\Delta Z\}=\{\Delta C_p\}_{\Psi=0^\circ}$$

$$[B]\ \{\Delta Z\}=\{\Delta C_p\}_{\Psi=90^\circ}$$

$$[C]\ \{\Delta Z\}=\{\Delta C_p\}_{\Psi=180^\circ}$$

$$[D]\ \{\Delta Z\}=\{\Delta C_p\}_{\Psi=270^\circ}$$

assigning weights α_1, α_2 ,α_3 , α_4 for the four azimuth locations:

$$\alpha_1[A]\ \{\Delta Z\}=\alpha_1\{\Delta C_p\}_{\Psi=0^\circ}$$

$$\alpha_2[B]\ \{\Delta Z\}=\alpha_2\{\Delta C_p\}_{\Psi=90^\circ}$$

$$\alpha_3[C]\ \{\Delta Z\}=\alpha_3\{\Delta C_p\}_{\Psi=180^\circ}$$

$$\alpha_4[D]\ \{\Delta Z\}=\alpha_4\{\Delta C_p\}_{\Psi=270^\circ}$$

the designer has an over-determined system of form:

$$\begin{bmatrix} \alpha_1[A] \\ \alpha_2[B] \\ \alpha_3[C] \\ \alpha_4[D] \end{bmatrix} \{\Delta Z\} = \begin{bmatrix} \alpha_1\{\Delta C_p\}_{\Psi=0^\circ} \\ \alpha_2\{\Delta C_p\}_{\Psi=90^\circ} \\ \alpha_3\{\Delta C_p\}_{\Psi=180^\circ} \\ \alpha_4\{\Delta C_p\}_{\Psi=270^\circ} \end{bmatrix} \qquad \text{(I)}$$

When this system is multiplied by the transpose of the coefficient matrix, a square system results:

$$\begin{bmatrix}\alpha_1[A] & \alpha_2[B] & \alpha_3[C] & \alpha_4[D]\end{bmatrix}\begin{bmatrix}\alpha_1[A]\\ \alpha_2[B]\\ \alpha_3[C]\\ \alpha_4[D]\end{bmatrix}\{\Delta Z\} = \begin{bmatrix}\alpha_1[A] & \alpha_2[B] & \alpha_3[C] & \alpha_4[D]\end{bmatrix}\begin{bmatrix}\alpha_1\{\Delta C_p\}_{\Psi=0^\circ}\\ \alpha_2\{\Delta C_p\}_{\Psi=90^\circ}\\ \alpha_3\{\Delta C_p\}_{\Psi=180^\circ}\\ \alpha_4\{\Delta C_p\}_{\Psi=270^\circ}\end{bmatrix}$$

When this system is solved, the designer will not have satisfied any of the above 4 equation sets exactly, but would have minimized the error in system (I) in a least square sense. Obviously, the more heavily weighted distributions are satisfied more accurately than the others.

The mission for which the aircraft is being designed will specify the relative importance between the different flight conditions, and this in turn will highlight certain azimuth stations. In this case a set of weight factors can be assigned for the different azimuth conditions, so the higher weight factor will converge faster to the target.

The design cycle is similar to the one used in the hover case. First, knowing the advance ratio as well as the rotor angle of attack, a lift distribution over the rotor is tailored to optimize the objective function that the designer is looking for, such as minimum induced power required, as an aerodynamic condition but also considering structural and dynamics requirements. This loading will be used to develop target pressure distributions at the radial 'control' stations at the azimuth angles considered. Using the least squares technique explained before in this section, a single airfoil is

designed to match the different pressure distributions in its radial position. This new geometry is fed back into the process for the new iteration. As in the hover case the process is stopped when convergence is reached.

3.3.2.3. Combined Flight Conditions.

Helicopters are such versatile machines that a typical mission will take them through a lot of different flight conditions, among which the most common ones will be hover and forward flight at different flight speeds. This is the reason why the designer does not give any value to a rotor optimized solely for the hover conditions or for the forward flight condition at some advance ratio. The actual design should consider all the possible flight conditions that the aircraft is likely to encounter.

The methodology presented here is easily adapted to consider these cases, where the design team will optimize for several flight conditions. Although it is very probable that the final design will not excel in any on the flight conditions, it will match all of them as close as possible in a least square sense.

To include two (or more) flight conditions in the design the process is as follows: Lift distributions must be developed for each flight condition, inflow angles correspondent to these distributions are computed; target pressure distributions are developed at the selected radial 'control' stations, and in the case of forward flight for the azimuth angles of

interest; an analysis run is performed for each of the flight conditions studied in the design and pressure distributions are computed for each of the positions where targets are specified. The over-specification problem is present here again, but the least squares technique presented in the previous sections will be used here. The designer will have to build the design matrices adding each flight condition and then solving for one ΔZ. In this way a single airfoil will match closer all the flow conditions that it is expected to encounter often.

Any possible combination of flight conditions can be considered in this way, the only requirement is the need for parallel analysis runnings of them all so they can be compared to the specified targets, but this can reduce significantly the design time since all possible flight conditions can be considered at once.

3.3.3. Inclusion Of Viscous Effects.

For the methodology to be complete and accepted as an efficient way for rotor design, viscous effects have to be considered. Although the fixed wing industry had started the research process for a method capable of designing a wing considering viscous effects, such as the usage of the Navier-Stokes equations in a 3-D space, parallel studies for the rotary wing industry are in its infancy.

In this work, the viscous effects will be included with the aid of strip theory, i.e. analyzing the boundary layer in a 2-D space, even when the pressure distributions were computed in an actual 3-D space. The full potential flow solver computes the pressure distributions along the blade, which will serve as an input to the 2-D compressible boundary layer code that will compute boundary layer thickness, displacement thickness and momentum thickness, among other quantities.

The rotor blade is then completely defined after this study is done, and the whole procedure is run in the following fashion: First of all the designer specifies the lift distribution over the rotor disc, as a function of the radial station for hover, and as a function of the radial and azimuth station for forward flight; with it he can tailor pressure distributions that will match this lift requirements as well as drag or moment considerations. Starting with the baseline rotor, the flow over it is computed and compared against the target distributions, the rotor is then modified until the convergence criteria is satisfied. At this point the 'fluid' airfoil is developed using only potential flow theory. Using the final pressure distributions, a boundary layer analysis is done and with it the displacement thickness, among other quantities, is computed. This displacement thickness is subtracted from the 'fluid' airfoil to obtain the 'solid' actual airfoil required to be built into the rotor blade.

This has been one of the aspects why the inclusion of viscous effects become necessary. There are also drag considerations that can not be analyzed unless some

viscous model is used in the design. Rather than computing what the drag will be for the final design, the designer can make use in advance of the viscous model to keep the drag to a target value. This will be done when the target pressure distributions are being tailored; when the pressure distribution is satisfying the lift coefficient, and keeping the moment coefficient within a certain range, the boundary layer analysis can be run with this pressure distribution as the input to check for the drag that it will produce. This can be done with the aid of the modified Squire-Young formula[45]:

$$C_d = 2\delta_{2_{te}} \left(\frac{U_{te}}{U_\infty} \right)^{\frac{5+H_{12_{te}}}{2}}$$

where: $H_{12\,te} = H_{12\,te}$ for $H_{12\,te} < 2.5$

$H_{12\,te} = 2.5$ for $H_{12\,te} > 2.5$

All the quantities needed in this formula will be computed by the boundary layer code. In this way the designer can tailor the target pressure distribution to some drag value, or some lift to drag ratio.

3.3.3.1. Hover Case.

As mentioned in the previous section, viscous effects are included mainly for two reasons: the computation of drag and the design of an actual solid airfoil. Computation of

drag can be considered in advance, so that the target pressure distributions are tailored to meet certain drag objective, as well as a check for the final design.

Due to the flow symmetry that is present during the hover condition, the inclusion of viscous effects are somewhat easy to perform. The pressure distribution that the airfoil will produce will be the same along one revolution and thus the displacement thickness will be constant along this revolution. In this case the boundary layer can be analyzed so that the displacement thickness is computed and subtracted from the 'fluid' airfoil so that the 'solid' airfoil is specified.

3.3.3.2. Forward Flight and Combination of Flight Conditions.

Viscous effects can be considered for any flight condition when the target pressure distributions are being tailored, to assure that the target distribution will not produce a drag higher than targeted. In the case of the hover condition, viscous analysis also helped to specify the solid airfoil which must be used to build the blade. In the case of forward flight, and thus for combinations of flight conditions also, this specification of the solid airfoil can not be done because the inverse design methodology will specify a fluid airfoil that will match all the target distributions as close as possible. This 'fluid' airfoil will produce several different pressure distributions along the blade revolution, which will in turn produce several different displacement thickness; it is not possible just to subtract this displacement thickness from the fluid airfoil, because the design will produce several

different 'solid' airfoils. This is the opposite to what should be obtained. A method to develop only one 'solid' airfoil from the subtraction of the different displacement thickness from several different 'fluid' airfoil has yet to be developed.

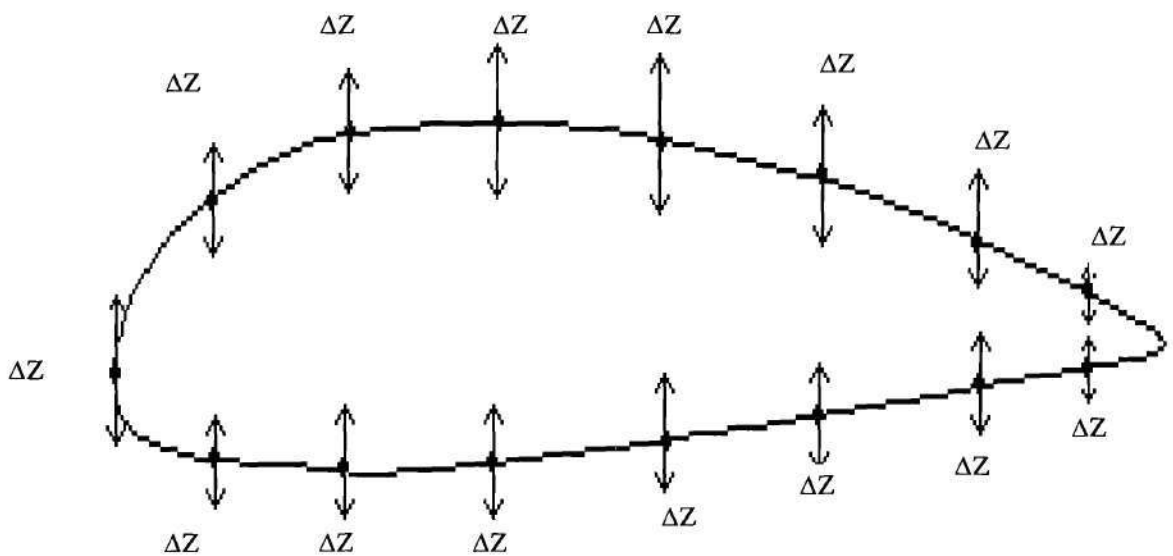

Figure 2.- Geometry modifications for the inverse design algorithm.

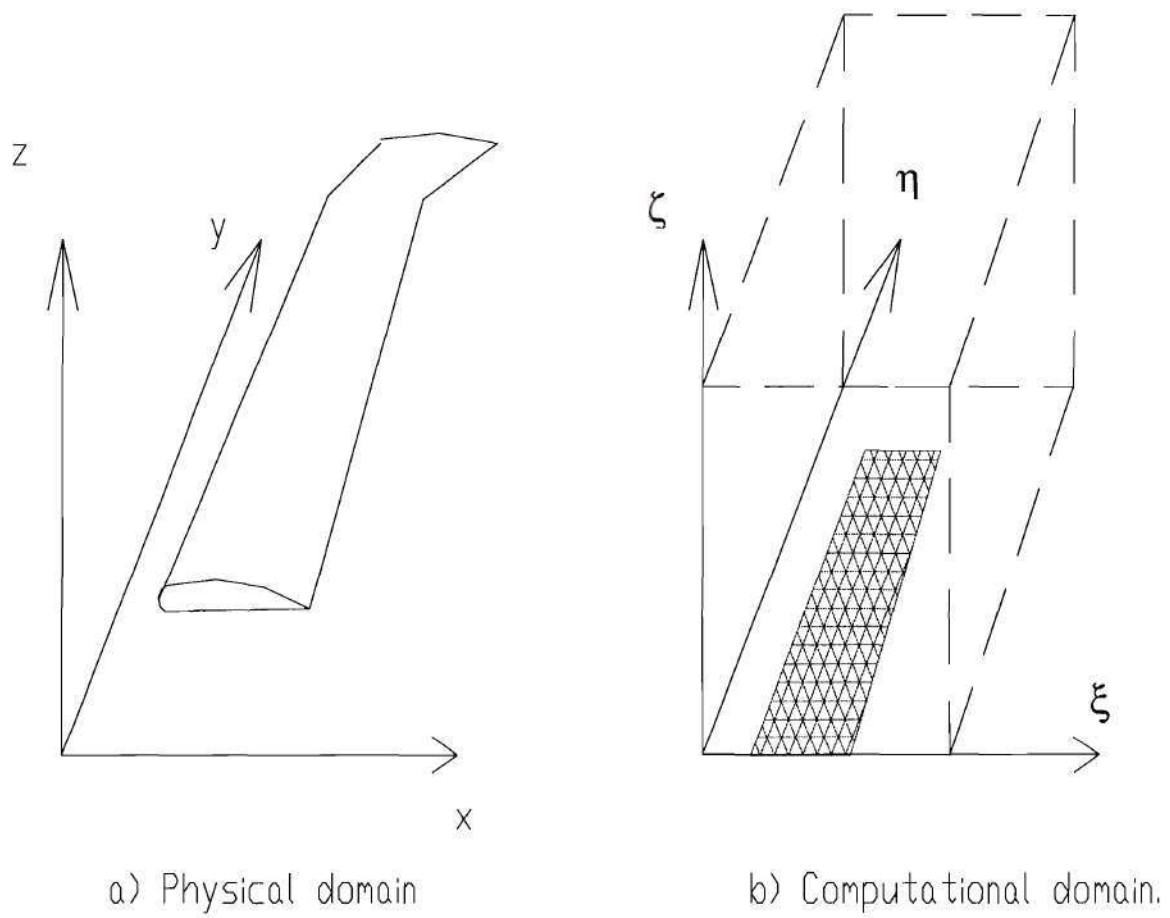

Figure 3. Physical and computational domains.

CHAPTER IV

CASE STUDIES

The presented methodology for rotor blade design has proved its capabilities and usefulness in a variety of cases. Different studies for hover, forward flight and combinations of both flight conditions had been tested with different rotor geometries, different flight conditions and different inflow characteristics. Results have been satisfactory in terms of achieving the performance goal. Although in some cases this required a significant amount of computer time, it is still less than the time required with traditional design methods. Some different cases, which had been used to test the method presented in the previous chapters will be detailed in the following sections.

4.1. Hover Case

Due to the fact that the blade is under the same flow conditions over the whole revolution, the hover flight condition is the simplest to analyze, and thus is the first case study in this work.

4.1.1. Matching a Specific Pressure Distribution in Hover.

A simple untwisted rotor with 6 feet radius, 6 inches chord and an NACA 0012 airfoil was taken as the initial geometry. Far wake effects were not considered here, and the goal was to find the blade geometry which will meet certain target aerodynamic characteristics at 3 radial control stations. Figures 4, 5 and 6 show the pressure distributions achieved by this starting rotor configuration at the selected control stations of 65%, 80% and 100% radial position. At this low pitch setting, the rotor was, as can be seen, lightly loaded. Target pressure distributions were prescribed at these three control stations. These target pressure distributions were chosen to significantly raise the C_T value from the baseline configuration. The target pressure distributions are shown in these same figures. The M_{tip} was set to 0.75 and the inflow angles were computed as $\alpha = 4° - (180\ v_i)/(\pi\Omega r)$, where the induced velocity, v_i, was obtained using an annular momentum and blade element code capable of computing the non-uniform induced velocities at different blade stations.

The inverse design methodology was now used to change the blade shape to achieve the desired C_p distributions. The design allows the leading edge z-values to change relative to the trailing edge, producing any twist required; and, of course, camber is also introduced.

After twenty design iterations between the modified Garabedian-McFadden (MGM) method solution and the flow solver, the target pressures were achieved over most of the rotor. Figures 4, 5 and 6 show the original, final and target C_p distributions at the selected radial stations. The original and final airfoil sections at these stations are shown on the same figures. It is clear that the design methodology was able to implement substantial changes to the blade twist and airfoil shape, in a fully automated manner.

This example has shown how robust the method is, when pressure distributions are to be matched. Airfoils are automatically generated and the computed pressure distributions are consistently converging towards the target distributions.

4.1.2. Matching a Lift Distribution in Hover.

In a second study, the configuration used was exactly the same as in the previous case, with the only addition of -9° linear twist. This example shows how a target lift distribution can be matched in the hover flight condition. For this example an automated procedure to develop target C_p distributions which will match the designated lift distribution was implemented, using the strategy given by Malone et. al[25]. As before, the inflow table compatible with this loading was computed with annular momentum blade element theory. After twenty design updates, the blade shape was modified to achieve the

target pressure distributions. In Figures 7, 8 and 9 the airfoils designed at these control stations are shown along with the original, target and final pressure distributions obtained at the specific control station. Figure 10 compares the lift distribution obtained after these twenty iterations against the original and target lift distributions. The target lift distribution developed for this example was selected to raise the C_T while keeping the induced velocity uniform to keep the induced power as low as possible.

The selected 'control' stations in this case were r/R=0.71, r/R=0.83 and r/R=1.0. Figure 10 shows that the target and final lift coefficients are very well matched at these stations. There is a region about r/R=0.9 to r/R=0.97 where they do not match as well as at the rest of the blade; of course, another 'control' station can be added in this region to enforce a better matching.

This case has shown how the methodology presented is capable of handling specified lift distributions for the hover condition.

4.2. Forward Flight Case

The forward flight condition, at any speed, requires a completely different approach due to the lack of symmetry in the rotor flow field. Since the blades will not be under the same flow condition along the revolution, they will produce a different pressure distribution for every azimuth station. Therefore, a specific target pressure distribution is also required for each azimuth station to be studied in the design case. More importantly, they need to be combined in some way so a single airfoil is designed for the whole revolution, not for every azimuth station. Theoretical details of the procedure used in this work are presented in the previous chapter and the practical details designing rotors for forward flight will be presented in the following sections.

4.2.1. Matching Pressure Distributions in Forward Flight.

The problem of designing rotors for forward flight cases was encouraged by the remarkable results obtained for the hover cases. This example shows the first steps of designing a rotor for the forward flight case.

In this case, all the control stations had a weight factor equal to 1, as a starting point for future studies. The original rotor used the NACA 0012 airfoil, with 30 feet radius and 2 feet chord. The inflow table was built by using the annular momentum and

blade element theory. The blade had a -10° built-in twist, $M_{tip} = 0.58$, and collective pitch of 16° while flying at a $\mu = 0.05$.

The selected control stations were placed at r/R=0.73, r/R=0.85 and r/R=1.0 and Ψ=90°, 180°, 270° and 360°. The load distribution, $L(r,\Psi)$, is not modified in this case, i.e. the distribution obtained from the original rotor is held, but the pressure distributions at the selected control stations were tailored using the Stratford recovery pressure profile. These C_p distributions matched the required C_l at the specific control station. Doing this, the induced power should remain constant, but the profile power is expected to decrease by selecting a pressure distribution which is on the verge of separation and produces less drag.

As mentioned in the previous chapters, the problem of over-specifying the design process is overridden by solving the problem in a least squares fashion, as explained in chapter three.

The design process was stopped after 10 iterations, since the obtained pressure distributions were considered to be close enough to the targets. A convergence criteria is introduced to check the design process development. This criteria is defined as:

$$CC = \frac{\sum_{k=1}^{l}\sum_{j=1}^{m}\alpha_k \sqrt{\frac{\sum_{i=1}^{n}\left(C_{p_{i,j,k}}{}^{actual} - C_{p_{i,j,k}}{}^{target}\right)^2}{n}}}{lm}$$

where CC is the convergence criteria, i is the index for the n number of points along the airfoil surface, j is the index for the m radial stations, and k is the index for the l azimuthal stations; finally α_k is the weight factor assigned to the azimuthal control station.

Figure 11 shows the convergence history for this example. This figure shows how the design process is converging toward the target. Figure 12 shows the three newly designed airfoils for r/R=0.73, 0.85 and 1.0 compared to the original NACA 0012 airfoil. Figures 13-24 compare the target pressure distributions and those obtained by the original rotor and the rotor built after the 10^{th} iteration for every control station. This case showed how to handle rotor design for the forward flight condition in its simplest case: matching specified pressure distributions at the control stations.

4.2.2. Weight Factors Effect.

In order to address the effect of the selected weight factors, a new case study is performed with the exact same specifications as the previous case, with the only difference of selecting weight factors. The Ψ=90° station was weighted with a 2, while the Ψ=180°

and 360° stations were assigned 1. Finally the 270° station was assigned a weight factor of 0.25. The geometry of the rotor, as well as the flight conditions, are kept the same as in the previous case.

The design process was also stopped after the 10th iteration since the obtained pressure distributions were considered to closely match the targets. Figure 25 shows the convergence history for this case; it is easily seen that the process is driving the solution toward the targets. Figure 26 shows the airfoils obtained for each selected radial station, and compares them against the original NACA 0012. A comparison between this figure and Figure 12 shows the effects of selecting different weight factors. Figures 27-38 show the target pressure distributions comparing them to the ones obtained by the original rotor and the rotor obtained after the 10th iteration at every control station.

4.2.3. Forward Flight In A Gazelle Helicopter.

The methodology was further tested by a more realistic case in which the gazelle helicopter was chosen. An inflow table produced by CAMRAD was available for the M_{tip}=0.63 and μ = 0.344 flight conditions. This inflow table was used as the input for the full potential flow code. The original rotor has a single airfoil all along the blade, with chord of 0.35 meters and radius equal to 5.25 meters. Collective and cyclic pitch angles were introduced in the inflow table.

Although the lift distribution was not modified in this case, different pressure distributions were generated by modifying the original distributions. These modifications were done with two major criteria in mind: 1) minimize separation present, which is checked with Stratford's[26] technique, and, 2) reduce wave drag by weakening any shock waves present.

Control stations were set at the 43%, 73% and 100% radial stations for this case; Figure 39 compares the designed airfoils after the 15th iteration against the original gazelle airfoil. In this case the airfoils were only slightly modified, probably because the gazelle rotor was designed for good performance at high speeds. The convergence history for this case is shown in Figure 40, which shows how the method is driving the design toward the targets. Figures 41-52 compare the target, original and final pressure distributions, showing the convergence at a every control station.

4.2.4. Design for Reduced Induced Torque in Forward Flight.

The objective in this example is to match a target lift distribution in forward flight. The lift distribution is specified so that it reduces the induced power required. In this case the original rotor had an NACA 0012 airfoil along the blade span with no taper and a chord of 2 feet. The radius was 30 feet with a built-in twist of -10° and the pitch angle

was fixed at 16.5°. Flight conditions were: M_{tip}=0.58 and μ = 0.05. The inflow table for these conditions was generated using the Drees' model[42].

A new lift distribution, and thus a new inflow table, was developed to reduce the induced torque. Figures 53-56 compare the original and target lift coefficient distributions along the blade for 4 azimuth stations 90° apart. Also shown in these figures, is the final lift coefficient distribution obtained after 10 iterations. The control stations were taken at r/R=0.43, r/R=0.73 and r/R=1.0 for Ψ=90°, 180°, 270° and 360°, but the final lift distribution is expected to match the target distribution everywhere.

At the 12 control stations selected, the target lift coefficient was translated into target pressure distributions which will drive the inverse design method. The pressure distributions were tailored to avoid separation wherever possible.

The design process was stopped after ten iterations. The convergence history for this example is shown Figure 57. It is easy to see that the process is again driving the design toward the target pressure distributions. Airfoils obtained at this point are compared against the original NACA 0012 in Figure 58. Note that the process has been able to modify camber, thickness and twist of the baseline blade to match the target pressure distributions. This design reduced the induced power required from 1180 to

1155 HP, a reduction of almost 3%. Original, target and final C_p distributions for the selected control stations are compared in Figures 59-70.

4.2.5. Matching Laminar Pressure Distributions in Forward Flight.

Among the many advantages of laminar flow is the reduction of viscous drag. Assuming the helicopter can achieve laminar flow over the rotor blades, less profile power would be required, specially if the outer sections of the blades are under this flow regime. Unfortunately, the assumption of laminar flow over a rotor blade seems to be extremely optimistic, if not unrealistic.

Turbulence is thrown into the flow by several different sources: Local Reynolds number at the blade radial station, strong tip vortex, skewed wake and rotor-fuselage interactions, among others. Almost every one of these is impossible to avoid, so a laminar regime is very unlikely to occur over the helicopter rotor. Nevertheless, since the rotor designer and the aerodynamicist will specify the target pressure distributions that are desired, laminar pressure distributions are easily tailored as targets. The method will be responsible of producing the airfoil distribution that will match them as close as possible. The case study presented here shows the differences observed in this type of analysis.

The rotor geometry, flow conditions and target lift distribution were specified exactly as in the previous example. Once this information was provided, the design methodology can be started and stopped when the convergence criteria is satisfied.

The most difficult aspect of this laminar flow analysis is the tendency of the flow to accelerate rapidly in the region close to the leading edge, thus increasing significantly the Reynolds number in this zone due to the high flow speed. This velocity peak is shown in the pressure distribution as a highly negative pressure coefficient, which usually appears in a region very close to the leading edge. The designer specifies the target distribution by relocating this point further aft, but this proved very hard to achieve. Most rotors will induce this high speed flow very close to the leading edge.

As mentioned before, this is not produced only by the airfoil shape, but also by other effects such as the tip vortex strength or tip speed, the chord of the blade, which will modify the local Reynolds number. All of them factors that will tend to produce a higher turbulence. In an attempt to reduce this velocity peak, the MGM coefficients, A, B and C were varied locally around the leading edge and up to the 25% chord point. This proved to have a beneficial effect in the way of minimizing the velocity peak. Unfortunately, the peak was not completely eliminated. Table I lists the MGM coefficient values used for this case. The interaction between these MGM coefficients and the velocity peak have to be studied in greater detail. As before, the convergence history is shown in Figure 71. It

can be seen there that the method is again driving the design toward the target pressure distributions. Original, final and target pressure distributions are compared in Figures 72-83 where this velocity peak can be seen. Figure 84 shows the newly design airfoils and compares them with the original airfoil.

4.3. Combined Flight Conditions

The designer will not consider any design as an optimum if it has only been optimized for a single particular flight condition, since the machine will fly in an infinite number of flight conditions. Optimizing a rotor for a particular flight condition, generally means a drawback at some other condition. In this methodology, a particular combination of flight conditions is selected from the mission specifications, so that the design is optimized for all of them simultaneously. The design will not satisfy these conditions exactly, but will produce a rotor that will minimize the difference in a least squared sense.

Two different cases are presented here. In the first one the rotor is optimized using potential flow theory. It is optimized for two different flight conditions separately and then an analysis is made to study how each design will perform the off-design condition for comparison purposes. The second case presented will make use of the full

methodology; making use of potential and viscous flow theory the rotor was optimized for two different flight conditions separately, as before, a comparison will be made between them but also against a third rotor designed for the two flight conditions simultaneously.

4.3.1. Rotor Design for Different Flight Conditions.

In this study one rotor was designed for the hover condition and another one was designed for the forward flight condition. A comparison made between these two rotors emphasized the importance of combining flight conditions during the design. The baseline rotor had a M_{tip}=0.58, chord equal to 2 feet, and used the NACA 0012 airfoil in a blade with 30 feet radius. The control stations are taken as r/R=0.43, r/R=0.73 and r/R=1.0 with Ψ=90°, 180°, 270° and 360° for the forward flight condition. This forward flight condition is specified as an advance ratio of 0.05 and a rotor angle of attack of 0.07° degrees.

The original rotor is first analyzed to compute its lift distribution as well as the pressure distributions for the selected flight conditions. Target lift and pressure distributions are tailored having the original distributions as a starting point. The lift distribution was modified so the induced power will be minimized, and pressure distributions were specified at the control stations once the required lift coefficient for that station was known. Even though a viscous analysis was not formally performed, the

target pressure distributions were tailored to avoid separation which is checked using the Stratford's technique.

As mentioned before, only potential theory was used in this case which means that the drag cannot be estimated. This will limit the designer to control the profile power but it will allow him to control the induced power, thus the comparison will be done by the ratio of thrust to induced power required.

Figures 85 and 86 compare the four rotors considered here, the original, the imaginary 'target' rotor and the rotors designed for hover and for forward flight. For the hover condition, results are as expected, since the best thrust to induced power ratio was achieved by the rotor specially designed for the hover condition. Although the rotor designed for forward flight also improves over the original rotor, and in fact is very close to the target rotor, one can not conclude that this will happen every time, since this might be only a coincidence. The fact that the rotor designed for hover performs better than the target rotor illustrates the fact of non-optimality of the target lift distributions.

For the forward flight case, results are not exactly as expected. Both designs, the rotor designed for hover and the rotor designed for forward flight improve substantially over the original rotor, but the fact that the rotor designed for hover shows a better performance than the rotor designed for forward flight highlights the importance of an

optimal lift distribution. In other words, the rotor designed for hover produces a lift distribution which requires less induced power than the target distribution or than the lift distribution produced by the rotor designed for forward flight.

The design methodology proposed here works to match the target pressure distributions specified at each control station rather than the target lift distributions. As can be seen in Figure 87, the convergence criteria is decreasing for both flight conditions; meaning that the obtained pressure distributions are closer to the targets after every iteration, as well as matching the target lift distributions, which can be seen in Figures 88-92, where it can be seen how each design matches its correspondent distribution better than the other rotor. The same behavior can be seen in Figures 93-107 where the original, target and final C_p distributions are compared. It can be seen here how the hover C_p distributions are better matched by the rotor designed for hover, as well as the rotor designed for forward flight matched better than the rotor design for hover the target C_p distributions in forward flight, despite the performance that any rotor can achieve. Figure 108 compares the airfoils designed for hover against the original NACA 0012, and Figure 109 compares this original airfoil against the airfoils design for the forward flight condition.

4.3.2. Rotor Design for a Combination of Flight Conditions.

In this example the full methodology is applied, a combination of hover and forward flight was specified as the most important flight conditions for the aircraft to be designed. Several designs and comparisons were made in this example to check for the method reliability. The rotor characteristics were given as M_{tip}=0.636, chord=0.47 feet, the original rotor used the VR7-0°T airfoil, with a radius of 13.1 feet. The control stations were taken as r/R=0.43, r/R=0.73 and r/R=1.0 with Ψ = 90°, 180°, 270° and 360° for forward flight. The forward flight condition was specified as an advance ratio of 0.21 and a rotor angle of attack of 7.3 degrees.

In order to test the methodology presented here, the performance of 5 different rotors was analyzed. These are: the original rotor, baseline from which the methodology starts; the 'target' rotor, an imaginary rotor that would produce the target lift and pressure distributions; the rotor optimized for the hover condition without considering any other aspect; the rotor optimized for the forward flight condition of μ=0.21 without considering any other flight condition; and the rotor optimized for the combination of the two flight conditions, hover and forward flight at μ = 0.21. The theoretical background on how these cases are combined is explained in chapter 3. In this section, details of the design as well as how these rotors perform is given.

Required inflow distributions for the original and target rotors (all other rotors use the target distributions) were computed using blade element theory with annular momentum. The original rotor was analyzed first in both flight conditions. The lift distributions obtained from the original rotor are modified so the new rotor will required less power is both flight conditions. Of course, the designer expects that there is no single rotor that will match both target lift distributions, but the method will produce a rotor which minimizes the difference for both specified conditions.

Specifying the target C_p distributions took several steps. Both lift distributions, for hover and forward flight, were modified for minimization of the induced power required; then the lift required was converted to actual target pressure distributions at the selected control stations. A boundary layer analysis was run to enforce that the drag produced by the target pressure distribution is less than the drag produced by the original pressure distribution. Profile power required will be minimized in this way.

When the rotor is hovering, the lift distribution is a function of radial position only, this simplifies the analysis; when the rotor is in forward flight, the lift distribution is a function of radial position as well as of azimuth angle. The designer will have to specify target pressure distributions at the radial and azimuthal control stations, that will minimize the profile power required and that when integrated will also minimize the induced power required.

Figures 110 and 111 show how these five rotors compare. The main variable through which they are compared is the thrust loading (thrust to total power ratio) due to slight modifications on the thrust produced by each of these rotors. It is easy to see from these figures how the newly designed rotors improve the hover performance. The fact that the rotor designed for forward flight shows the highest improvement on hover performance was not expected and it highlights the importance of optimality of the target lift distributions.

The three newly designed rotors perform about the same in forward flight. The forward flight case shows little variation from the original rotor. This is shown in Figure 112 where the convergence rate is shown. It is easy to see that the design has arrived to a steady state. In this example, the rotors designed for the combination of flight conditions or for forward flight achieved the lowest value for the convergence criteria at the fifth iteration, but the rotor designed for hover is still improving.

Figures 113-117 compare the lift coefficient distributions obtained for hover and forward flight at Ψ=90°, 180°, 270° and 360°. Figures 118-132 compare the target, original and final C_p distributions obtained for the rotors designed for hover, forward flight and the combination of flight conditions. It can be seen here that the rotor designed for hover matched better the target C_p distributions for hover as well as the rotor designed for

forward flight matched better the target C_p distributions for forward flight. The rotor designed for the combination of flight conditions matched close both conditions, which emphasized the power of the proposed methodology to design rotors for any combination of flight conditions.

Figures 133-135 compare the newly designed airfoils for each flight condition against the VR-7 (0° t. e. tab) original airfoil. It is noted here the different designs achieved by considering different flight conditions.

Table I. MGM coefficients used for the laminar flow study case.

Lower Surface				Upper Surface			
X/Chord	A	B	C	X/Chord	A	B	C
1				0			
0.95	5	5	5	0.005	5	5	5
0.9	5	5	5	0.0125	5	5	5
0.85	5	5	5	0.025	10	10	10
0.8	5	5	5	0.05	10	10	10
0.75	5	5	5	0.075	10	10	10
0.7	5	5	5	0.1	10	10	10
0.65	5	5	5	0.15	30	30	30
0.6	5	5	5	0.2	30	30	30
0.55	5	5	5	0.25	15	15	15
0.5	5	5	5	0.26	5	5	5
0.45	5	5	5	0.27	5	5	5
0.4	5	5	5	0.28	5	5	5
0.35	5	5	5	0.29	5	5	5
0.34	5	5	5	0.3	5	5	5
0.33	5	5	5	0.31	5	5	5
0.32	5	5	5	0.32	5	5	5
0.31	5	5	5	0.33	5	5	5
0.3	5	5	5	0.34	5	5	5
0.29	5	5	5	0.35	5	5	5
0.28	5	5	5	0.4	5	5	5
0.27	5	5	5	0.45	5	5	5
0.26	5	5	5	0.5	5	5	5
0.25	15	15	15	0.55	5	5	5
0.2	30	30	30	0.6	5	5	5
0.15	30	30	30	0.65	5	5	5
0.1	10	10	10	0.7	5	5	5
0.075	10	10	10	0.75	5	5	5
0.05	10	10	10	0.8	5	5	5
0.025	10	10	10	0.85	5	5	5
0.0125	5	5	5	0.9	5	5	5
0.005	5	5	5	0.95	5	5	5
0				1			

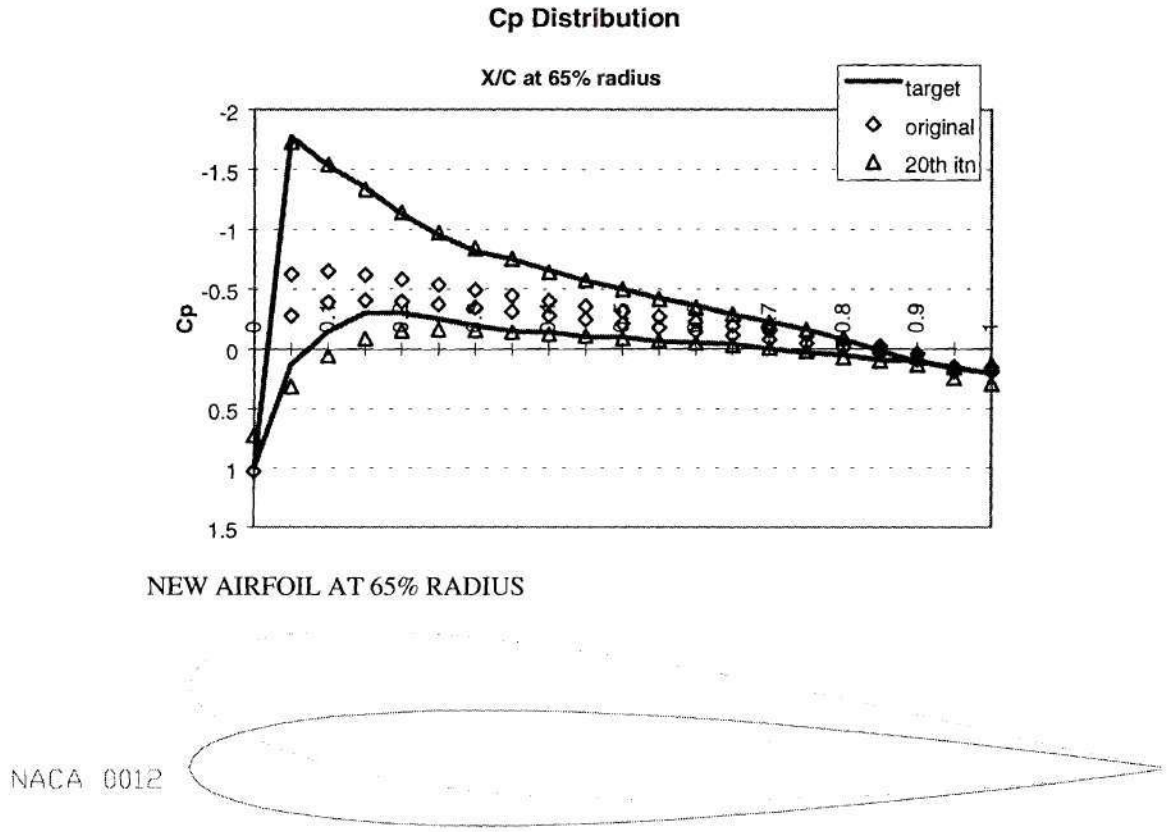

Figure 4. Comparison of C_p distribution at r/R=0.65 for a case study where the objective is to match the target pressure distributions.

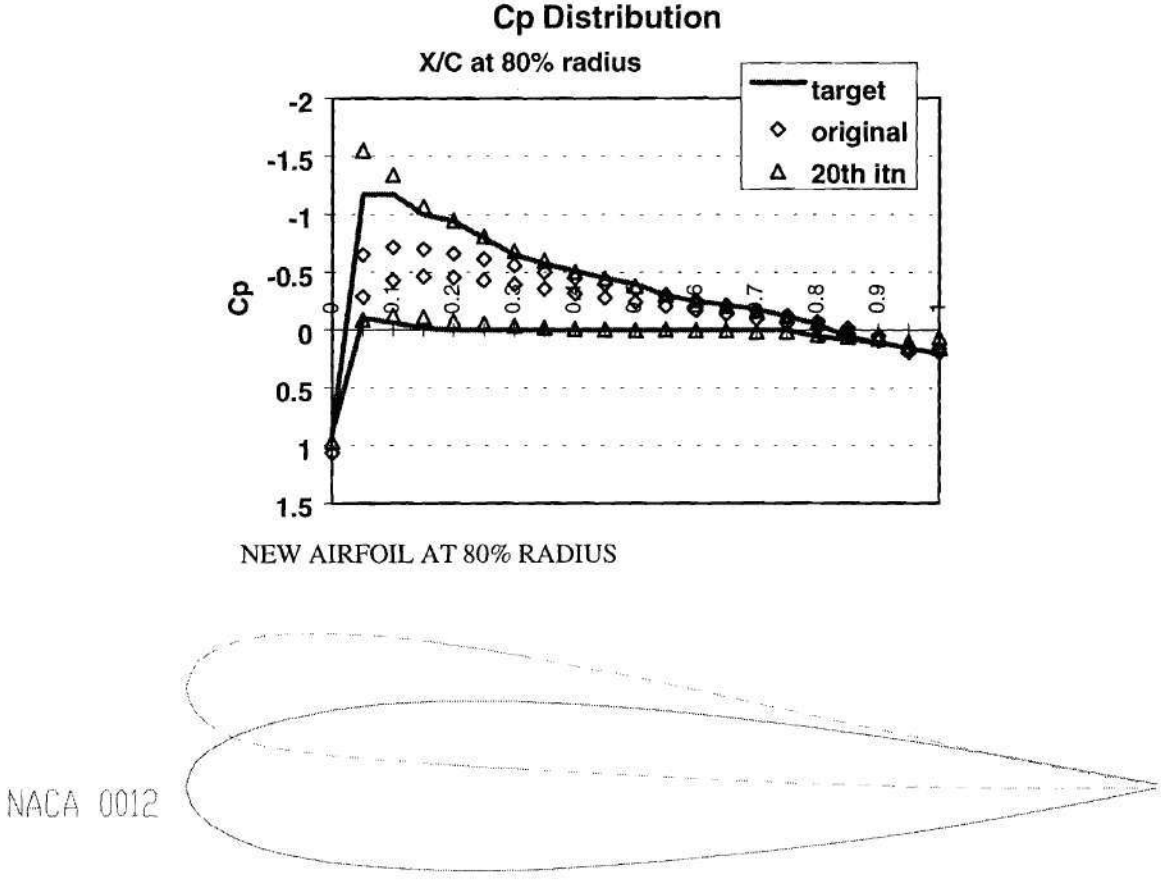

Figure 5. Comparison of C_p distribution at r/R=0.8 for a case study where the objective is to match the target pressure distributions.

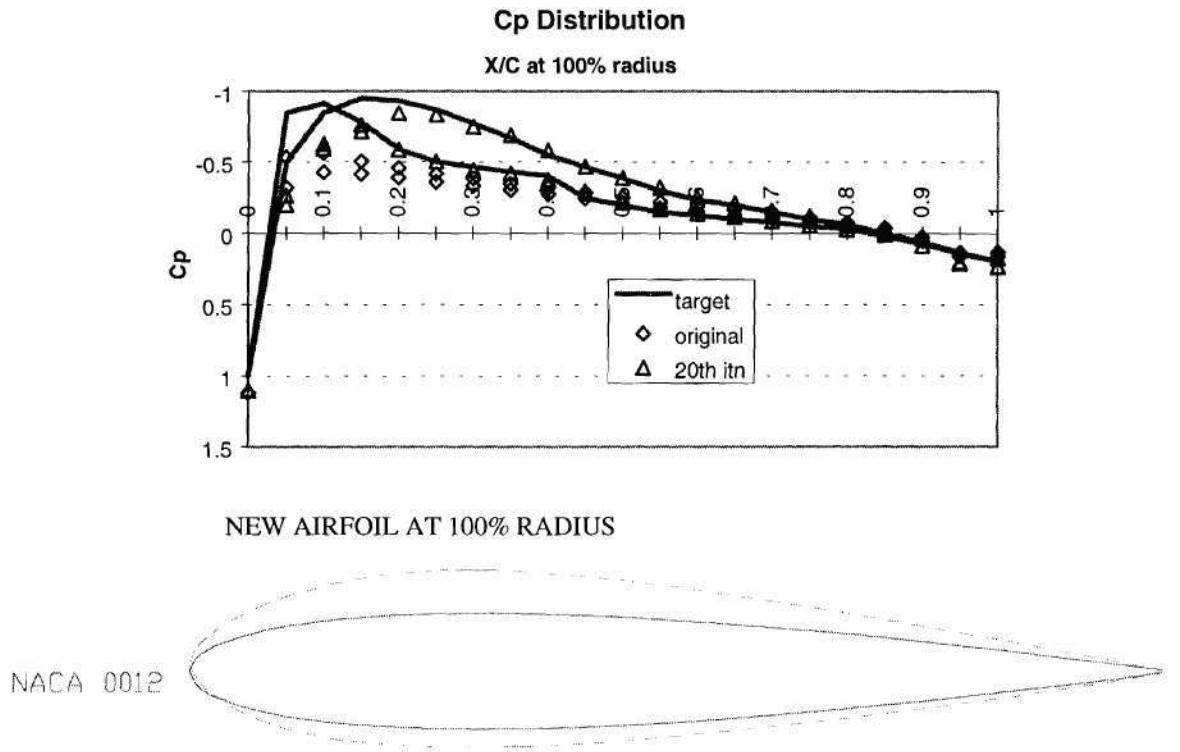

Figure 6. Comparison of C_p distribution at r/R=1.0 for a case study where the objective is to match the target pressure distributions.

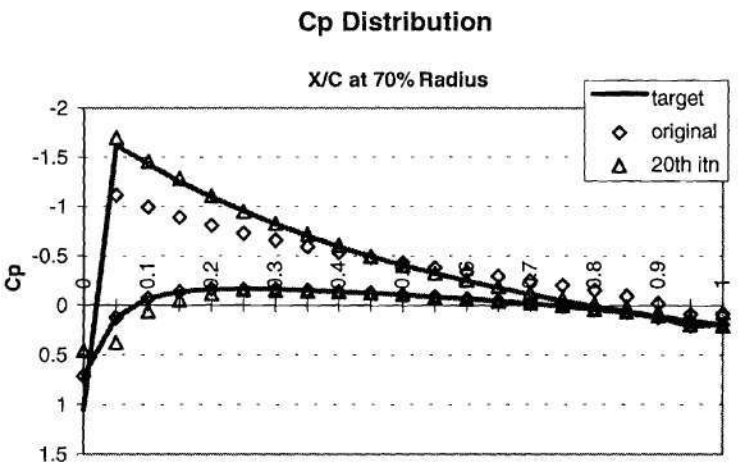

NEW AIRFOIL AT 70% RADIUS

Figure 7. Comparison of airfoils and C_p distribution at r/R=0.70 for case study in which the goal was to match a lift coefficient distribution.

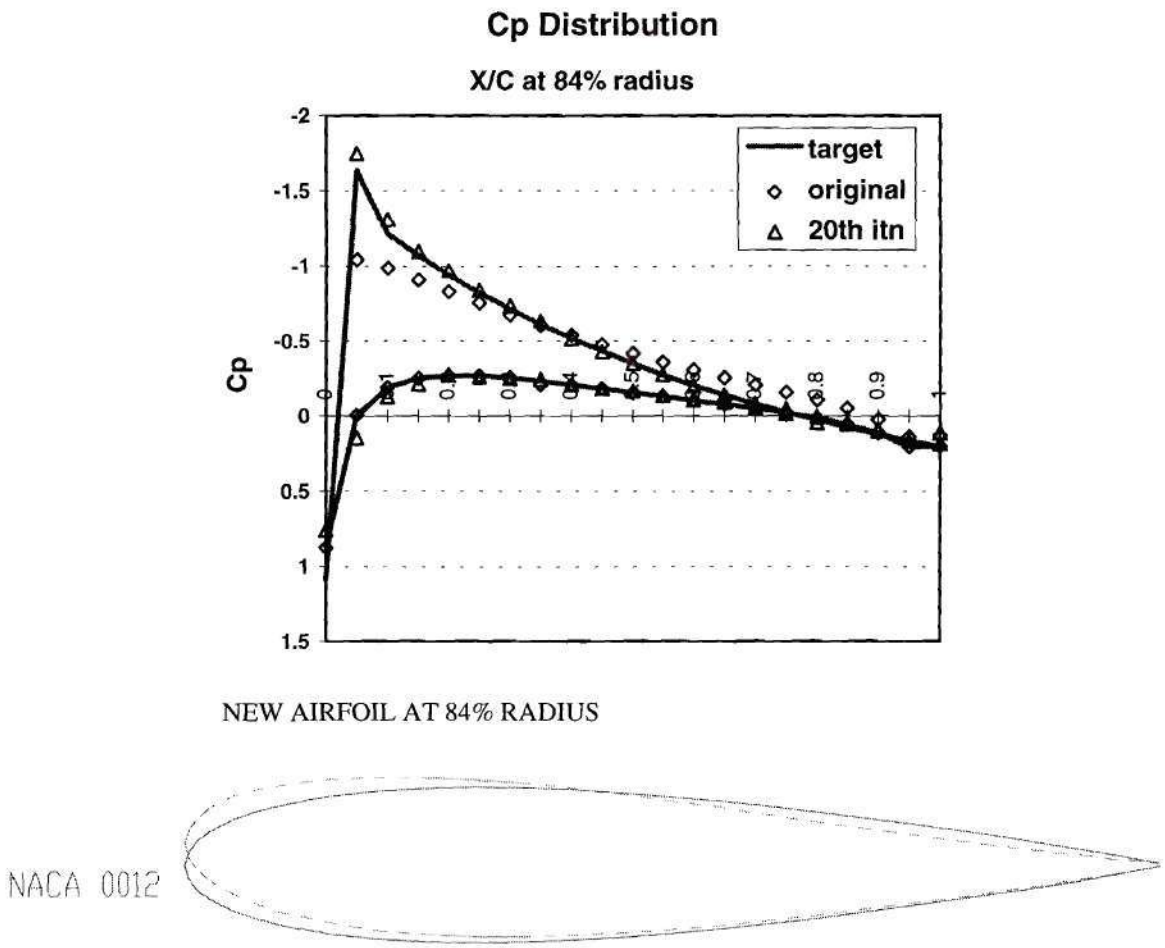

Figure 8. Comparison of airfoils and C_p distribution at r/R=0.84 for case study in which the goal was to match a lift coefficient distribution.

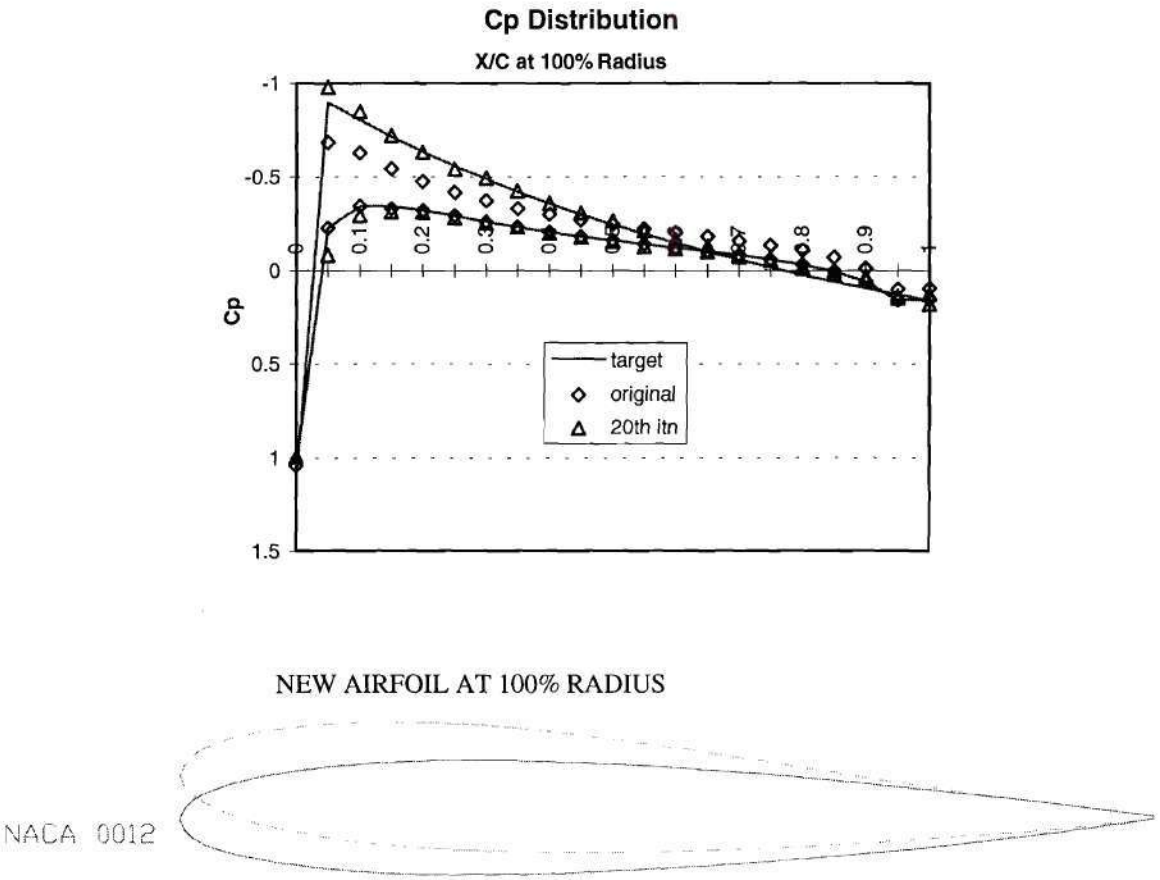

Figure 9. Comparison of airfoils and C_p distribution at r/R=1.0 for case study in which the goal was to match a lift coefficient distribution.

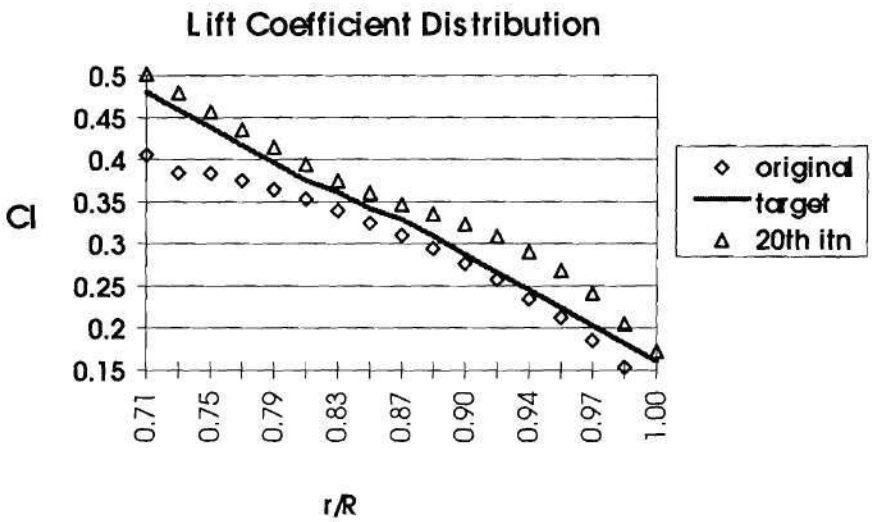

Figure 10. Comparison of C_l distribution for case study in which the goal was to match a lift coefficient distribution.

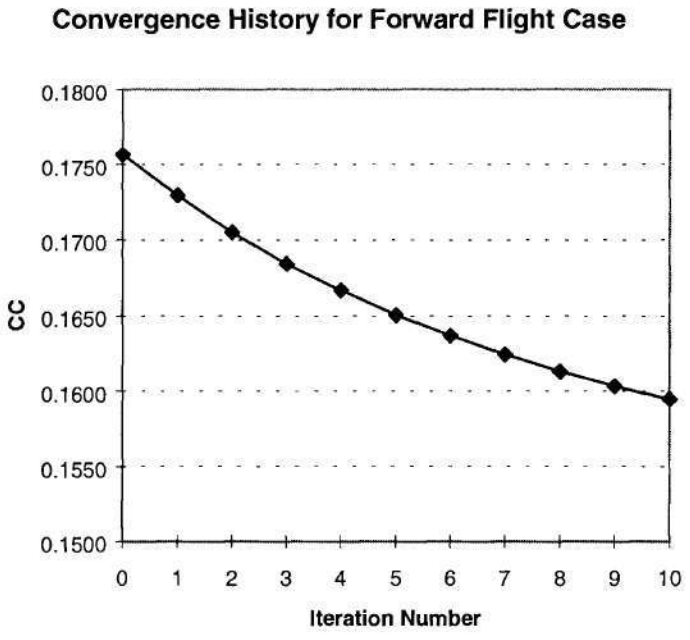

Figure 11. Convergence rate for forward flight study case in which the objective is to match target C_p distributions.

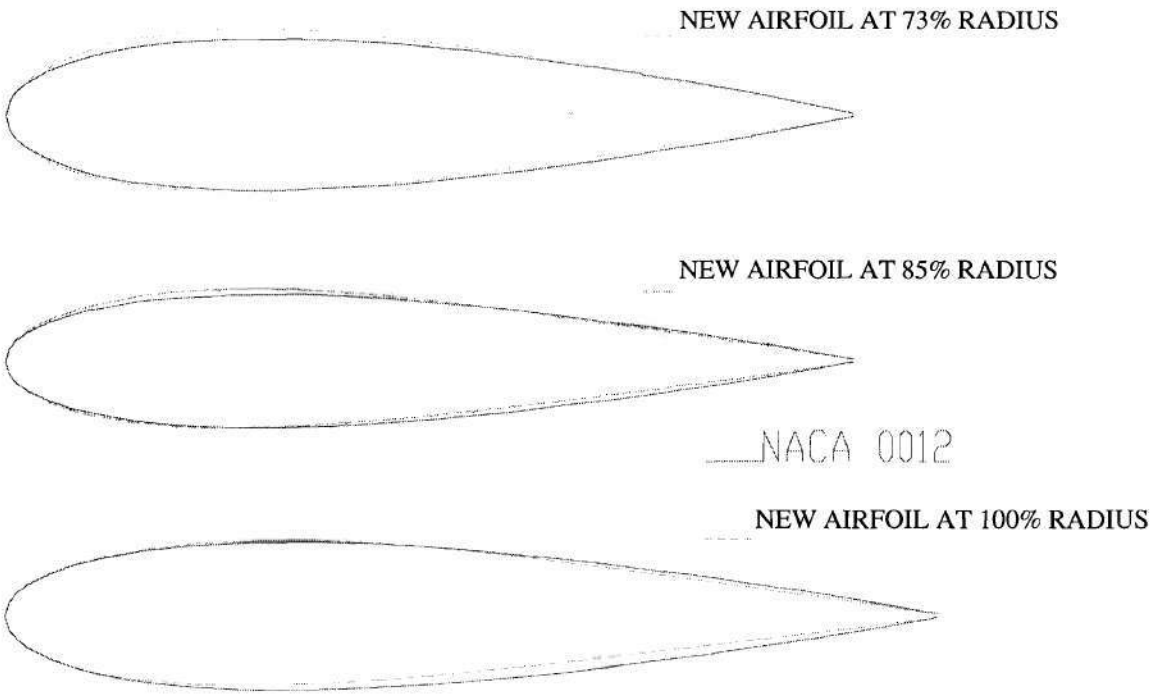

Figure 12. Airfoil comparison for forward flight study case in which the objective was to match target C_p distributions.

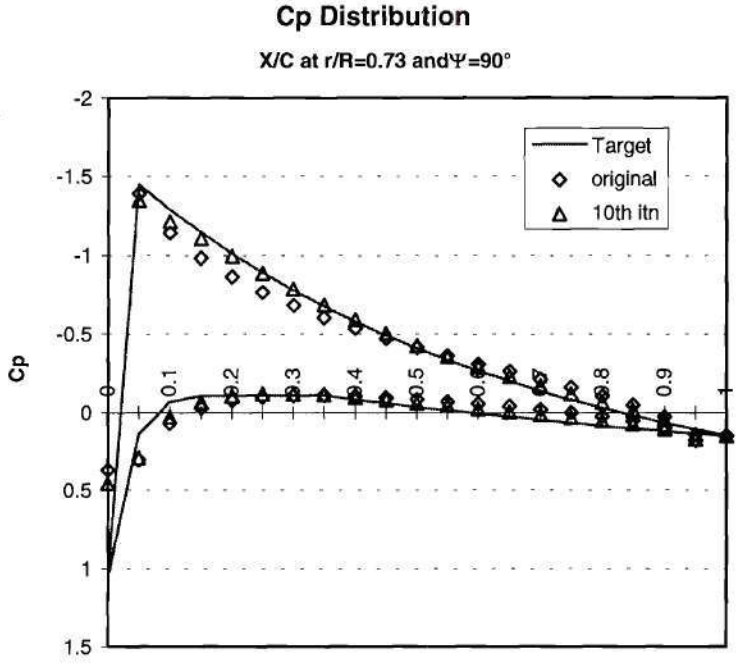

Figure 13. Pressure distribution comparison at r/R=0.73 and Ψ=90° for forward flight study case in which the objective was to match target C_p distributions.

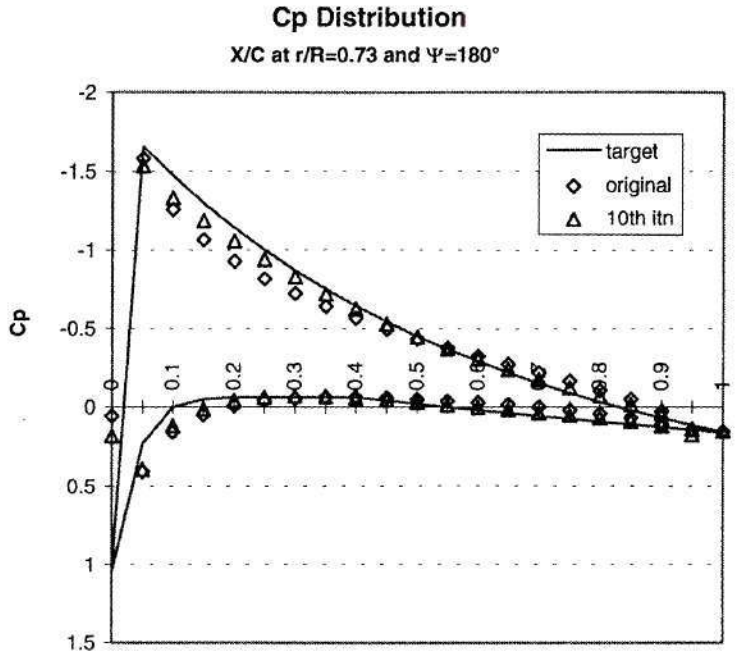

Figure 14. Pressure distribution comparison at r/R=0.73 and Ψ=180° for forward flight study case in which the objective was to match target C_p distributions.

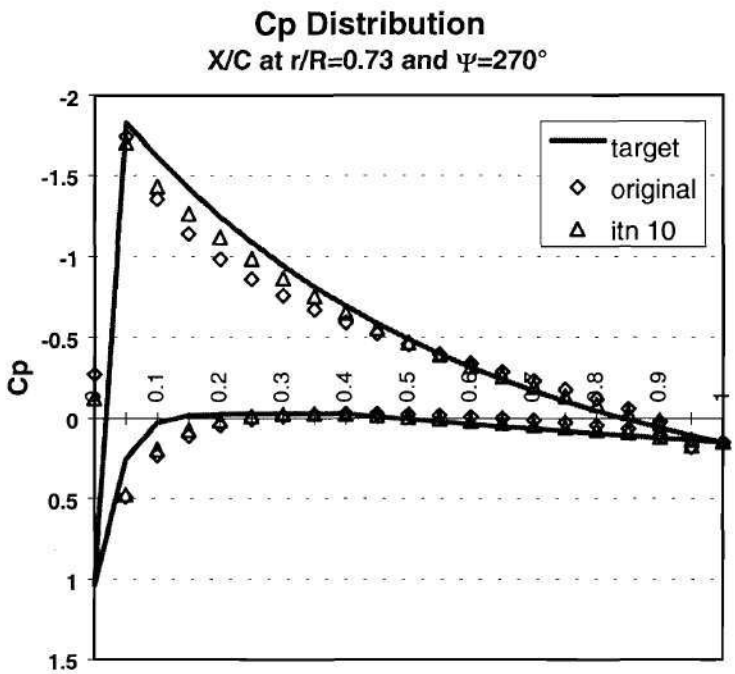

Figure 15. Pressure distribution comparison at r/R=0.73 and Ψ=270° for forward flight study case in which the objective was to match target C_p distributions.

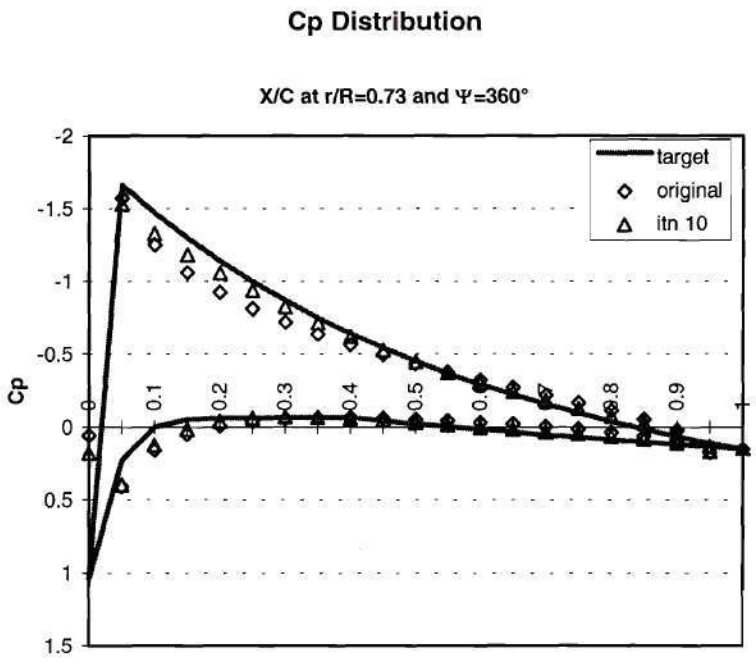

Figure 16. Pressure distribution comparison at r/R=0.73 and Ψ=360° for forward flight study case in which the objective was to match target C_p distributions.

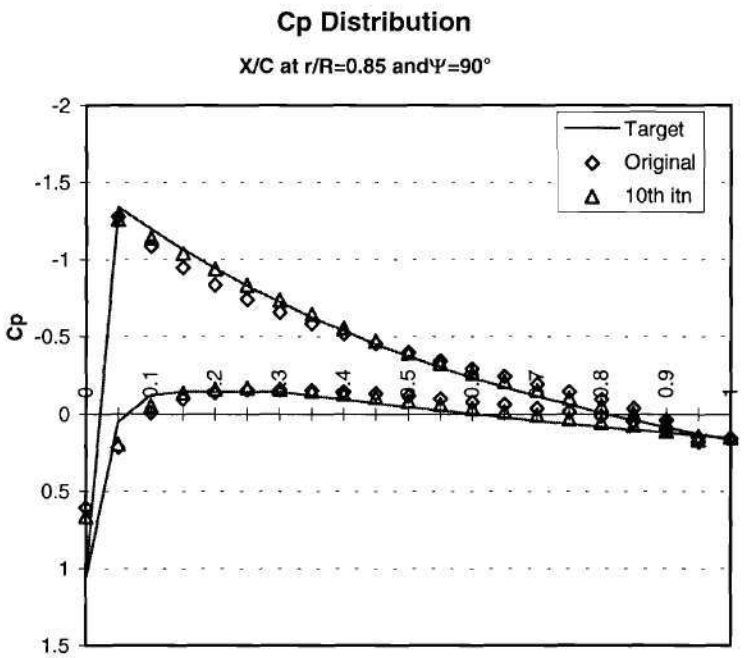

Figure 17. Pressure distribution comparison at r/R=0.85 and Ψ=90° for forward flight study case in which the objective was to match target C_p distributions.

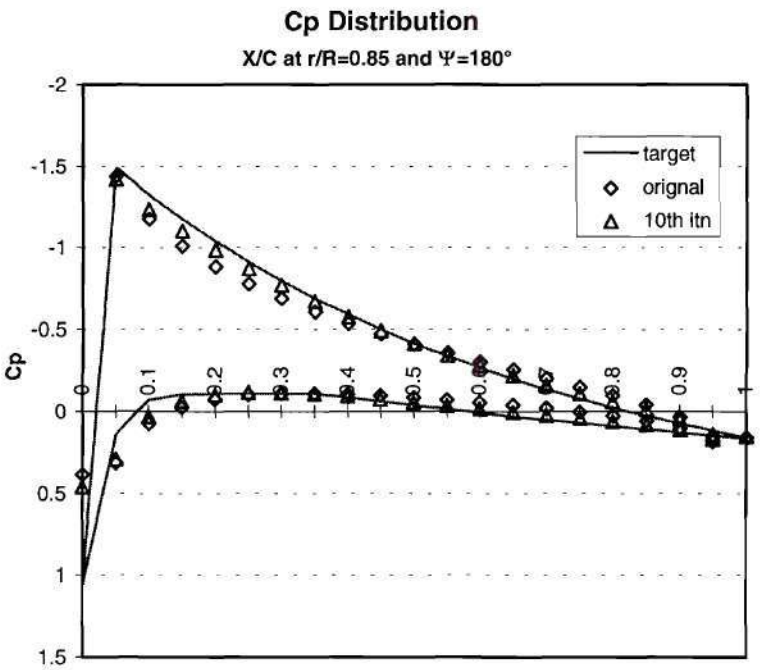

Figure 18. Pressure distribution comparison at r/R=0.85 and Ψ=180° for forward flight study case in which the objective was to match target C_p distributions.

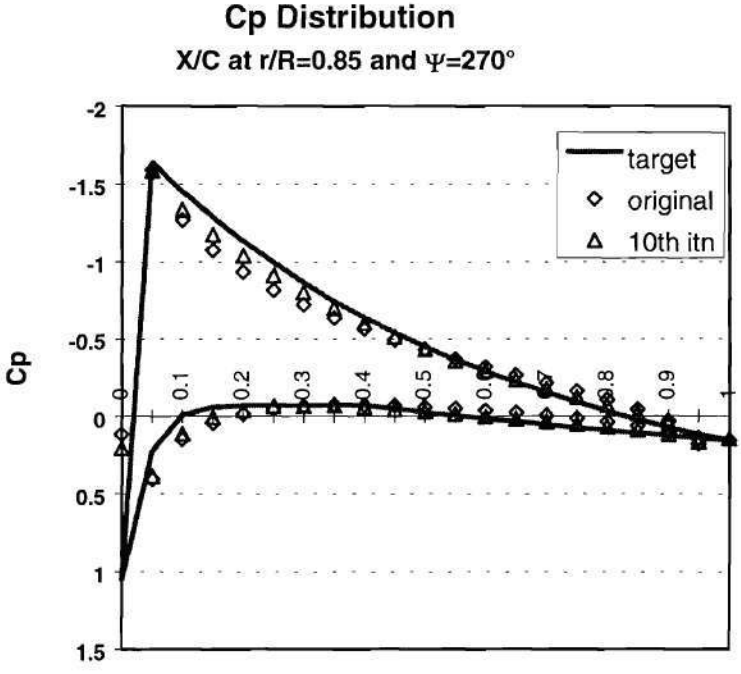

Figure 19. Pressure distribution comparison at r/R=0.85 and Ψ=270° for forward flight study case in which the objective was to match target C_p distributions.

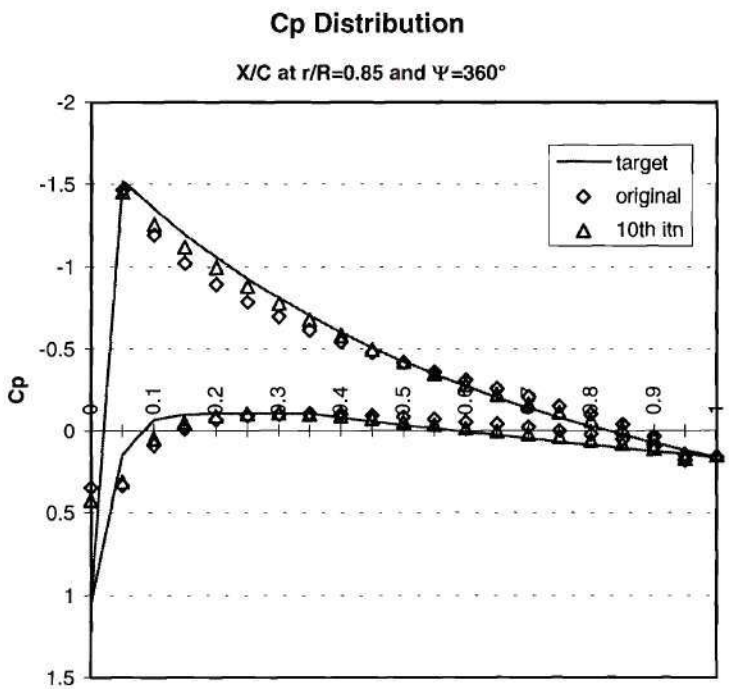

Figure 20. Pressure distribution comparison at r/R=0.85 and Ψ=360° for forward flight study case in which the objective was to match target C_p distributions.

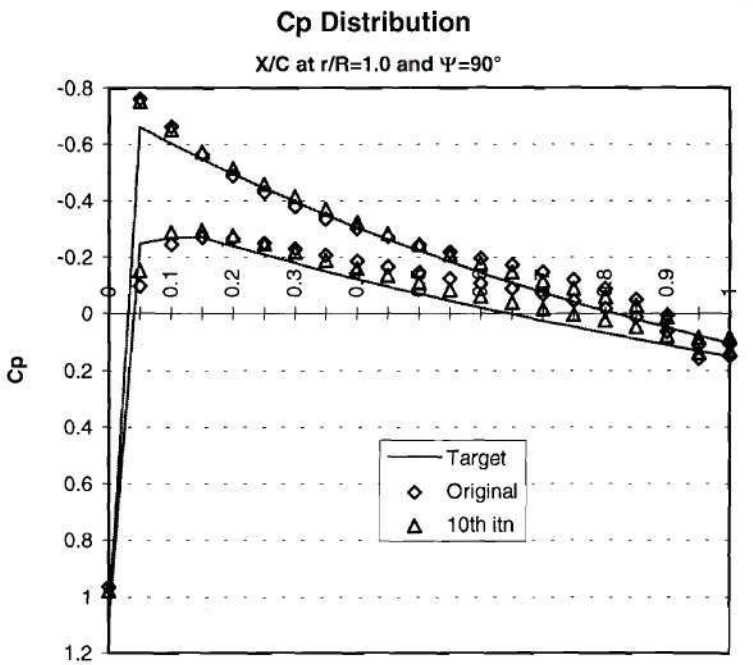

Figure 21. Pressure distribution comparison at r/R=1.0 and Ψ=90° for forward flight study case in which the objective was to match target C_p distributions.

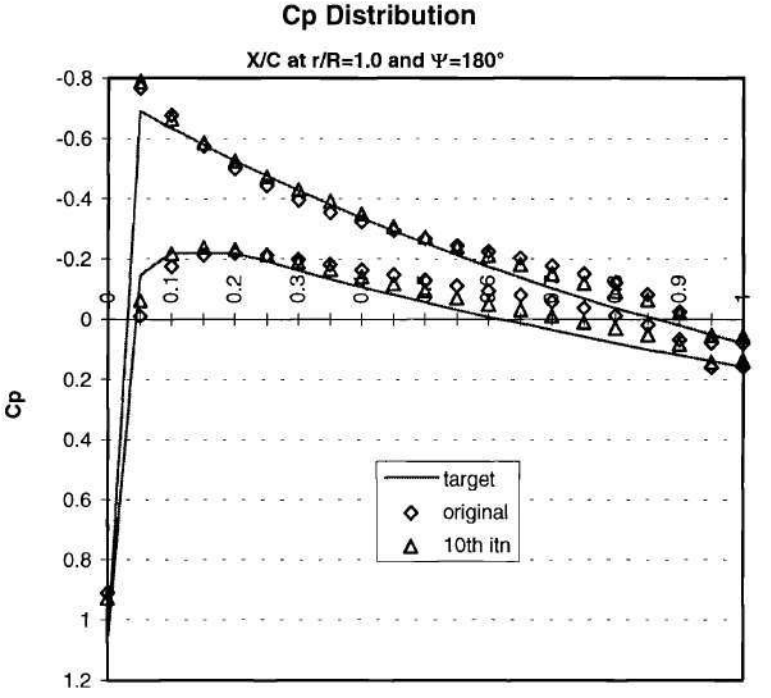

Figure 22. Pressure distribution comparison at r/R=1.0 and Ψ=180° for forward flight study case in which the objective was to match target C_p distributions.

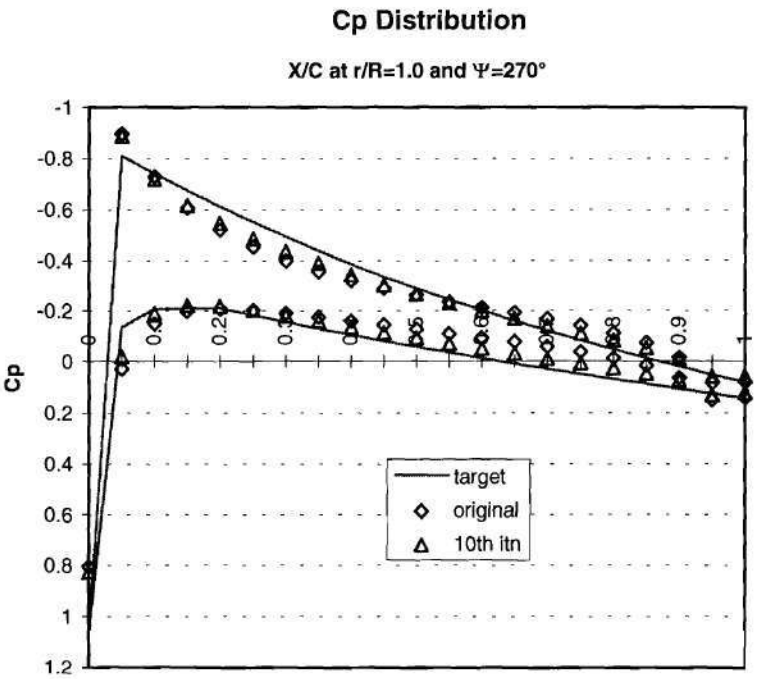

Figure 23. Pressure distribution comparison at r/R=1.0 and Ψ=270° for forward flight study case in which the objective was to match target C_p distributions.

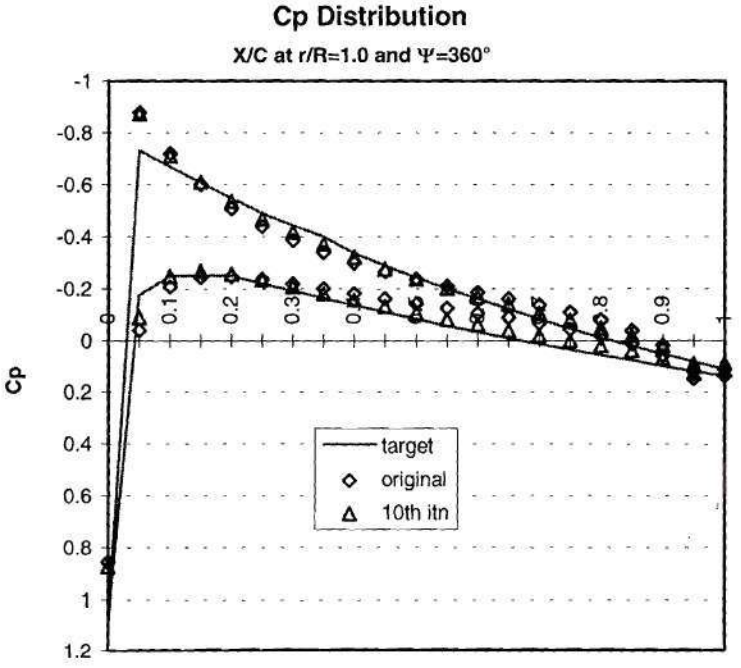

Figure 24. Pressure distribution comparison at r/R=1.0 and Ψ=360° for forward flight study case in which the objective was to match target C_p distributions.

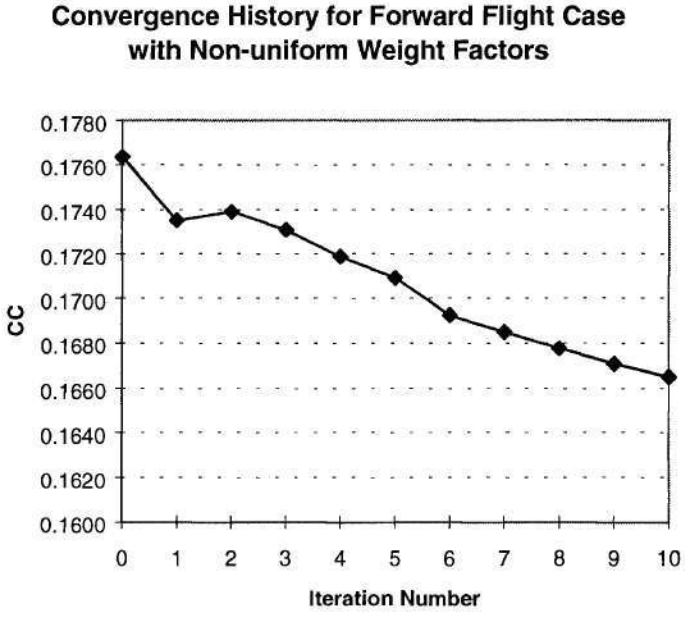

Figure 25. Convergence rate for forward flight case with non-uniform weight factors in which the objective is match target C_p distributions.

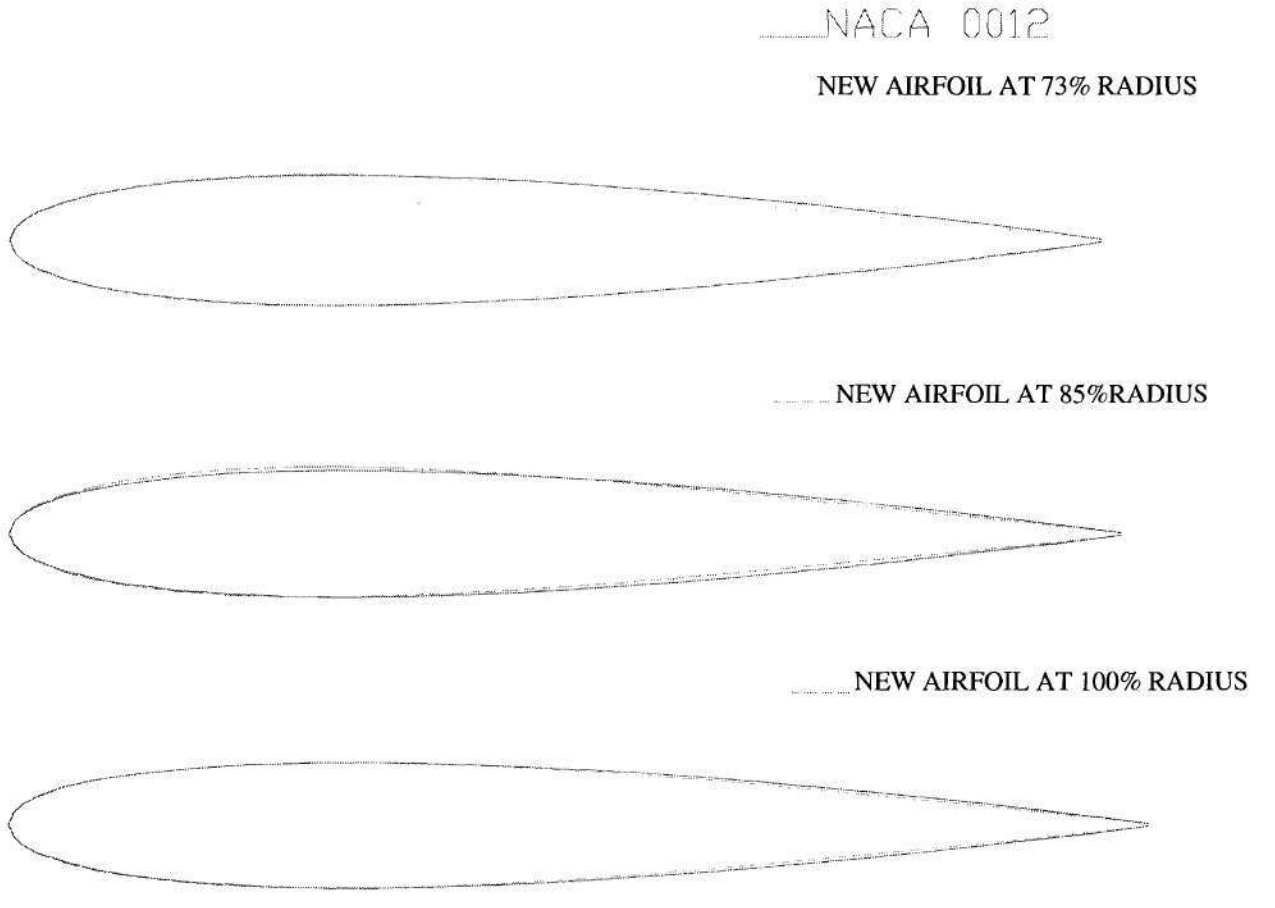

Figure 26. Airfoil Comparison for forward flight study case with non-uniform weight factors in which the objective is to match target C_p distributions.

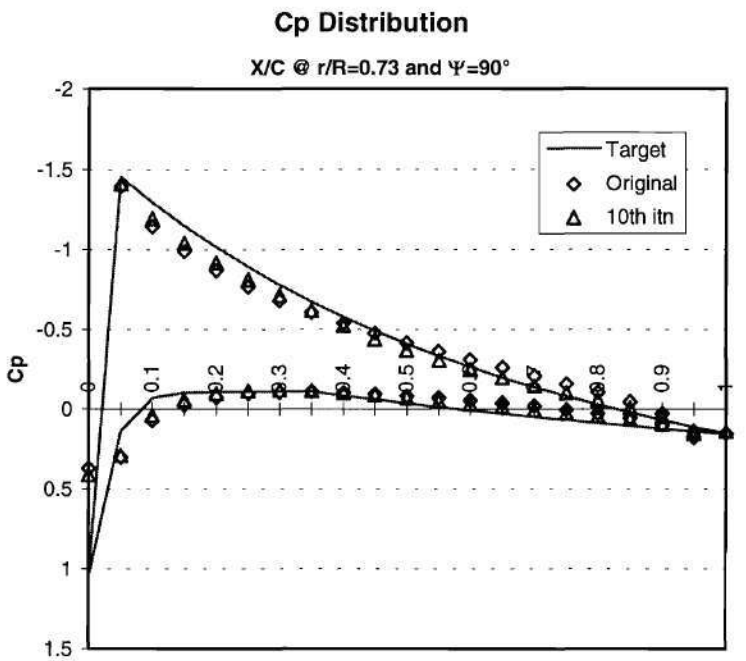

Figure 27. Pressure distribution comparison at r/R=0.73 and Ψ=90° for forward flight study case with non-uniform weight factors in which the objective was to match C_p distributions.

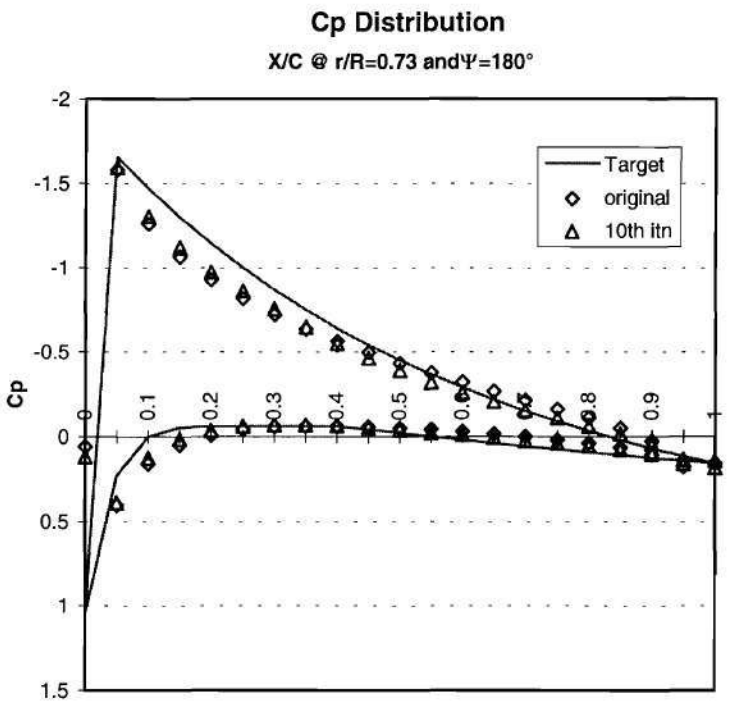

Figure 28. Pressure distribution comparison at r/R=0.73 and Ψ=180° for forward flight study case with non-uniform weight factors in which the objective was to match C_p distributions.

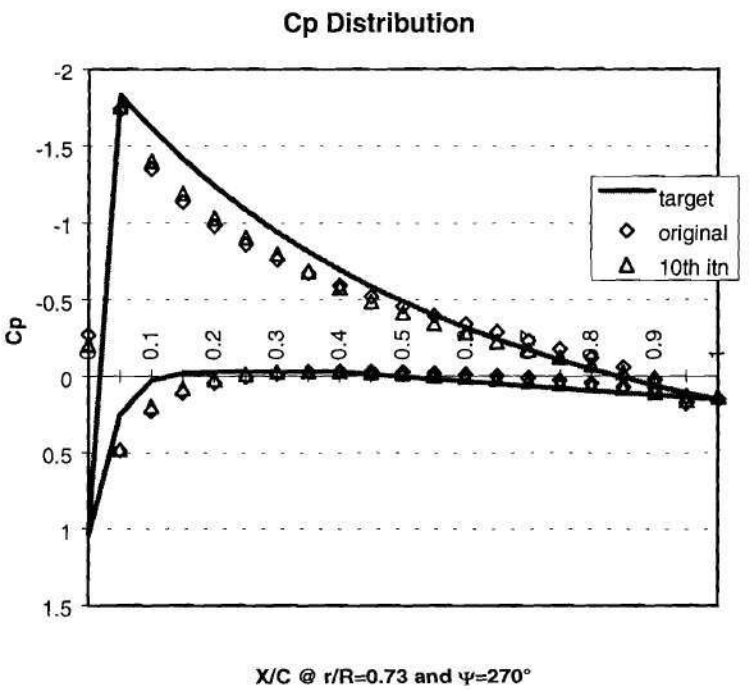

Figure 29. Pressure distribution comparison at r/R=0.73 and Ψ=270° for forward flight study case with non-uniform weight factors in which the objective was to match C_p distributions.

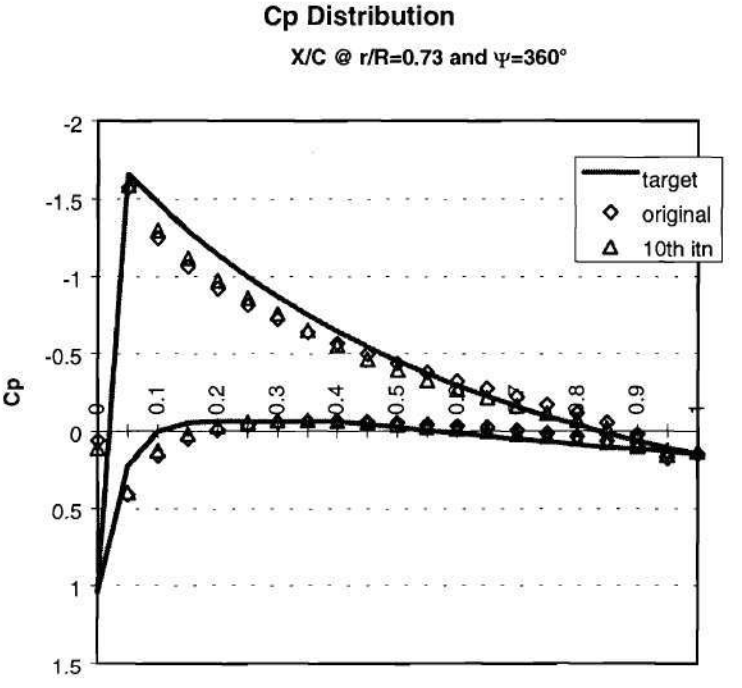

Figure 30. Pressure distribution comparison at r/R=0.73 and Ψ=360° for forward flight study case with non-uniform weight factors in which the objective was to match C_p distributions.

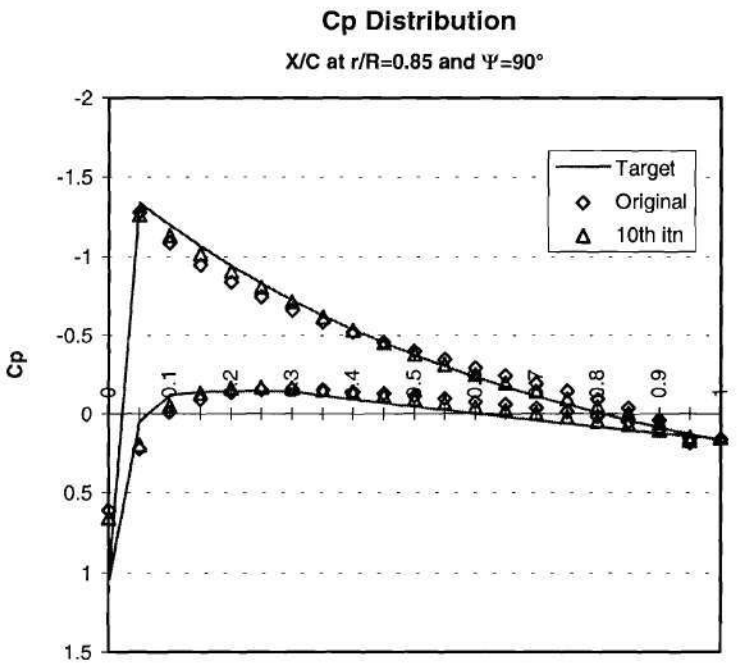

Figure 31. Pressure distribution comparison at r/R=0.85 and Y=90° for forward flight study case with non-uniform weight factors in which the objective was to match C_p distributions.

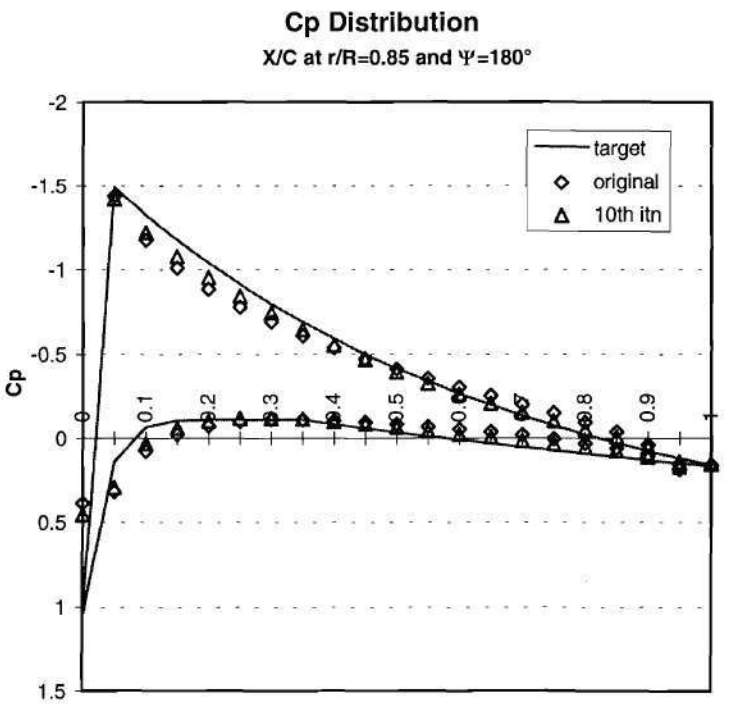

Figure 32. Pressure distribution comparison at r/R=0.85 and Y=180° for forward flight study case with non-uniform weight factors in which the objective was to match C_p distributions.

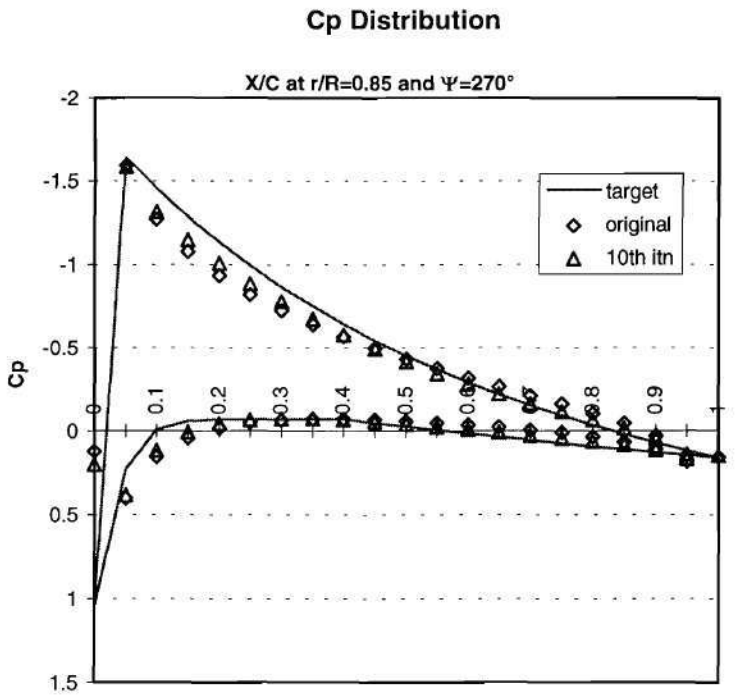

Figure 33. Pressure distribution comparison at r/R=0.85 and Y=270° for forward flight study case with non-uniform weight factors in which the objective was to match C_p distributions.

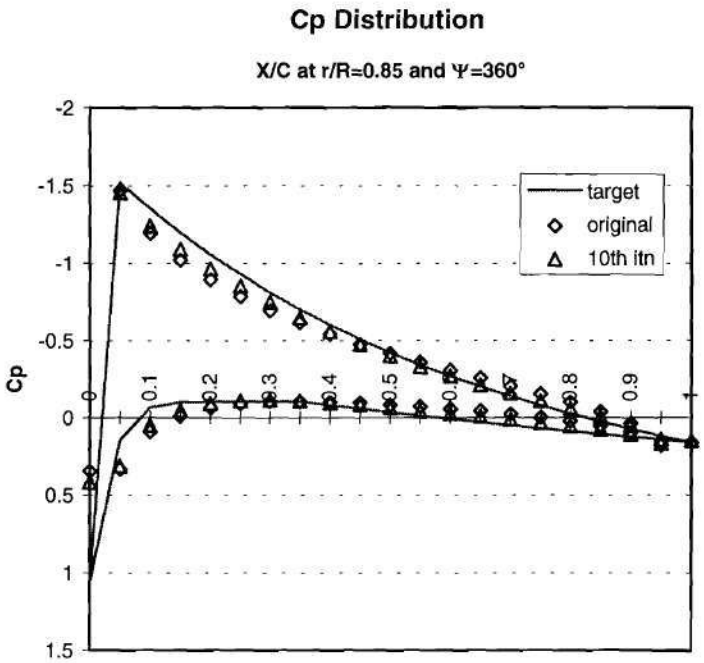

Figure 34. Pressure distribution comparison at r/R=0.85 and Y=360° for forward flight study case with non-uniform weight factors in which the objective was to match C_p distributions.

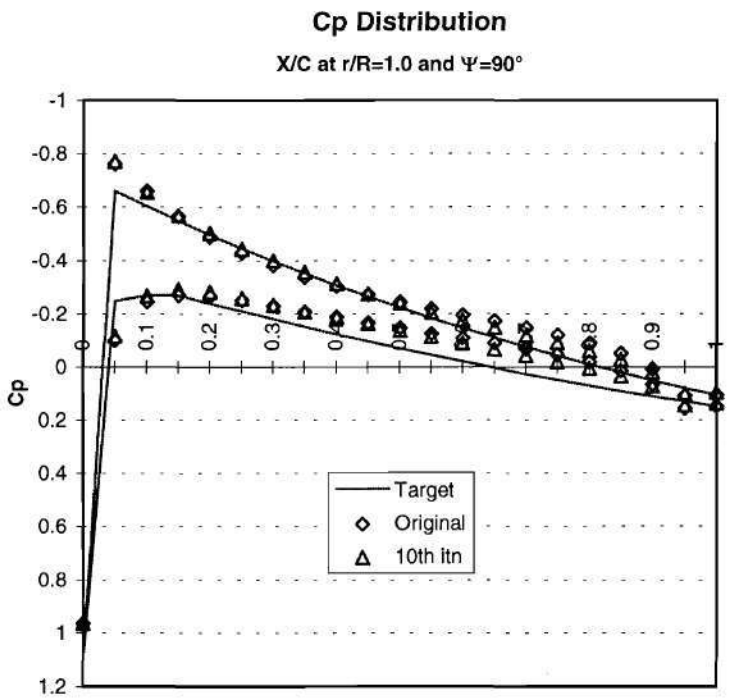

Figure 35. Pressure distribution comparison at r/R=1.0 and Y=90° for forward flight study case with non-uniform weight factors in which the objective was to match C_p distributions.

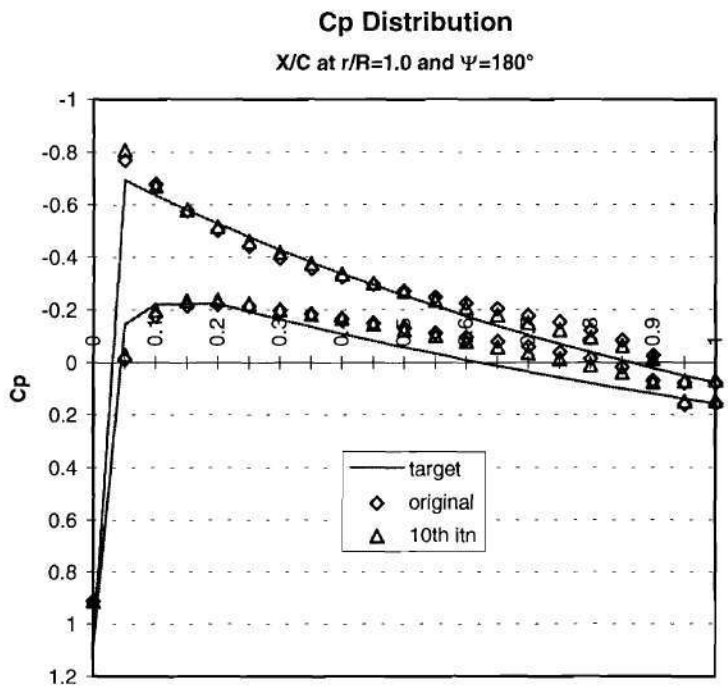

Figure 36. Pressure distribution comparison at r/R=1.0 and Y=180° for forward flight study case with non-uniform weight factors in which the objective was to match C_p distributions.

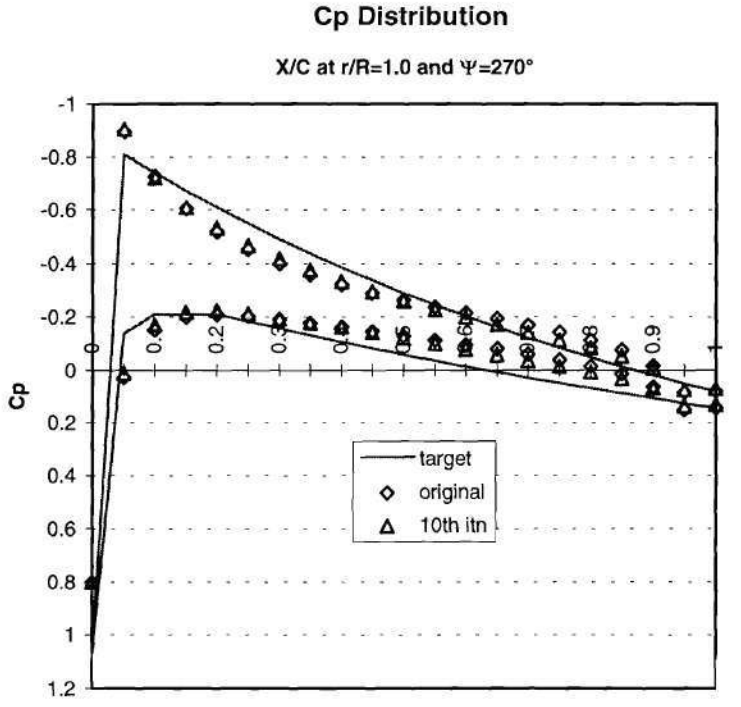

Figure 37. Pressure distribution comparison at r/R=1.0 and Y=270° for forward flight study case with non-uniform weight factors in which the objective was to match C_p distributions.

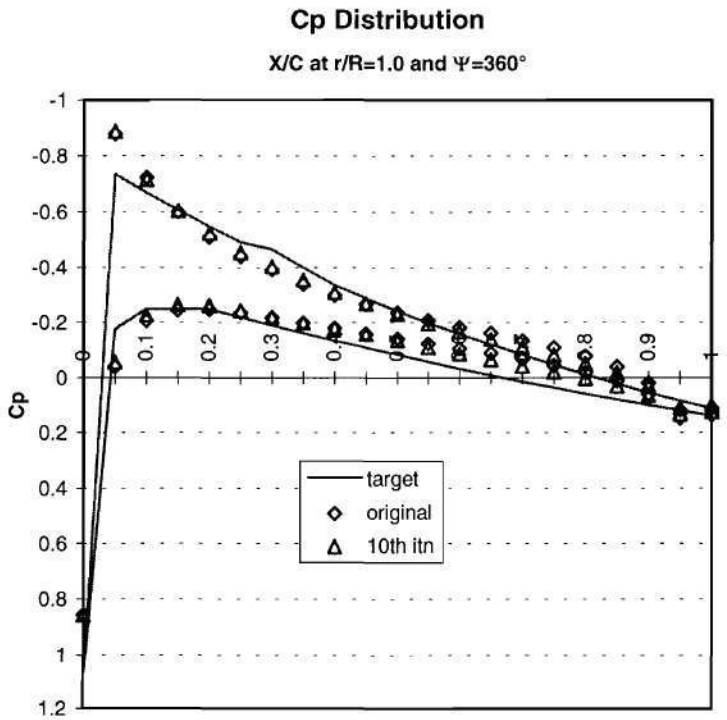

Figure 38. Pressure distribution comparison at r/R=1.0 and Y=360° for forward flight study case with non-uniform weight factors in which the objective was to match C_p distributions.

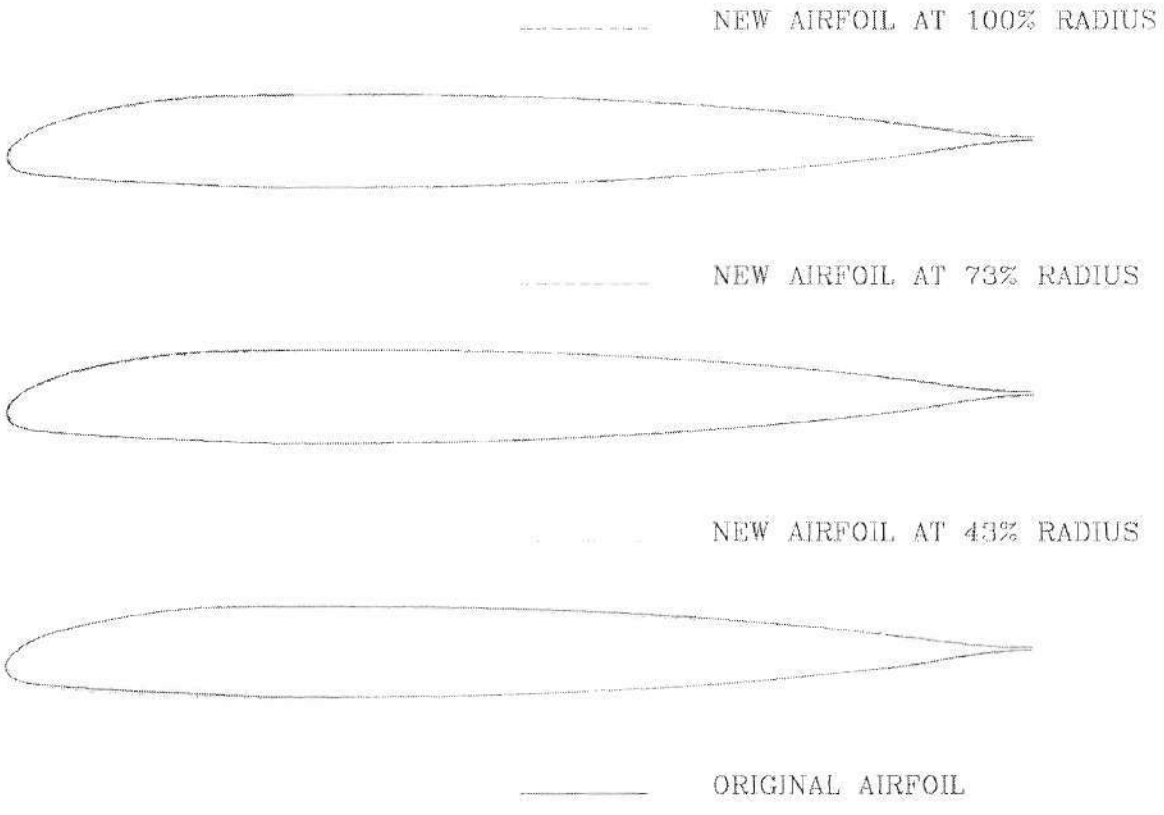

Figure 39. Airfoil Comparison for gazelle study at high speed flight.

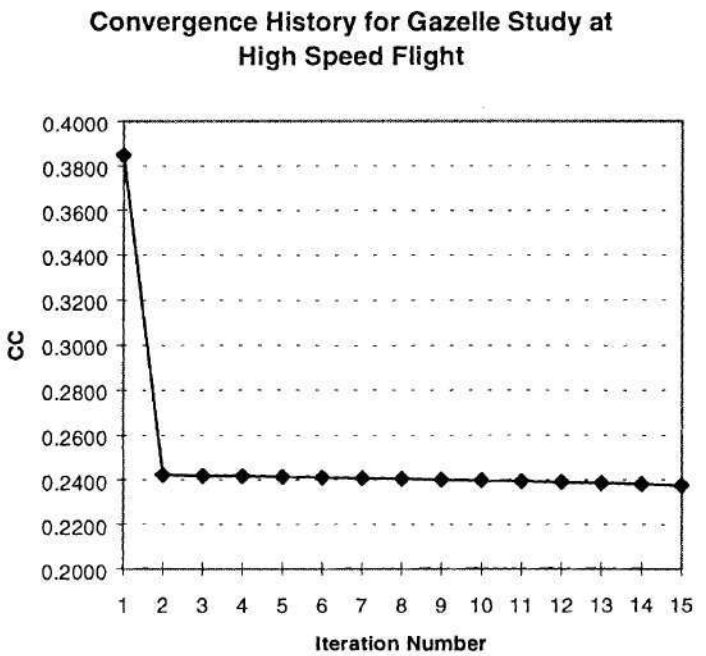

Figure 40. Convergence rate for gazelle study at high speed flight.

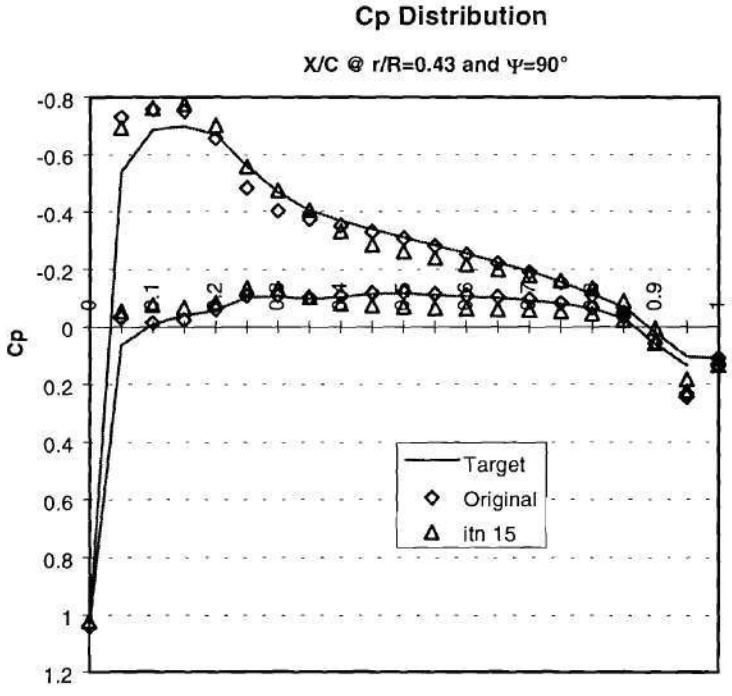

Figure 41. Pressure distribution comparison at r/R=0.43 and Ψ=90° for gazelle study in high speed flight.

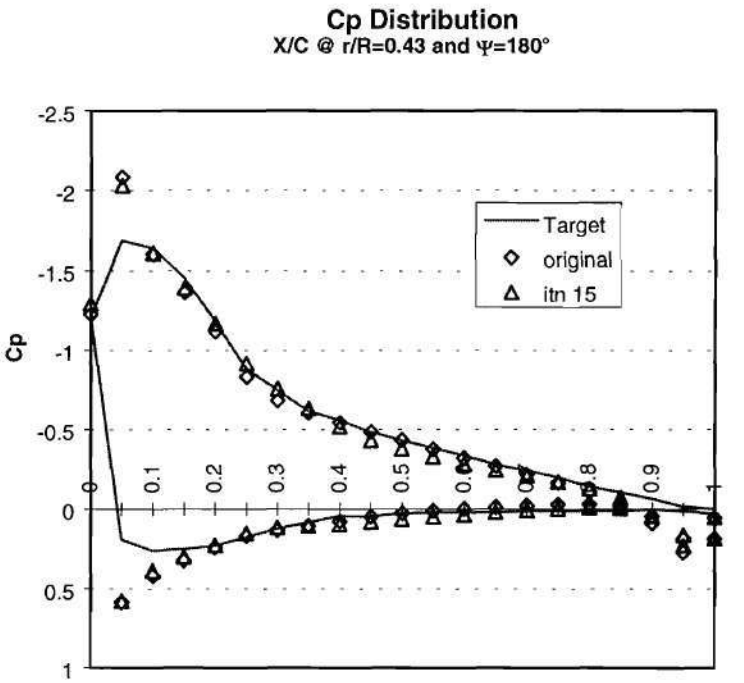

Figure 42. Pressure distribution comparison at r/R=0.43 and Ψ=180° for gazelle study in high speed flight.

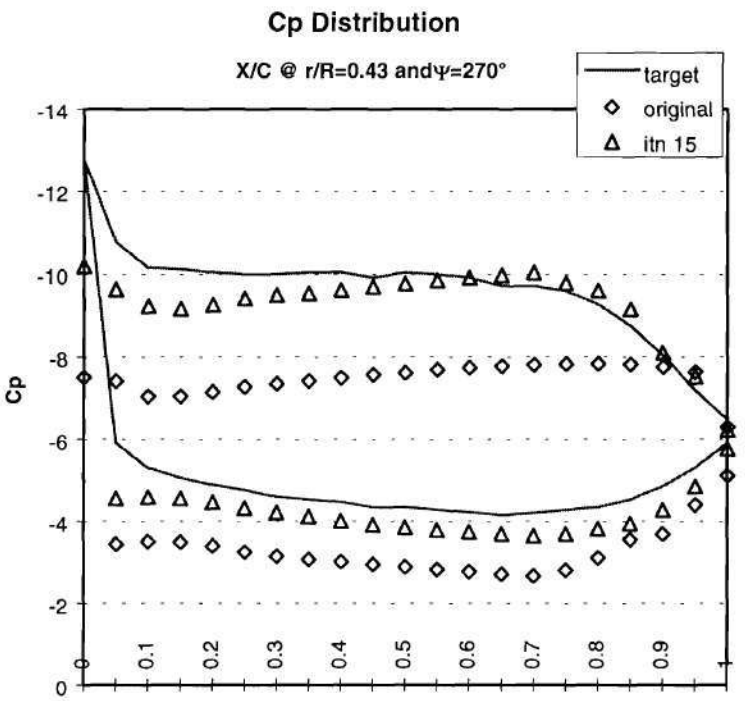

Figure 43. Pressure distribution comparison at r/R=0.43 and Ψ=270° for gazelle study in high speed flight.

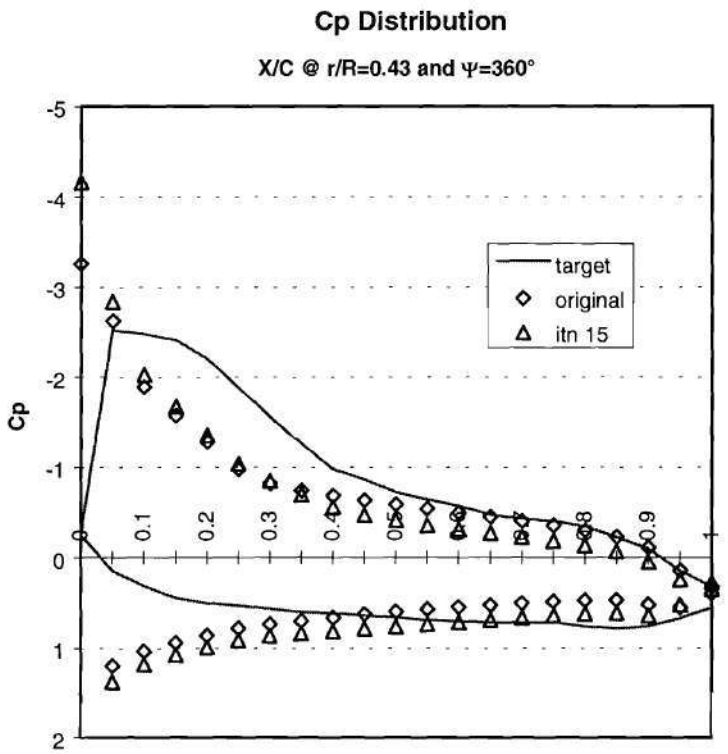

Figure 44. Pressure distribution comparison at r/R=0.43 and Ψ=360° for gazelle study in high speed flight.

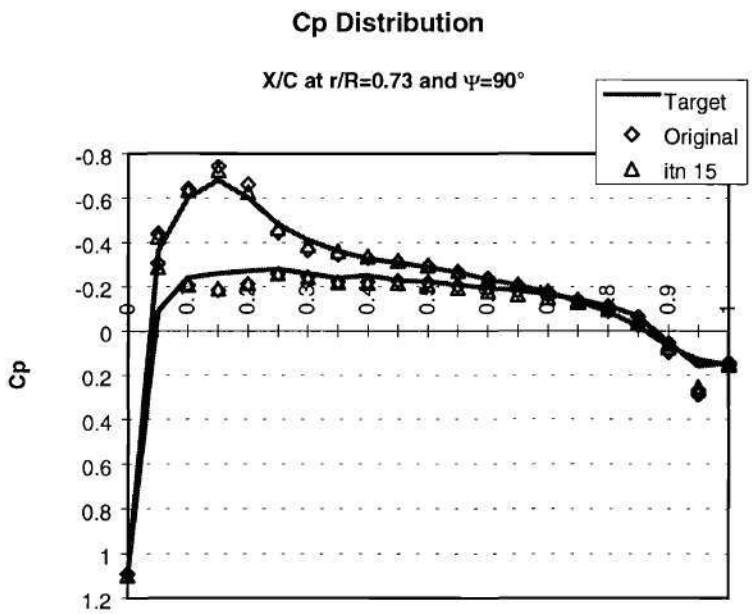

Figure 45. Pressure distribution comparison at r/R=0.73 and Ψ=90° for gazelle study in high speed flight.

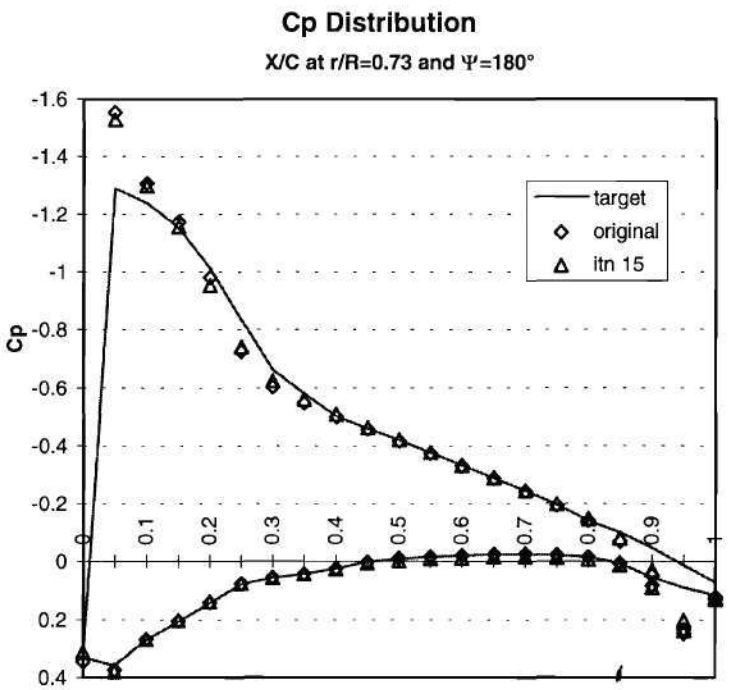

Figure 46. Pressure distribution comparison at r/R=0.73 and Ψ=180° for gazelle study in high speed flight.

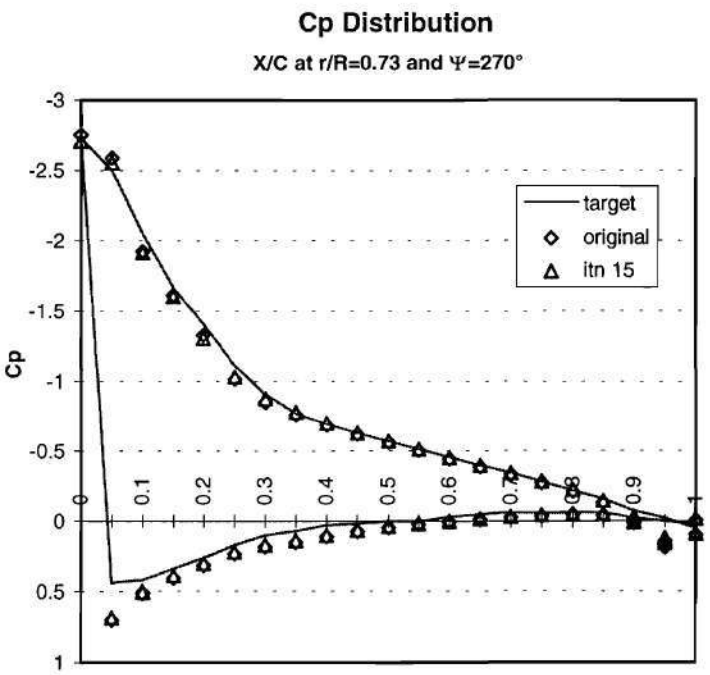

Figure 47. Pressure distribution comparison at r/R=0.73 and Ψ=270° for gazelle study in high speed flight.

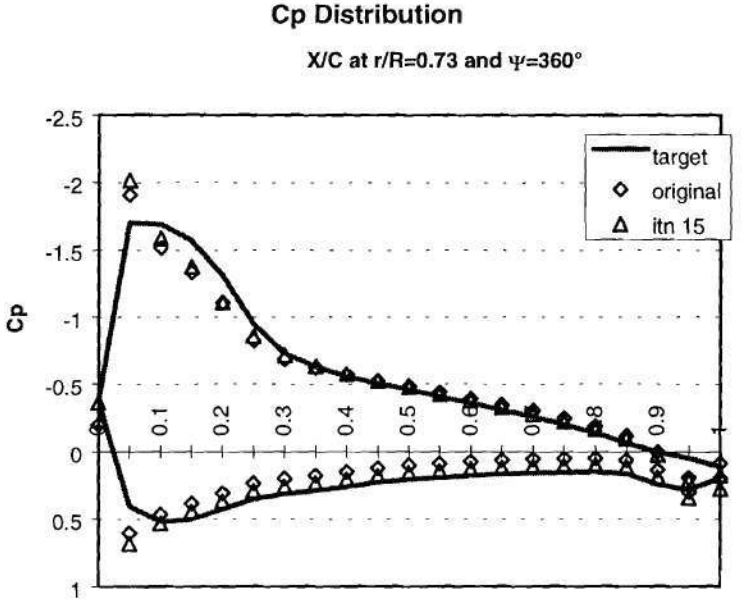

Figure 48. Pressure distribution comparison at r/R=0.73 and Ψ=360° for gazelle study in high speed flight.

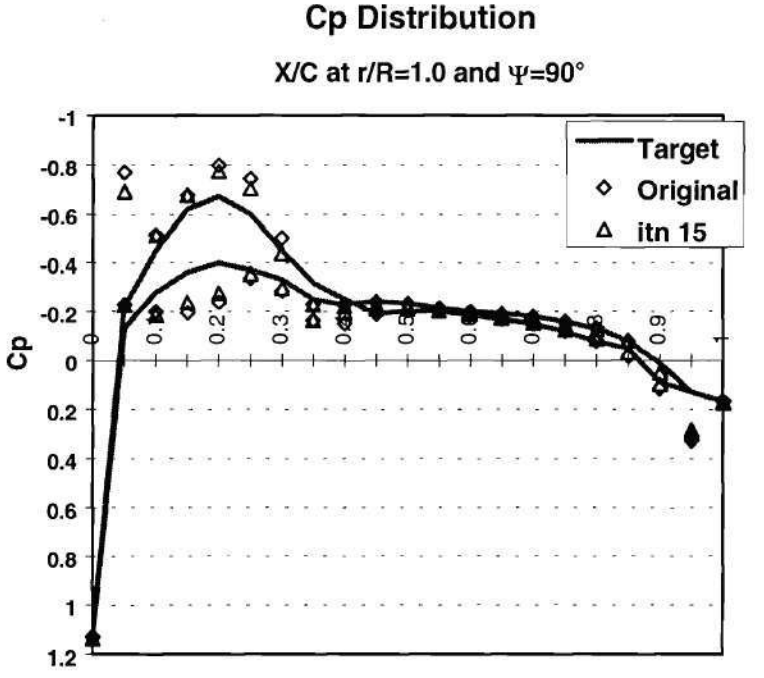

Figure 49. Pressure distribution comparison at r/R=1.0 and Ψ=90° for gazelle study in high speed flight.

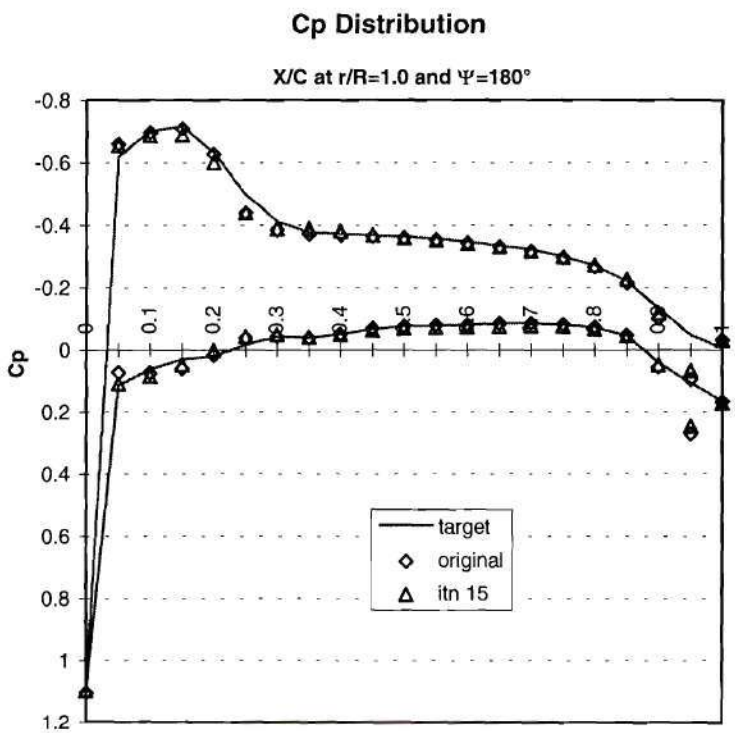

Figure 50. Pressure distribution comparison at r/R=1.0 and Ψ=180° for gazelle study in high speed flight.

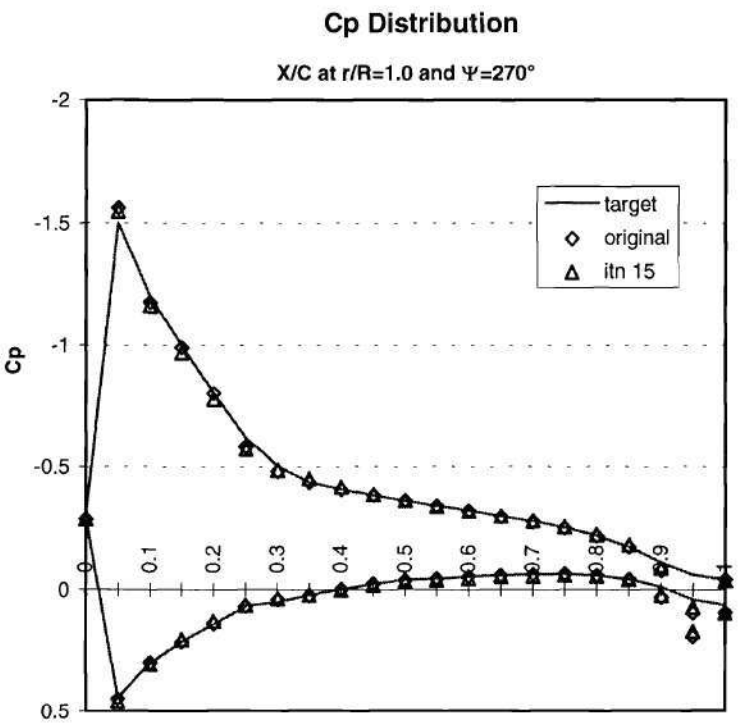

Figure 51. Pressure distribution comparison at r/R=1.0 and Ψ=270° for gazelle study in high speed flight.

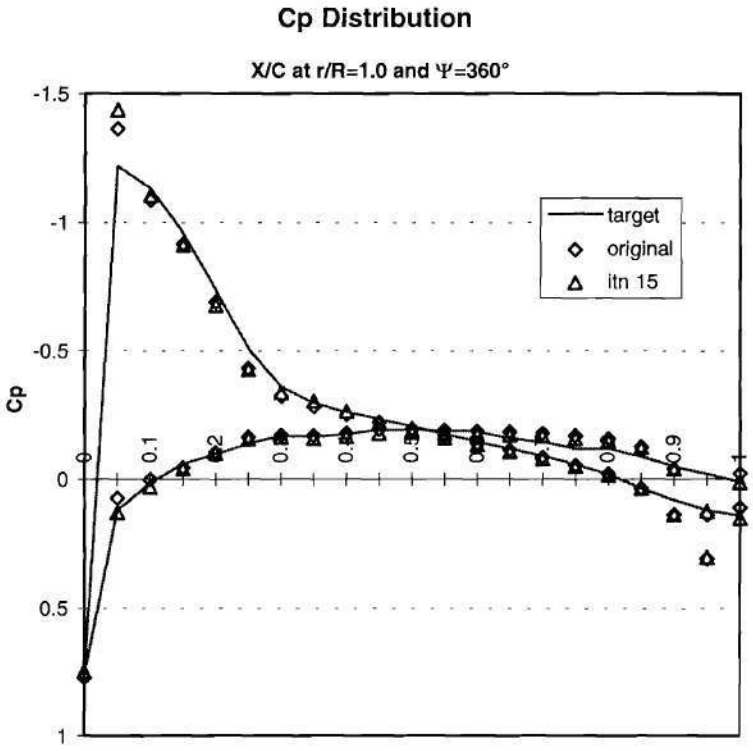

Figure 52. Pressure distribution comparison at r/R=1.0 and Ψ=360° for gazelle study in high speed flight.

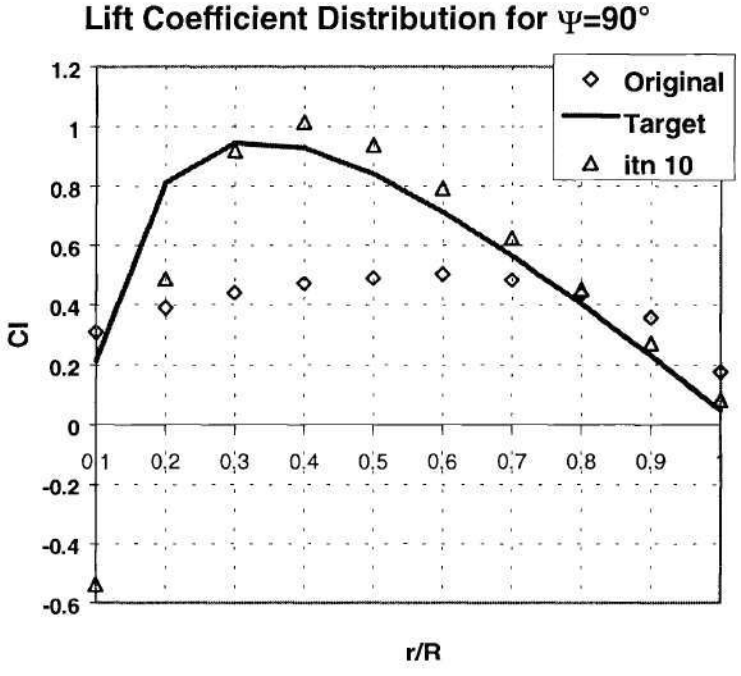

Figure 53. Lift coefficient distribution for Ψ=90° for induced torque reduction study case.

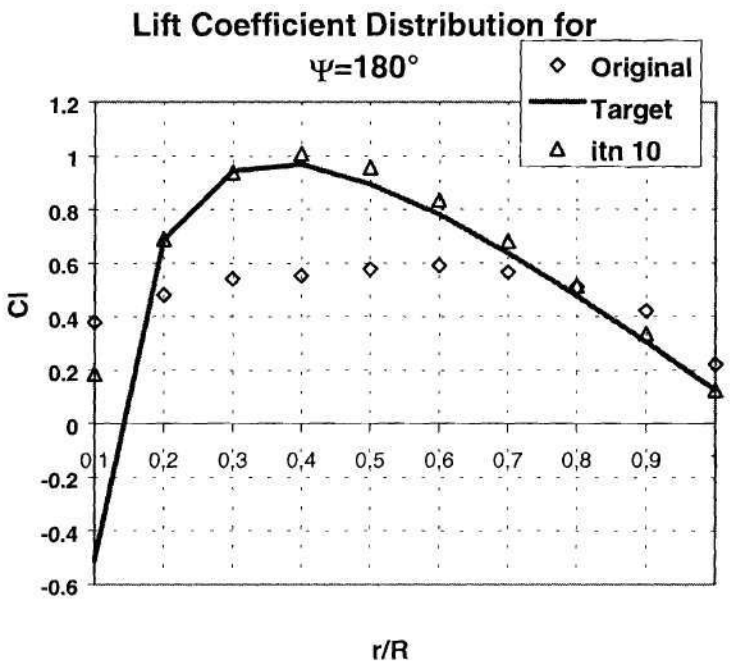

Figure 54. Lift coefficient distribution for Ψ=90° for induced torque reduction study case.

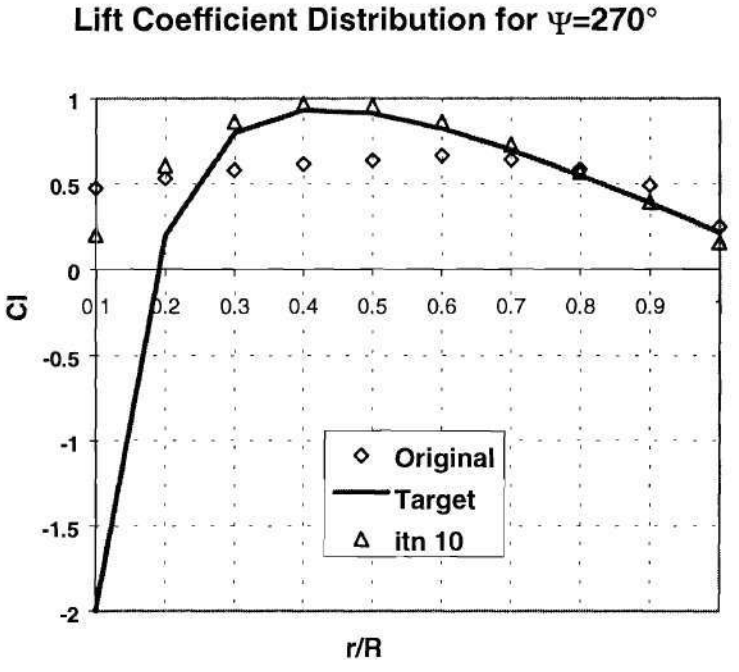

Figure 55. Lift coefficient distribution for Ψ=270° for induced torque reduction study case.

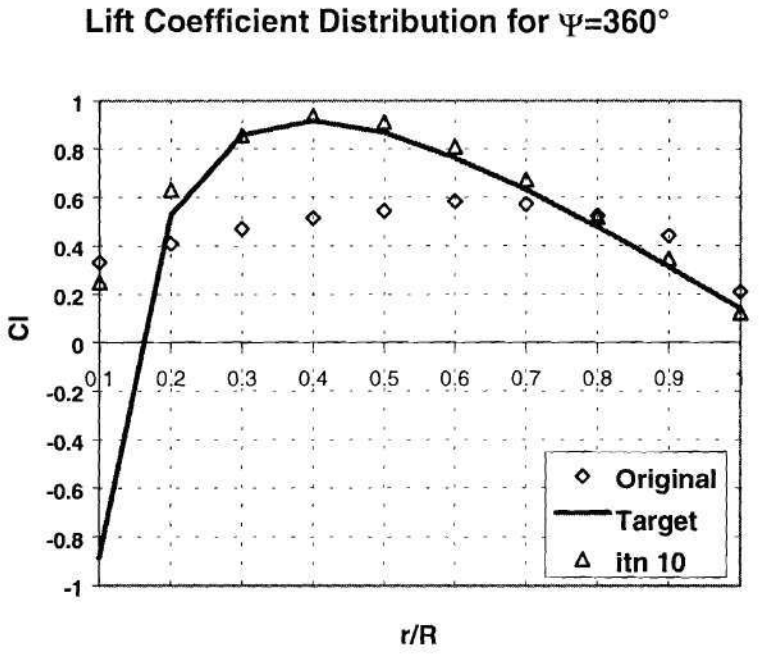

Figure 56. Lift coefficient distribution for Ψ=360° for induced torque reduction study case.

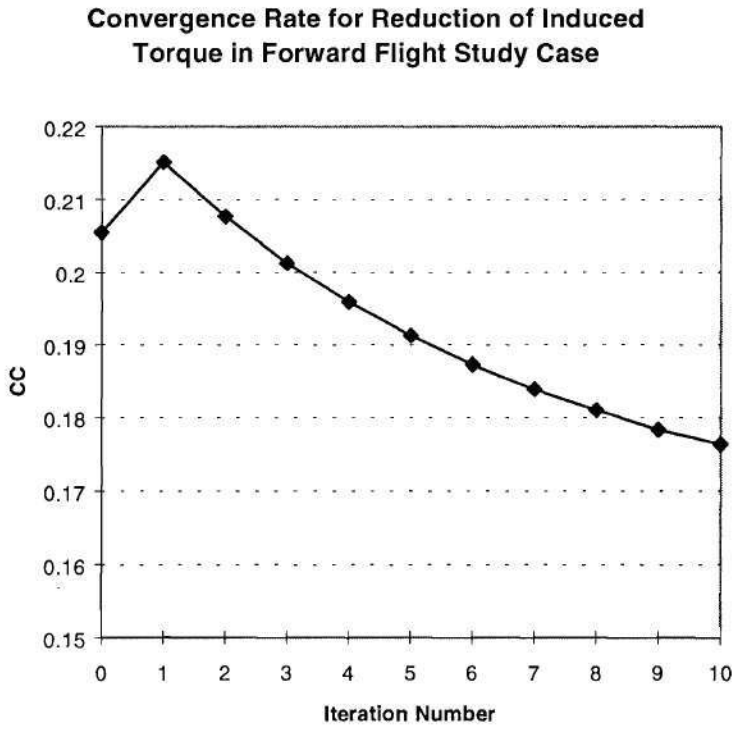

Figure 57. Convergence rate for induced torque reduction in forward flight study case.

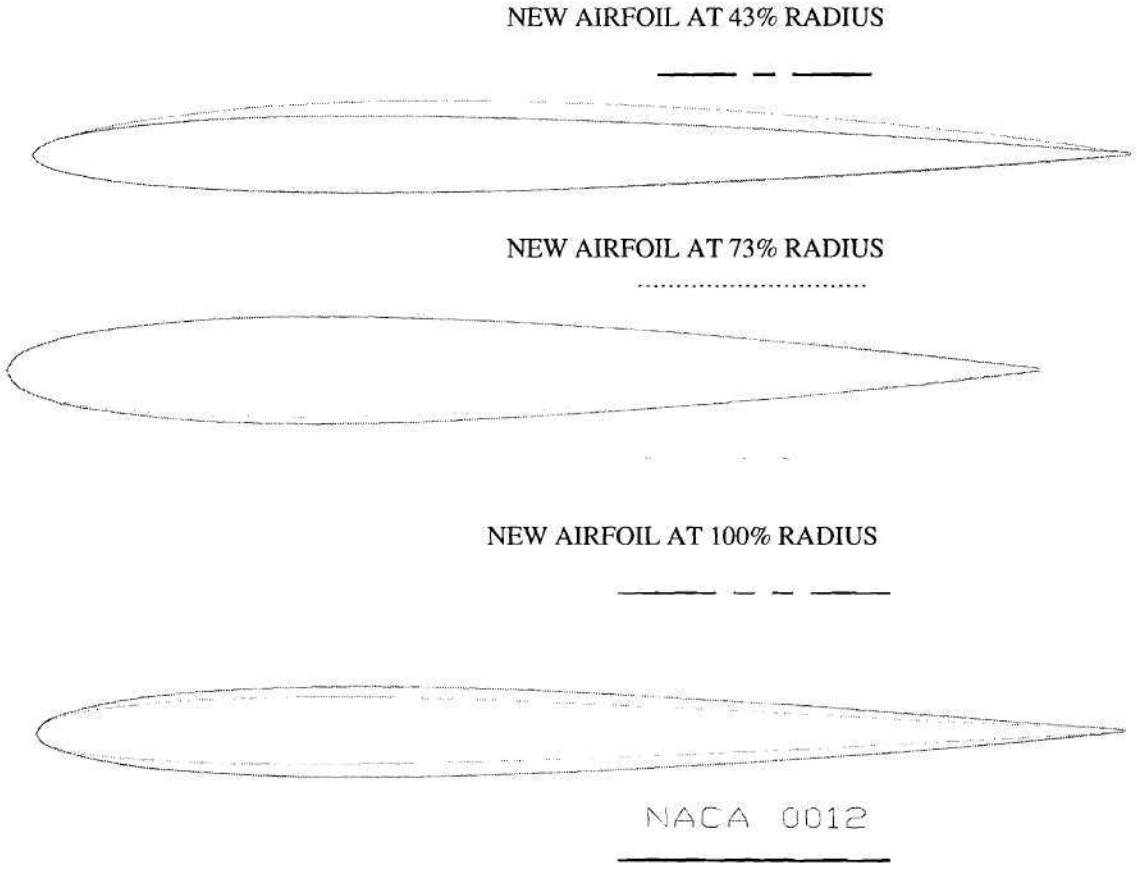

Figure 58. Airfoil comparison for induced torque reduction in forward flight study case.

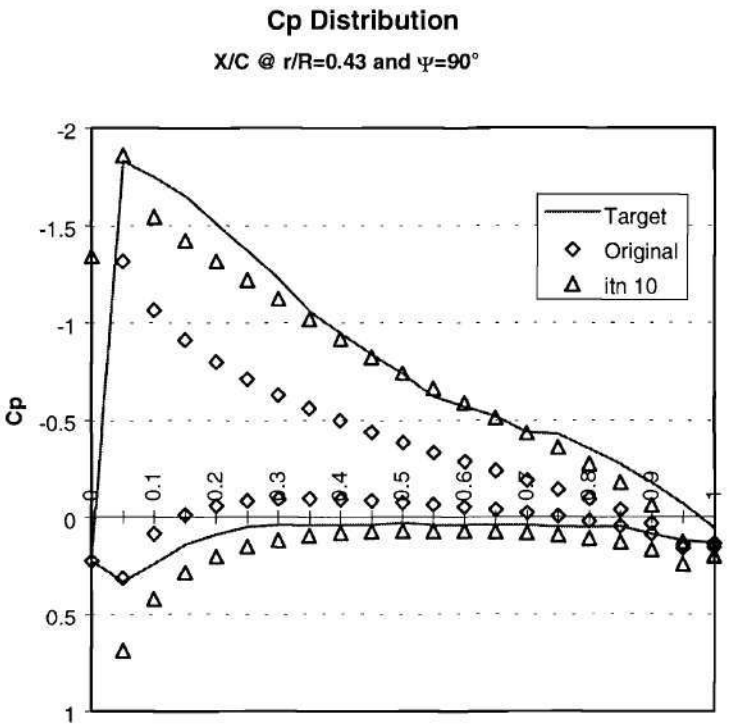

Figure 59. Pressure distribution comparison at r/R=0.43 and Ψ=90° for induced torque reduction in forward flight study case.

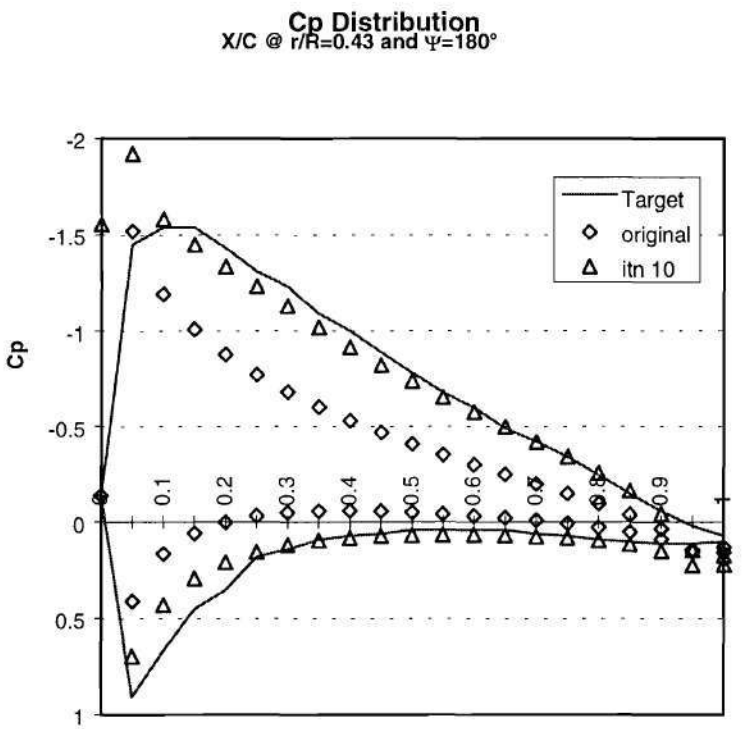

Figure 60. Pressure distribution comparison at r/R=0.43 and Ψ=180° for induced torque reduction in forward flight study case.

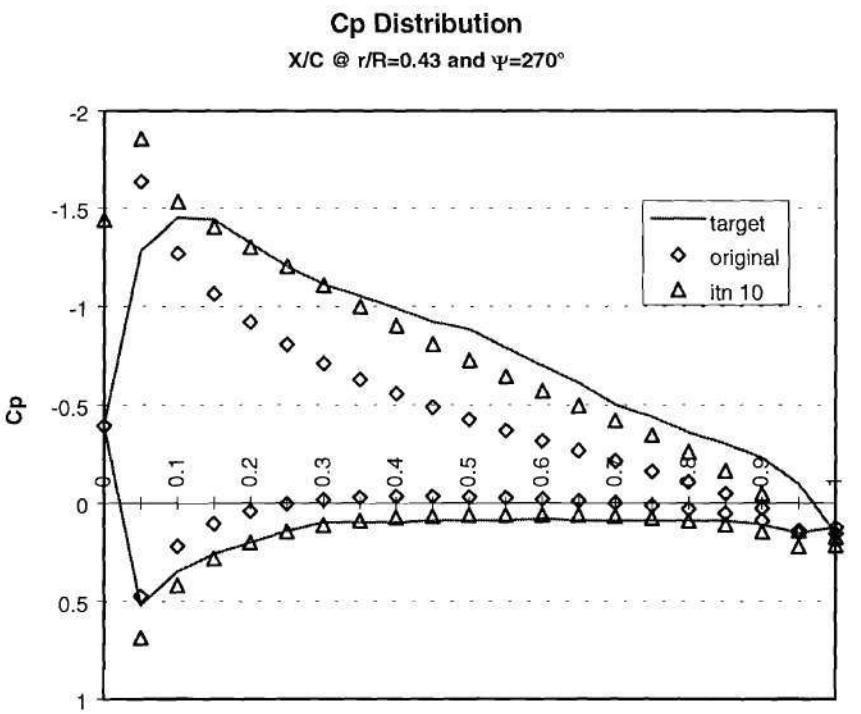

Figure 61. Pressure distribution comparison at r/R=0.43 and Ψ=270° for induced torque reduction in forward flight study case.

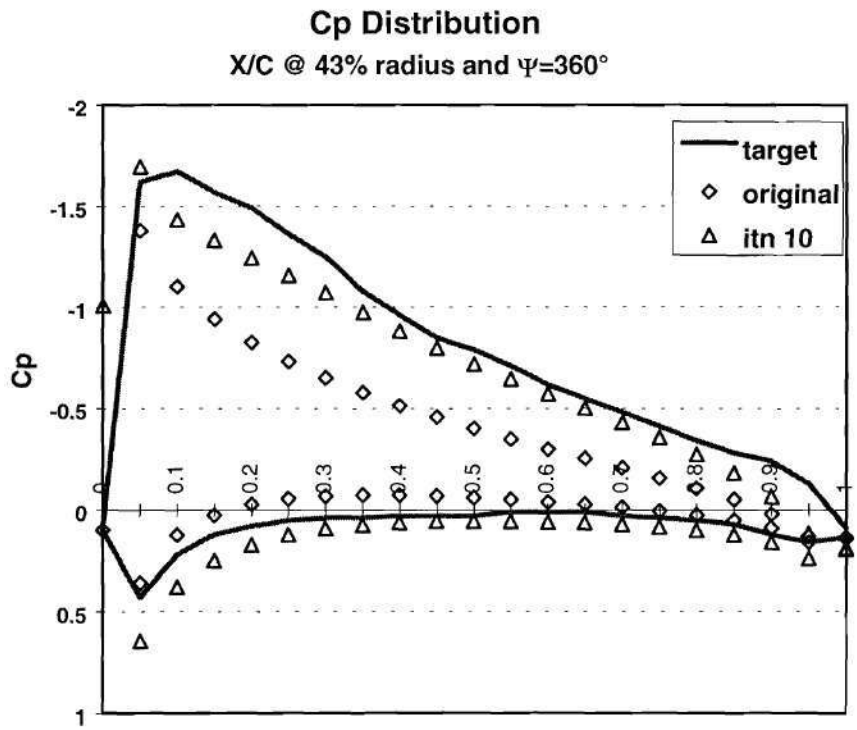

Figure 62. Pressure distribution comparison at r/R=0.43 and Ψ=360° for induced torque reduction in forward flight study case.

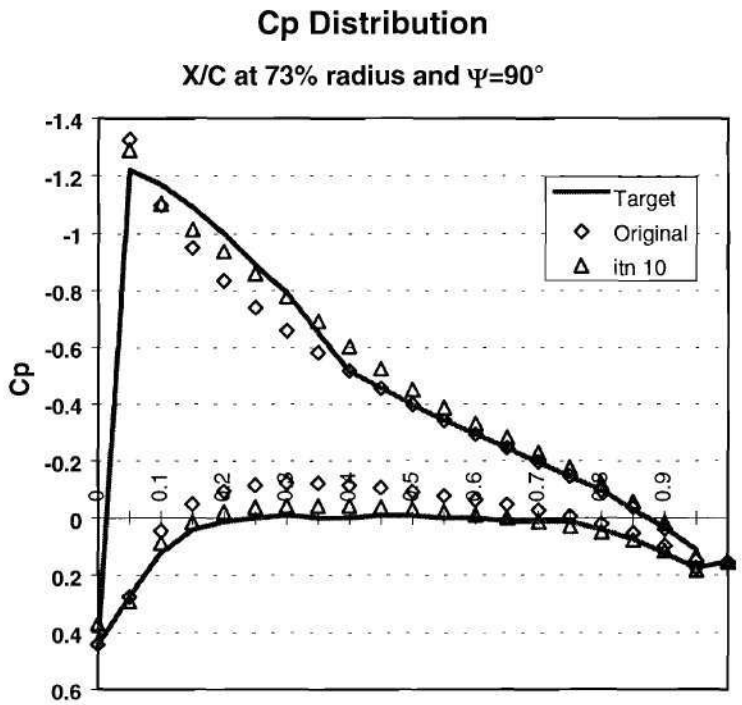

Figure 63. Pressure distribution comparison at r/R=0.73 and Ψ=90° for induced torque reduction in forward flight study case.

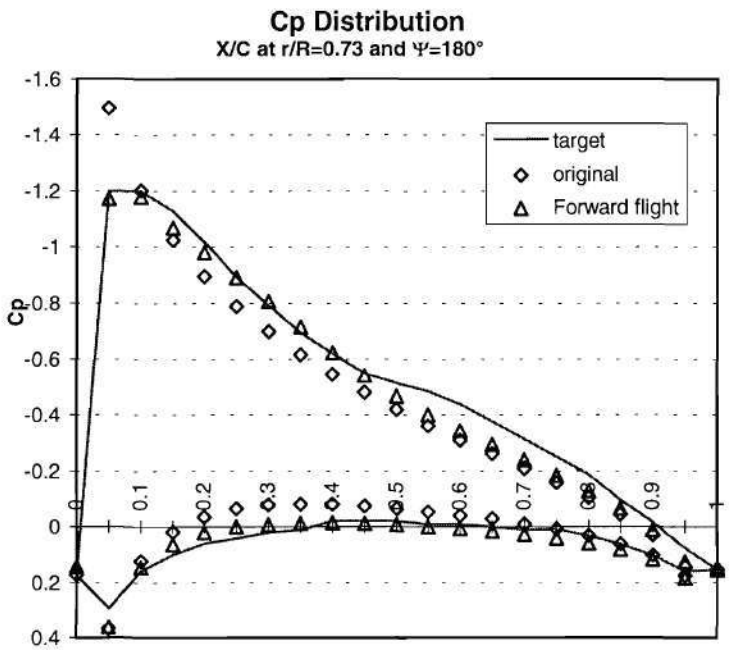

Figure 64. Pressure distribution comparison at r/R=0.73 and Ψ=180° for induced torque reduction in forward flight study case.

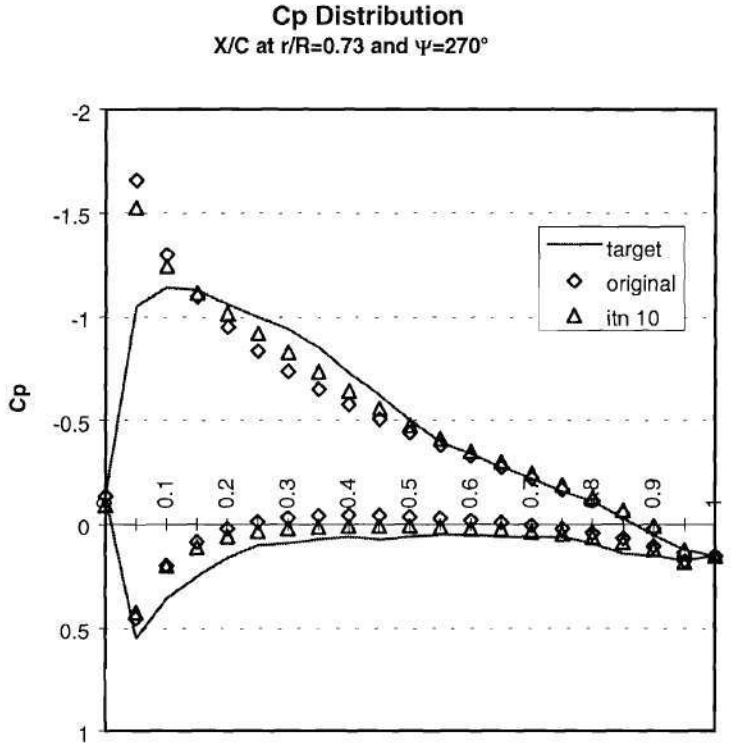

Figure 65. Pressure distribution comparison at r/R=0.73 and Ψ=270° for induced torque reduction in forward flight study case.

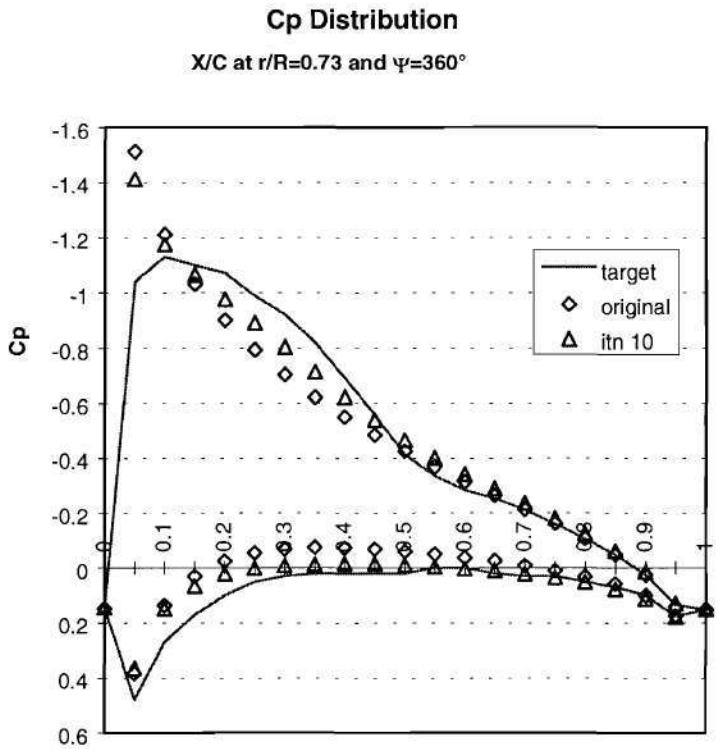

Figure 66. Pressure distribution comparison at r/R=0.73 and Ψ=360° for induced torque reduction in forward flight study case.

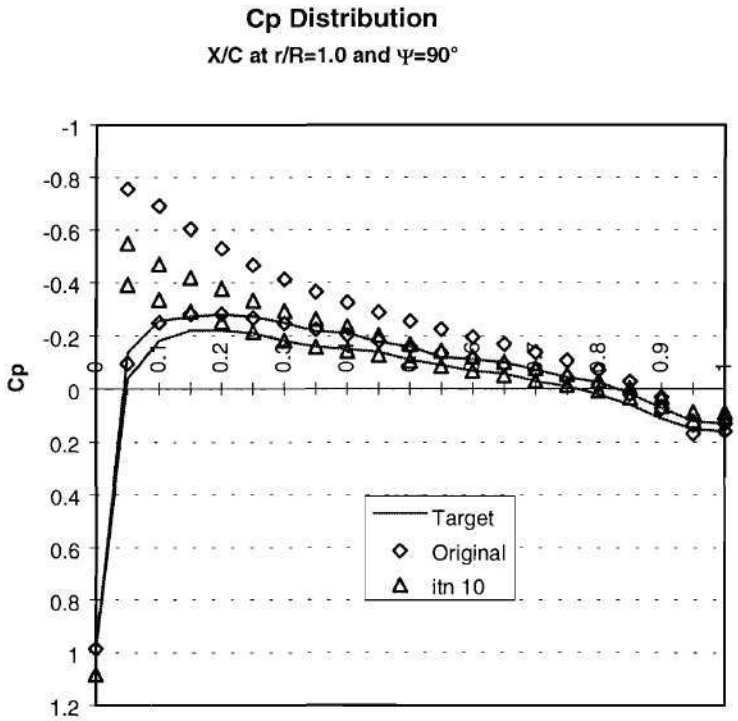

Figure 67. Pressure distribution comparison at r/R=1.0 and Ψ=90° for induced torque reduction in forward flight study case.

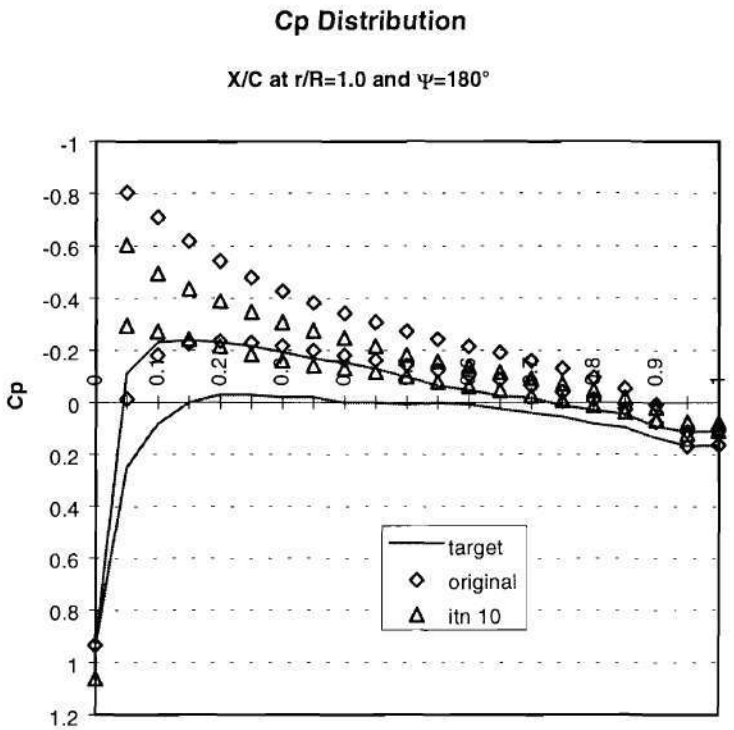

Figure 68. Pressure distribution comparison at r/R=1.0 and Ψ=180° for induced torque reduction in forward flight study case.

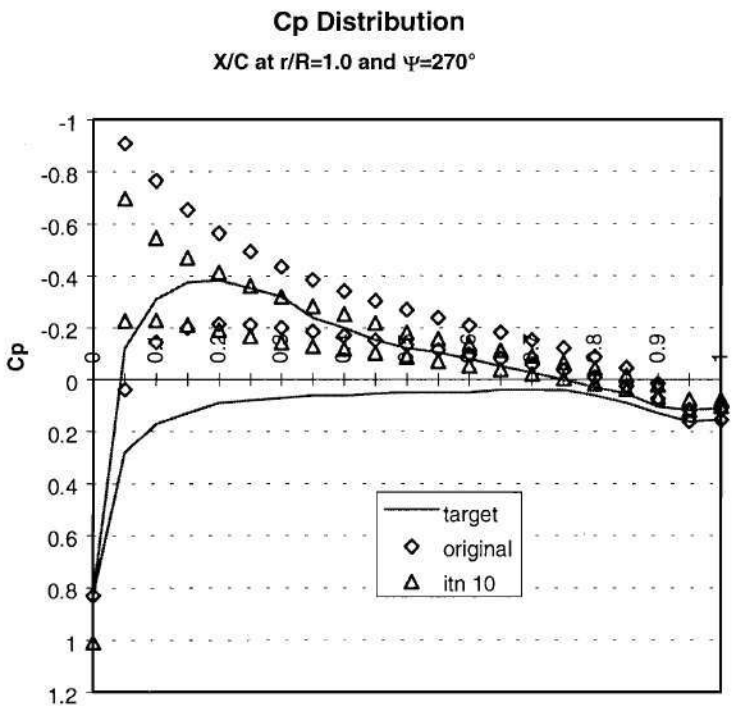

Figure 69. Pressure distribution comparison at r/R=1.0 and Ψ=270° for induced torque reduction in forward flight study case.

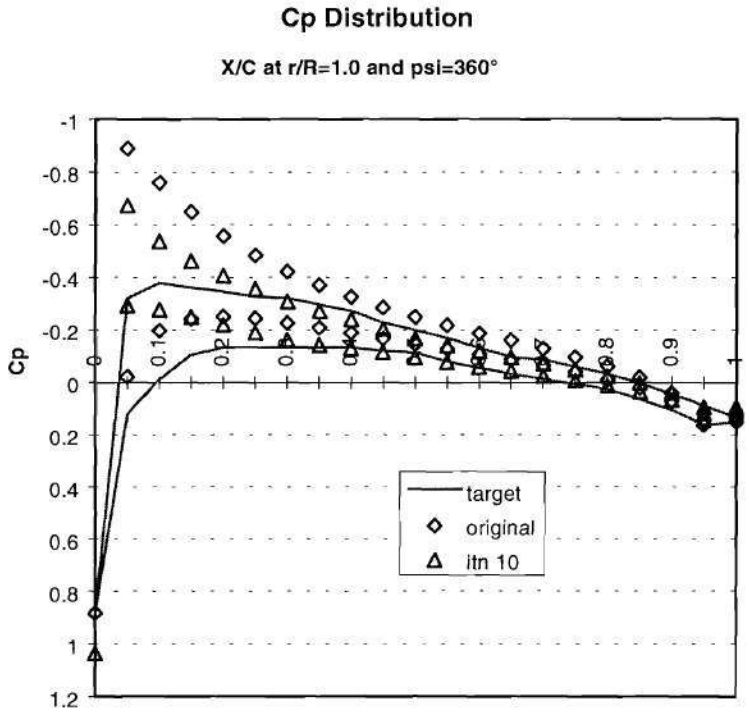

Figure 70. Pressure distribution comparison at r/R=1.0 and Ψ=360° for induced torque reduction in forward flight study case.

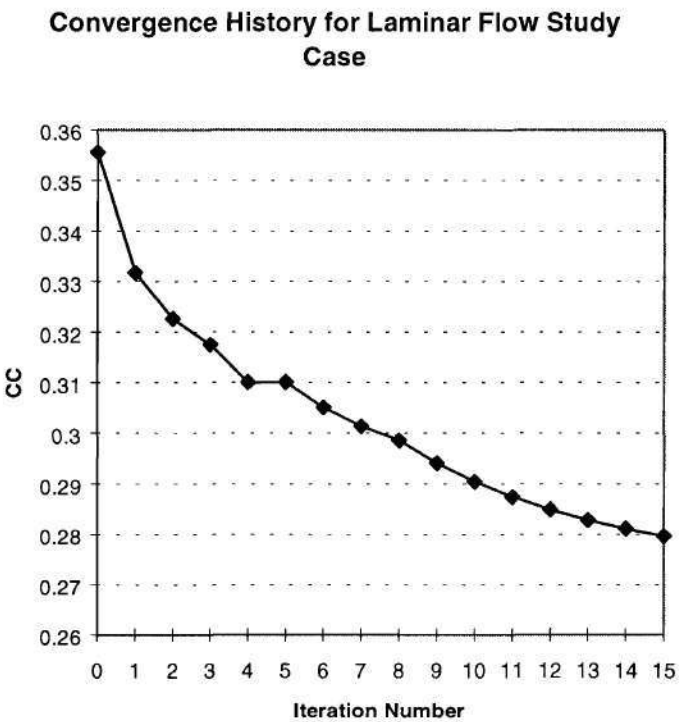

Figure 71. Convergence rate for laminar flow in forward flight study case.

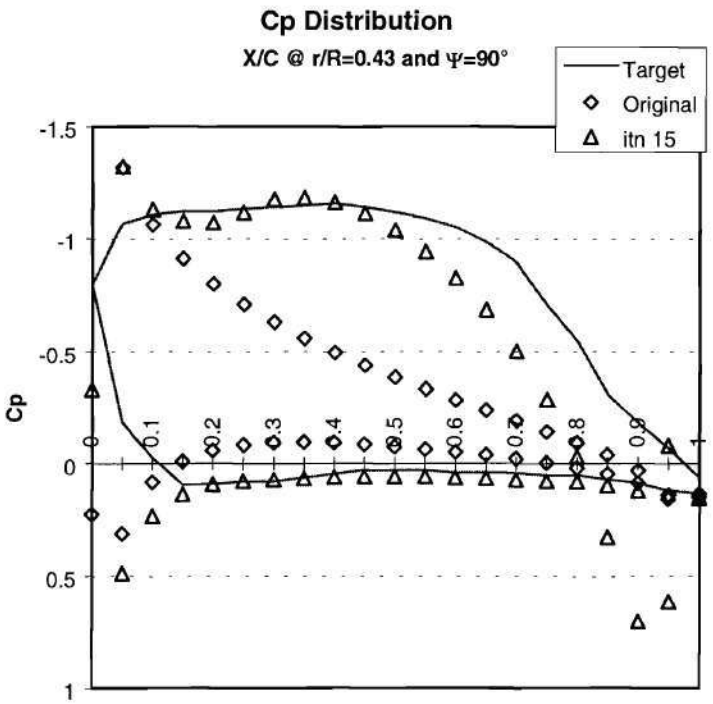

Figure 72. Pressure distribution comparison at r/R=0.43 and Ψ=90° for laminar flow in forward flight study case.

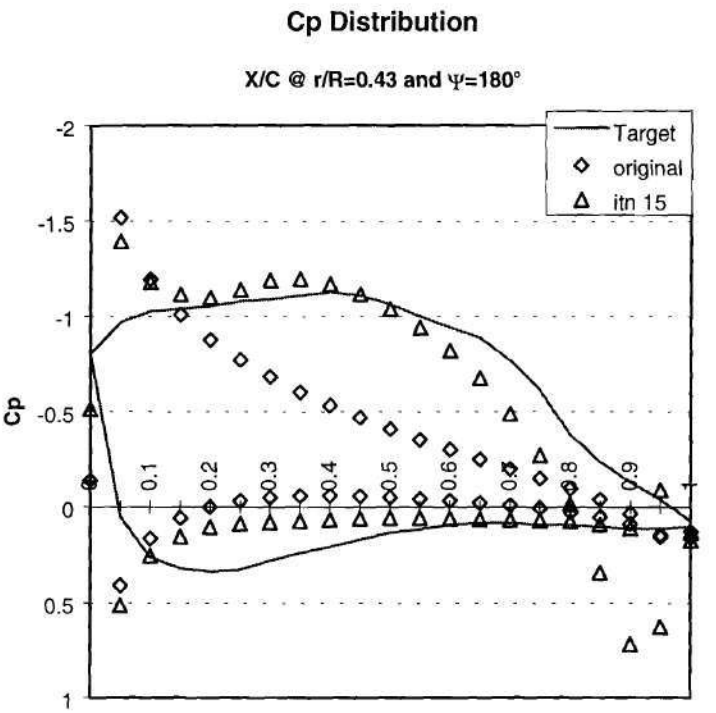

Figure 73. Pressure distribution comparison at r/R=0.43 and Ψ=180° for laminar flow in forward flight study case.

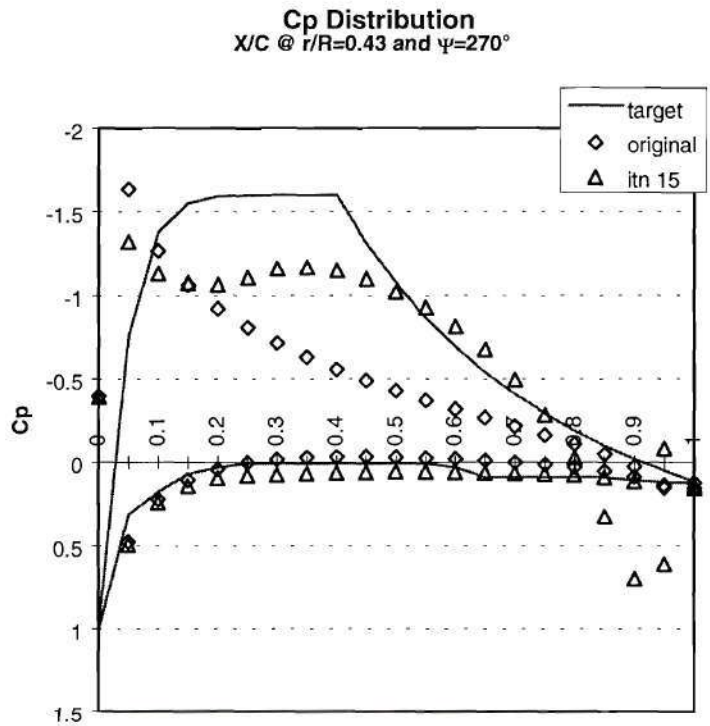

Figure 74. Pressure distribution comparison at r/R=0.43 and Ψ=270° for laminar flow in forward flight study case.

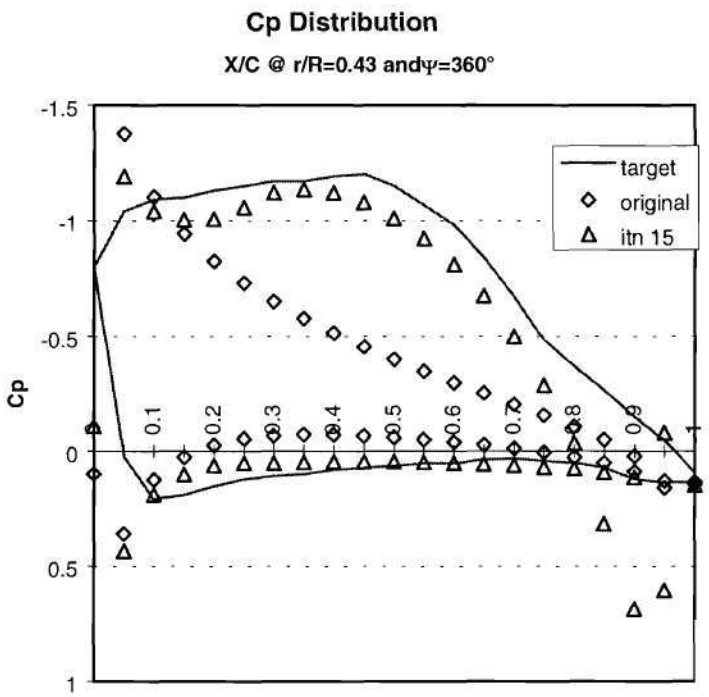

Figure 75. Pressure distribution comparison at r/R=0.43 and Ψ=360° for laminar flow in forward flight study case.

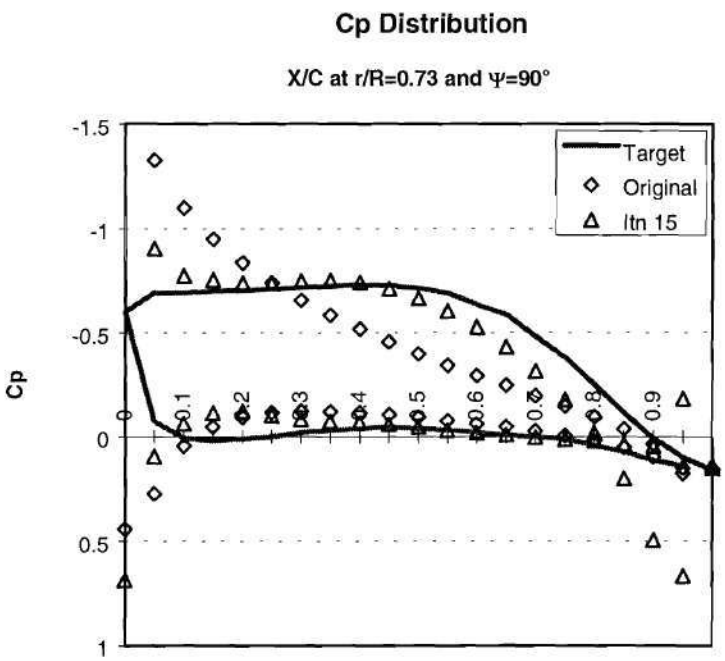

Figure 76. Pressure distribution comparison at r/R=0.73 and Ψ=90° for laminar flow in forward flight study case.

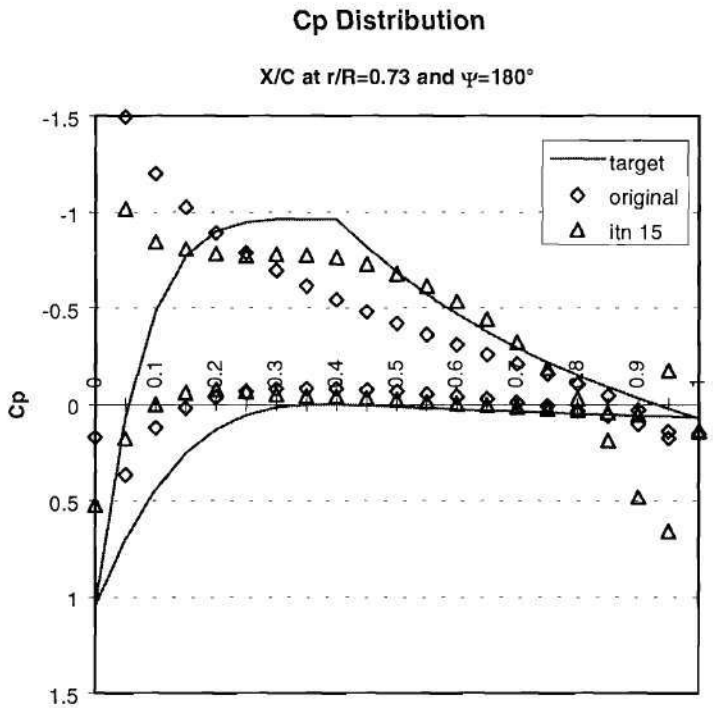

Figure 77. Pressure distribution comparison at r/R=0.73 and Ψ=180° for laminar flow in forward flight study case.

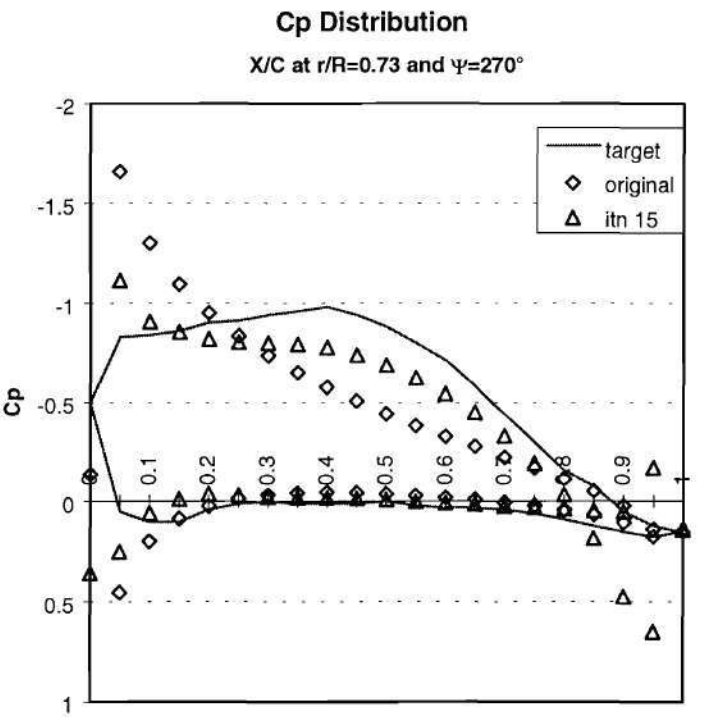

Figure 78. Pressure distribution comparison at r/R=0.73 and Ψ=270° for laminar flow in forward flight study case.

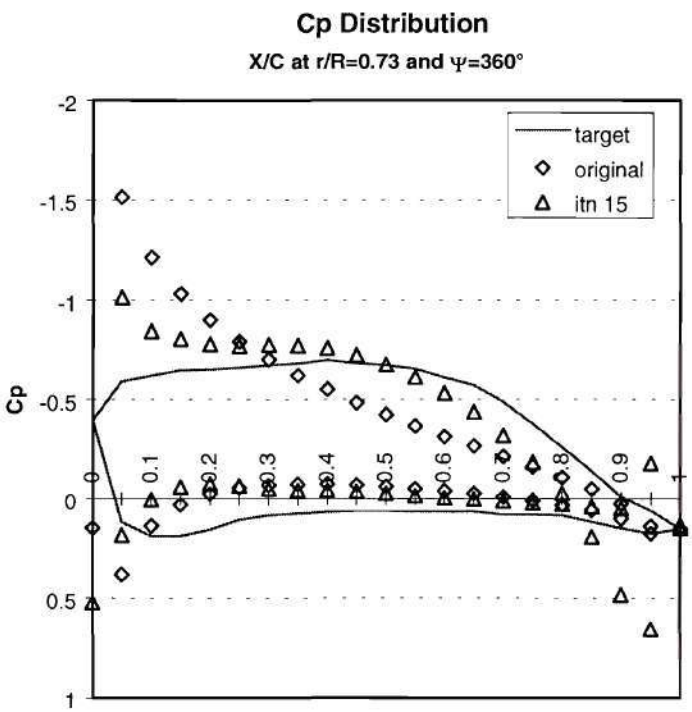

Figure 79. Pressure distribution comparison at r/R=0.73 and Ψ=360° for laminar flow in forward flight study case.

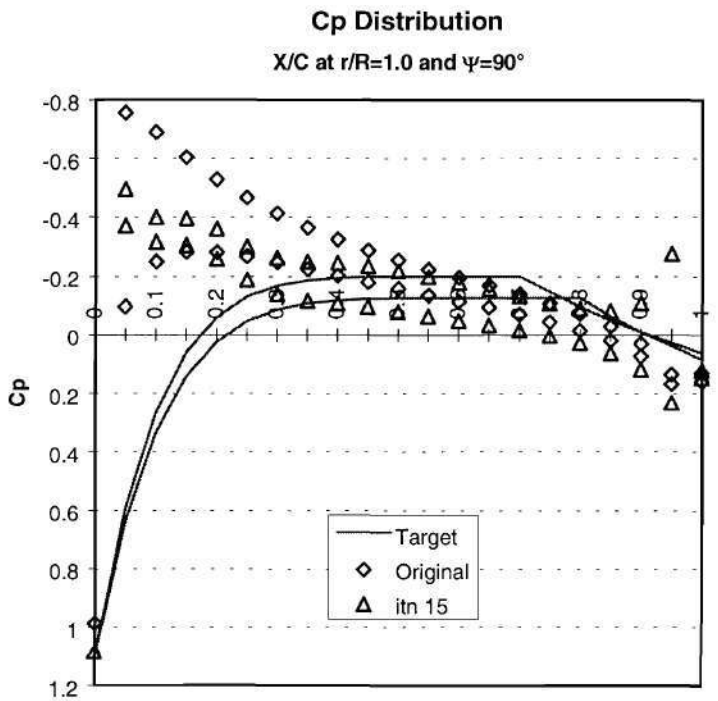

Figure 80. Pressure distribution comparison at r/R=1.0 and Ψ=90° for laminar flow in forward flight study case.

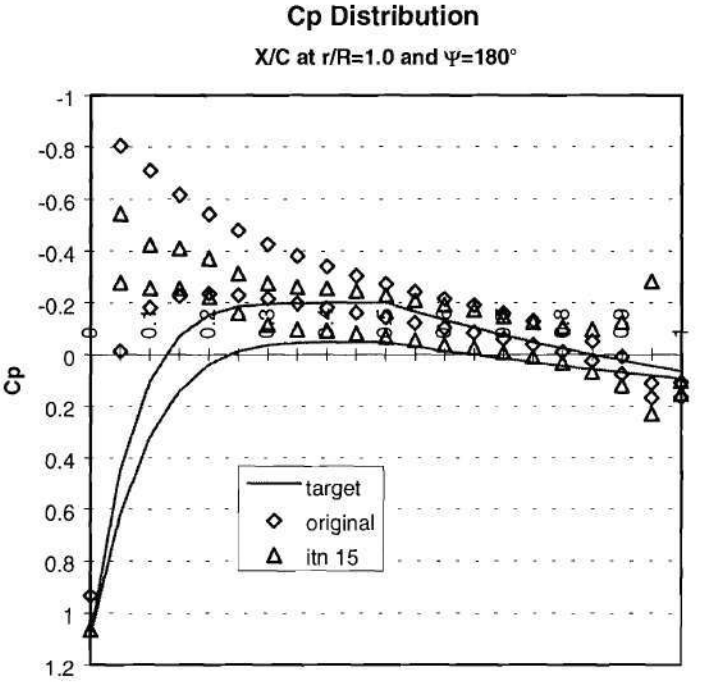

Figure 81. Pressure distribution comparison at r/R=1.0 and Ψ=180° for laminar flow in forward flight study case.

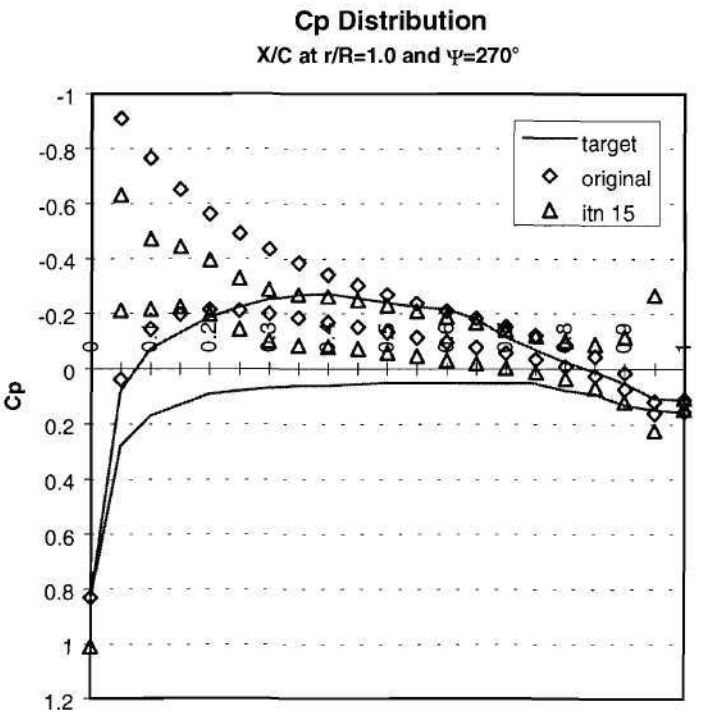

Figure 82. Pressure distribution comparison at r/R=1.0 and Ψ=270° for laminar flow in forward flight study case.

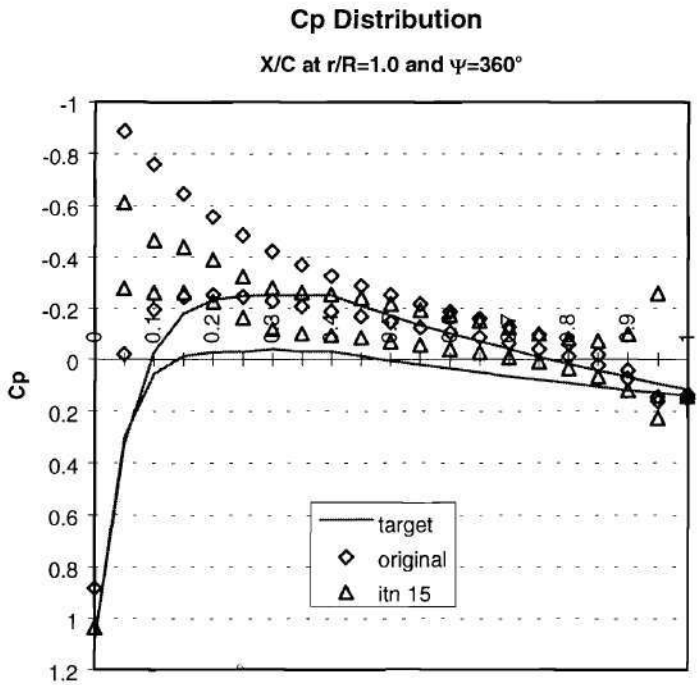

Figure 83. Pressure distribution comparison at r/R=1.0 and Ψ=360° for laminar flow in forward flight study case.

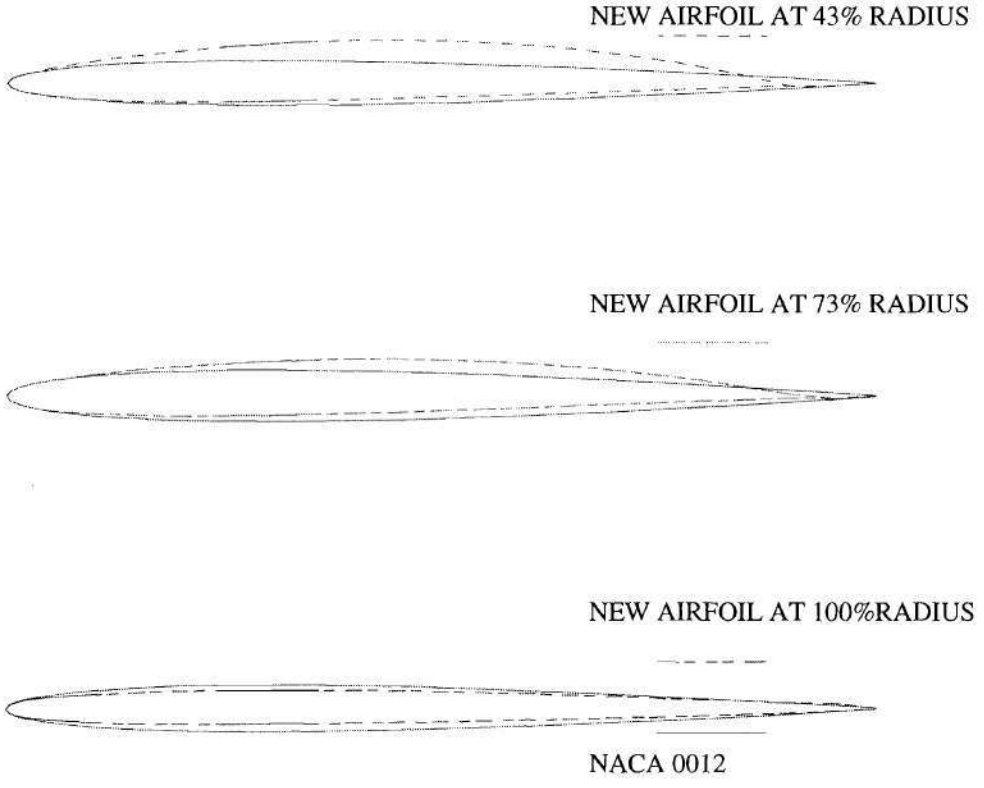

Figure 84. Airfoil comparison for laminar flow in forward flight study case.

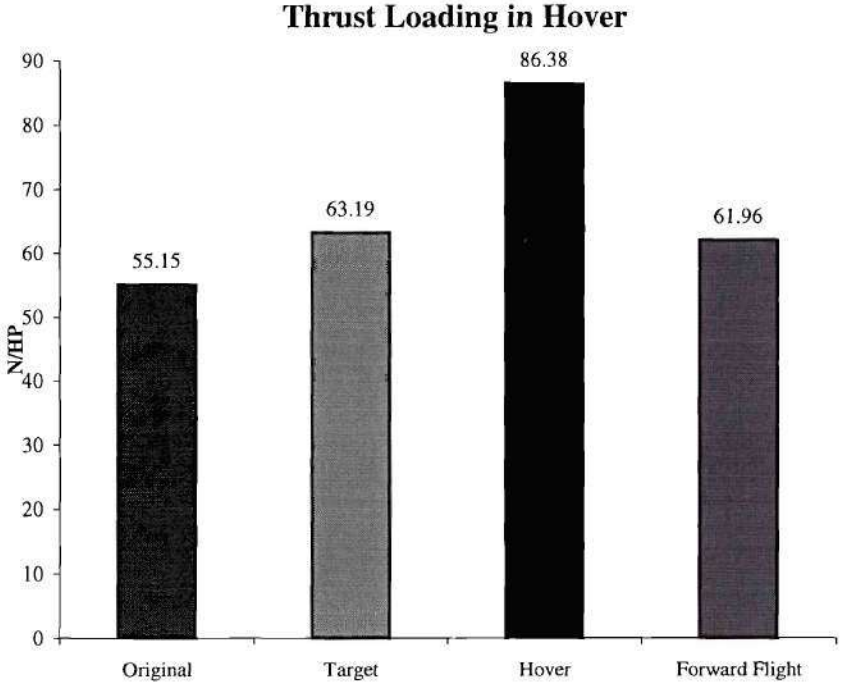

Figure 85. Performance comparison of different rotors in hover for example on different flight conditions.

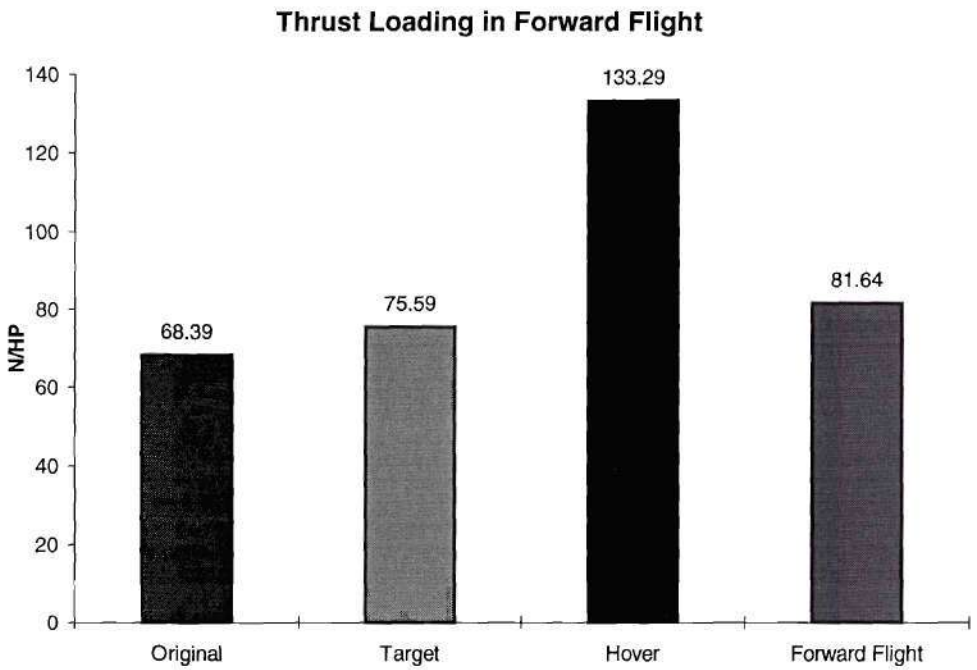

Figure 86. Performance comparison of different rotors in forward flight for example on different flight conditions.

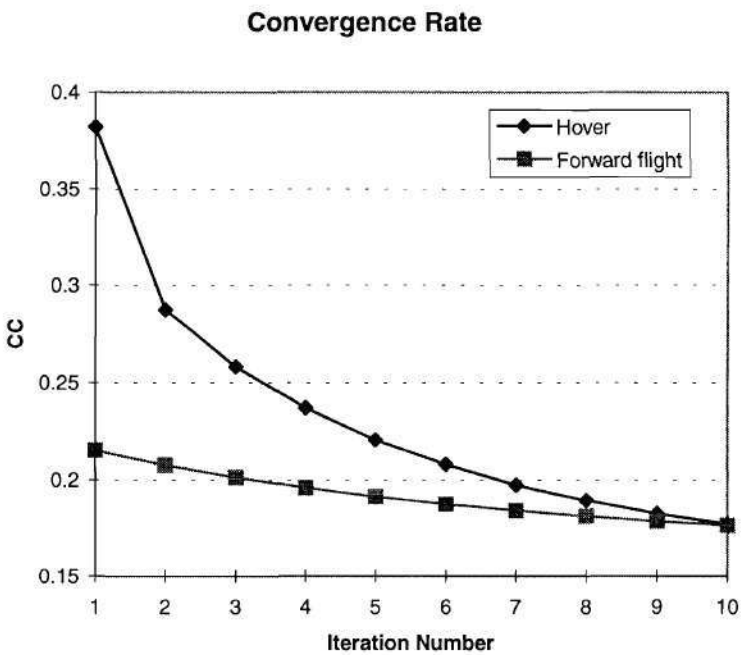

Figure 87. Convergence rate for example on different flight conditions.

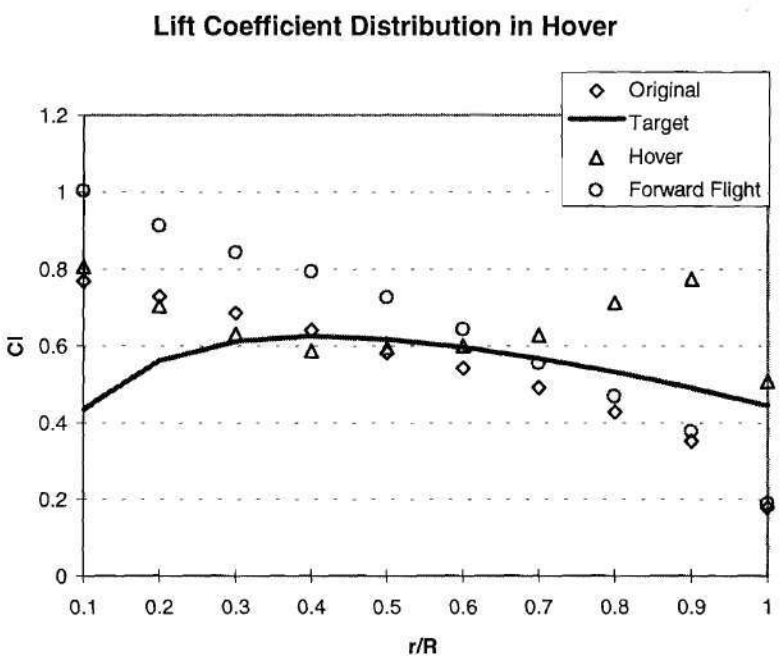

Figure 88. Comparison of lift coefficient distributions for example on different flight conditions.

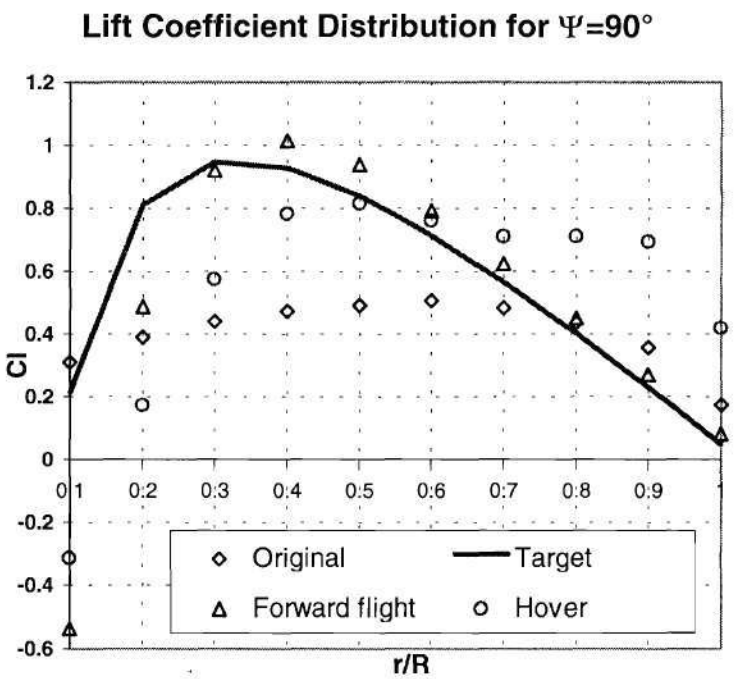

Figure 89. Comparison of lift coefficient distributions in forward flight at Ψ=90° for example on different flight conditions.

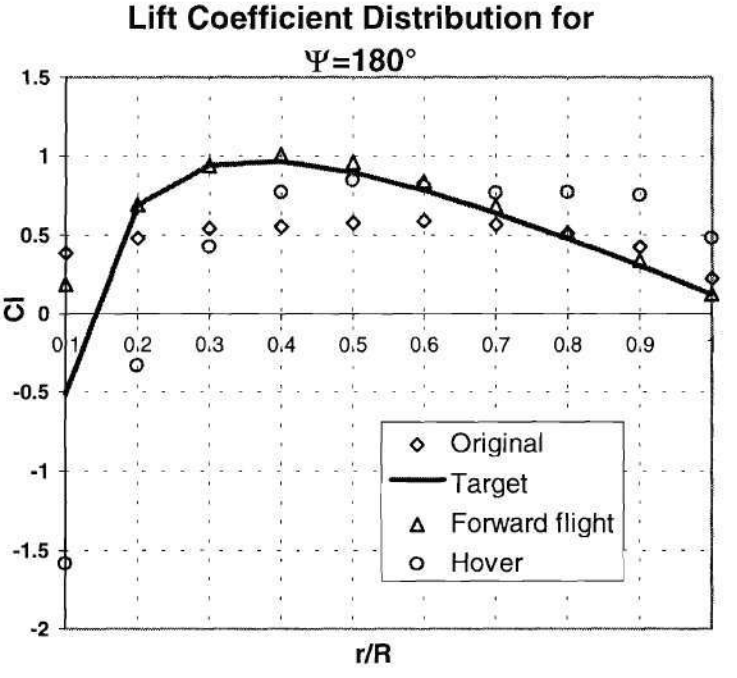

Figure 90. Comparison of lift coefficient distributions in forward flight at Ψ=180° for example on different flight conditions.

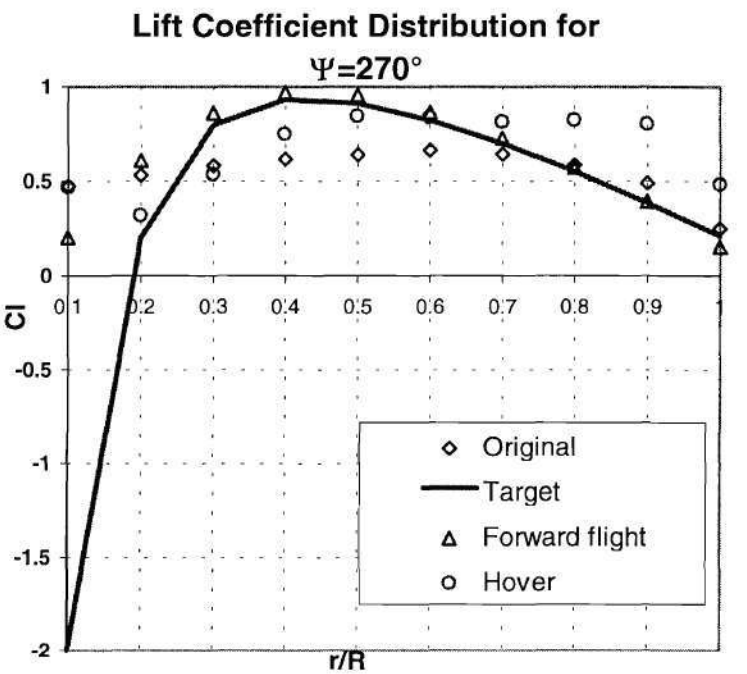

Figure 91. Comparison of lift coefficient distributions in forward flight at Ψ=270° for example on different flight conditions

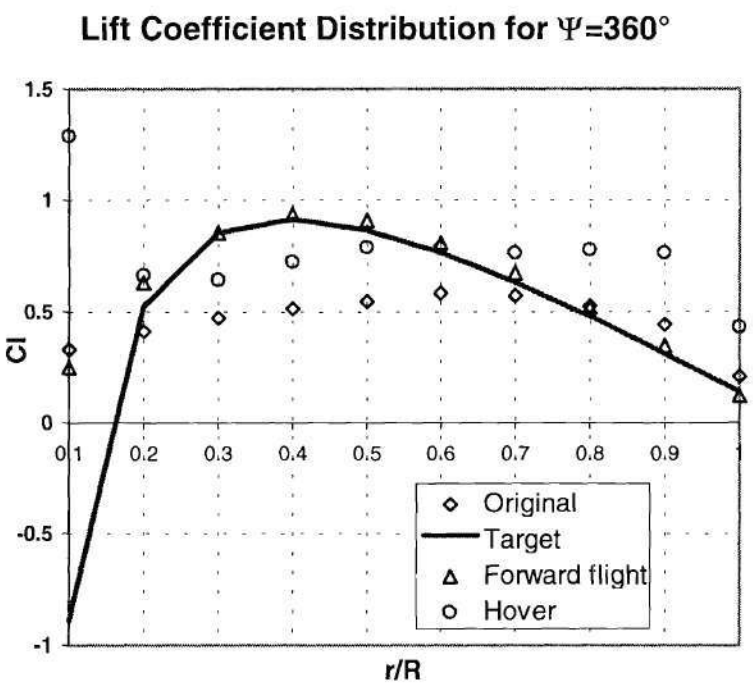

Figure 92. Comparison of lift coefficient distributions in forward flight at Ψ=360° for example on different flight conditions.

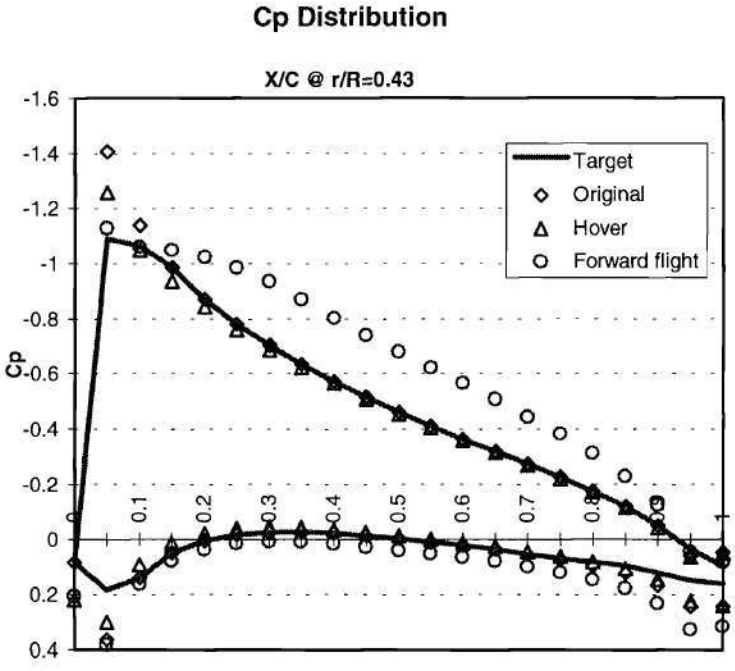

Figure 93. Comparison of pressure distributions in hover at r/R=0.43 for example on different flight conditions.

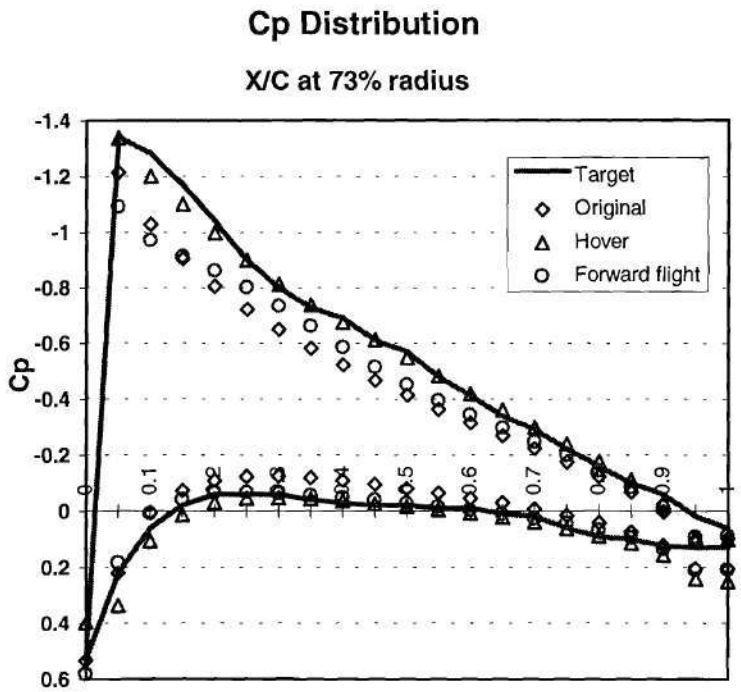

Figure 94. Comparison of pressure distributions in hover at r/R=0.73 for example on different flight conditions.

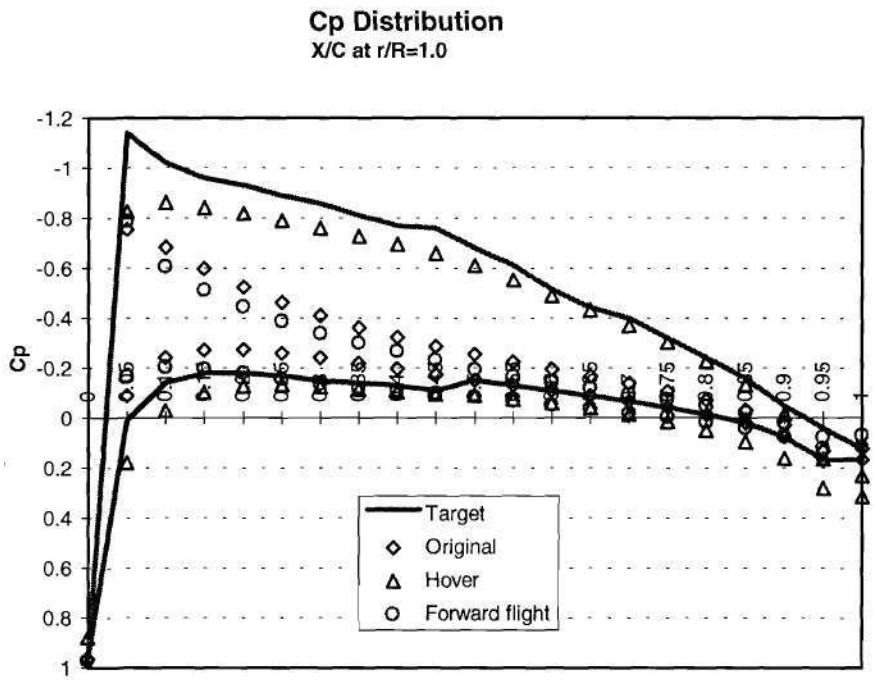

Figure 95. Comparison of pressure distributions in hover at r/R=1.0 for example on different flight conditions.

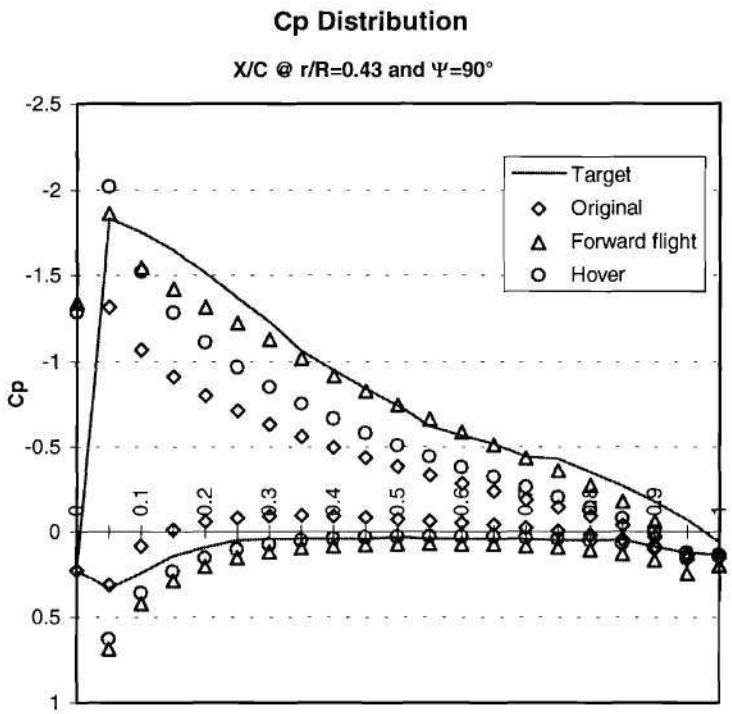

Figure 96. Comparison of pressure distributions in forward flight at r/R=0.43 and Ψ=90° for example on different flight conditions.

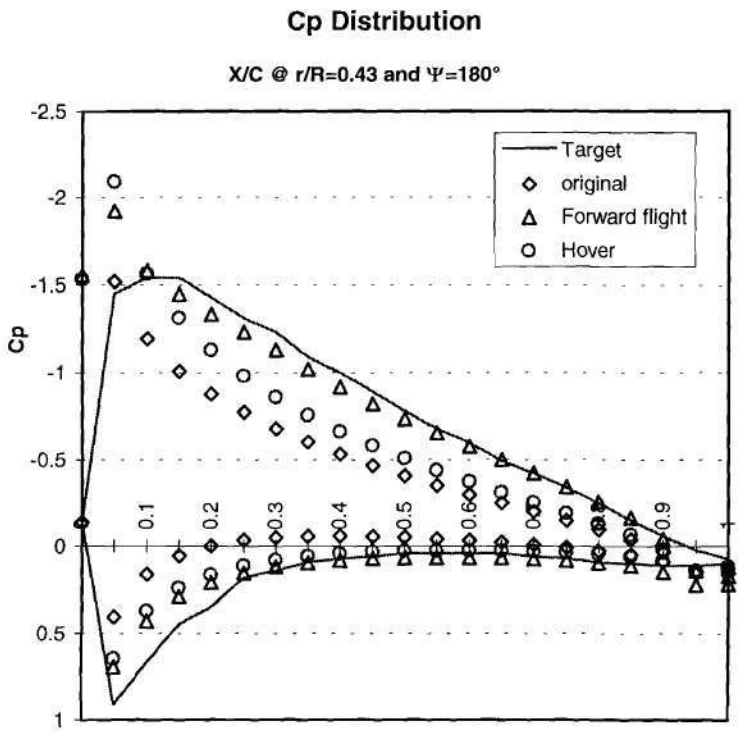

Figure 97. Comparison of pressure distributions in forward flight at r/R=0.43 and Ψ=180° for example on different flight conditions.

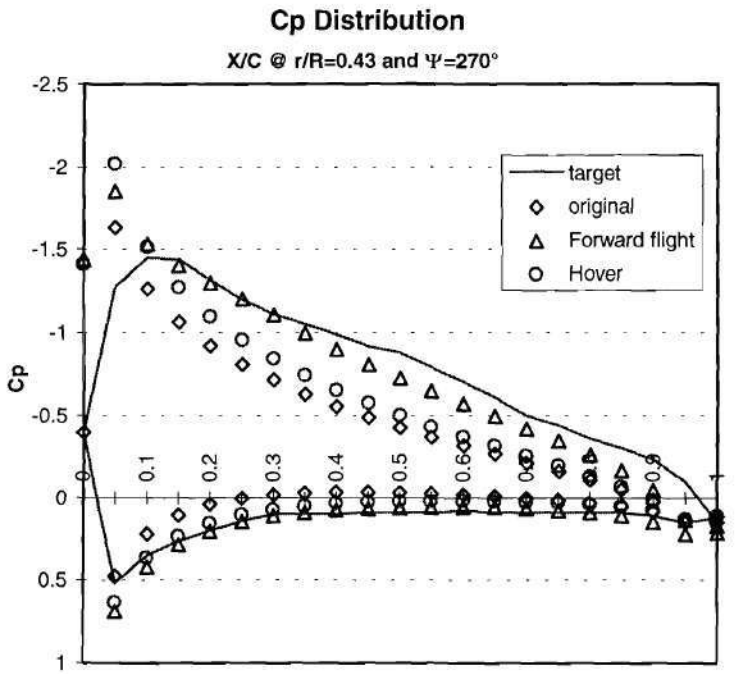

Figure 98. Comparison of pressure distributions in forward flight at r/R=0.43 and Ψ=270° for example on different flight conditions.

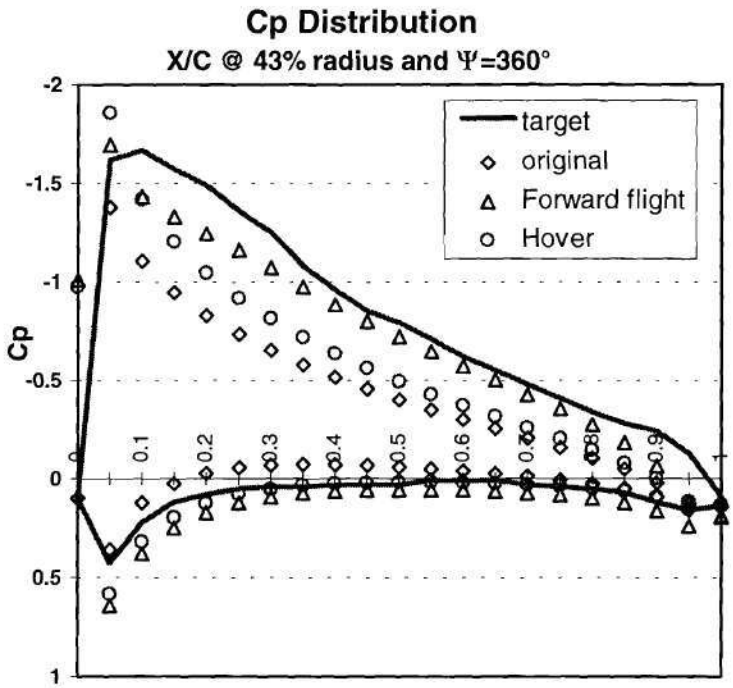

Figure 99. Comparison of pressure distributions in forward flight at r/R=0.43 and Ψ=360° for example on different flight conditions.

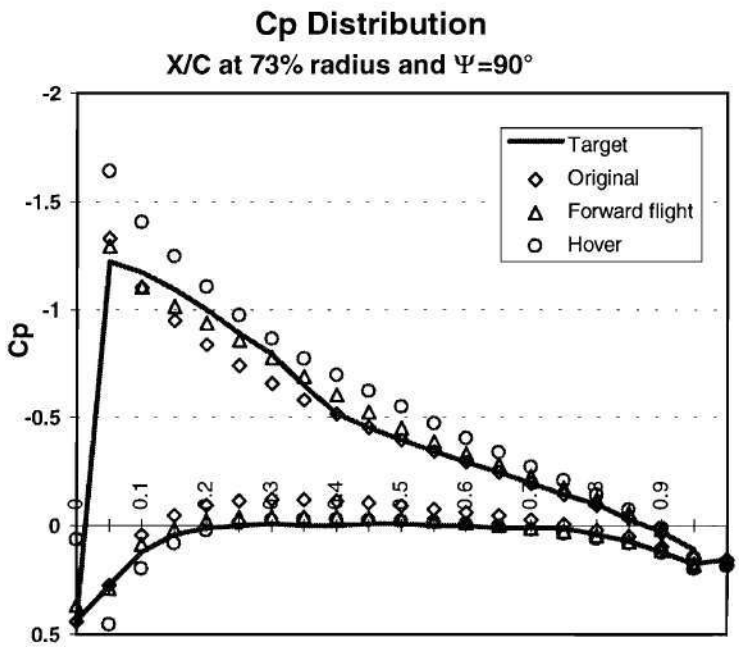

Figure 100. Comparison of pressure distributions in forward flight at r/R=0.73 and Ψ=90° for example on different flight conditions.

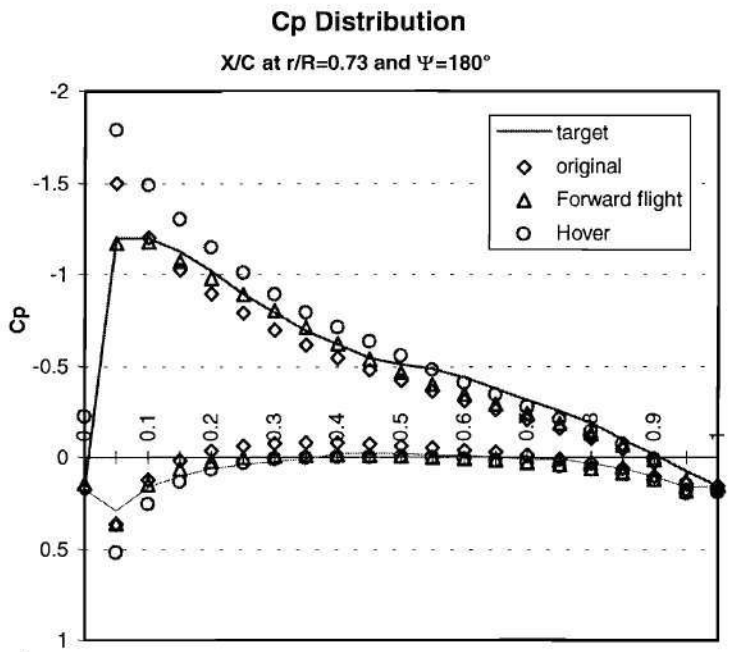

Figure 101. Comparison of pressure distributions in forward flight at r/R=0.73 and Ψ=180° for example on different flight conditions.

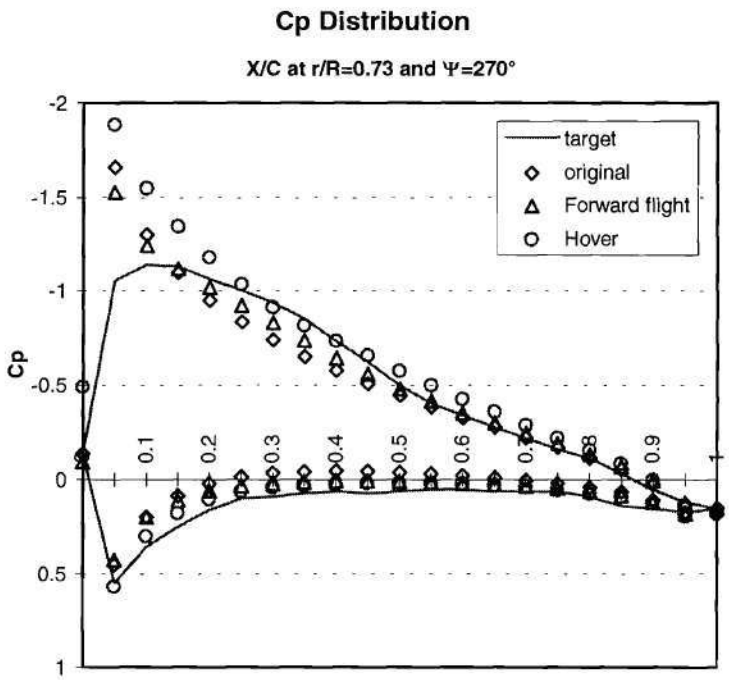

Figure 102. Comparison of pressure distributions in forward flight at r/R=0.73 and Ψ=270° for example on different flight conditions.

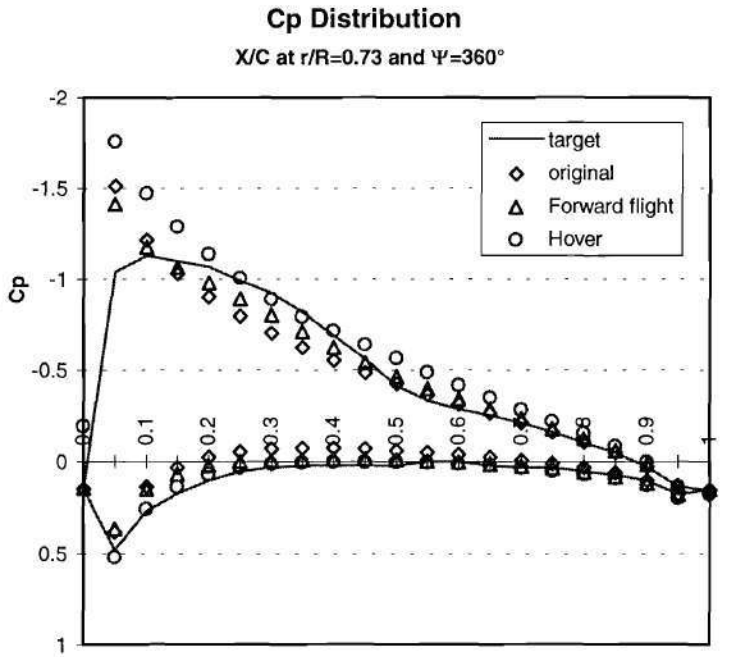

Figure 103. Comparison of pressure distributions in forward flight at r/R=0.73 and Ψ=360° for example on different flight conditions.

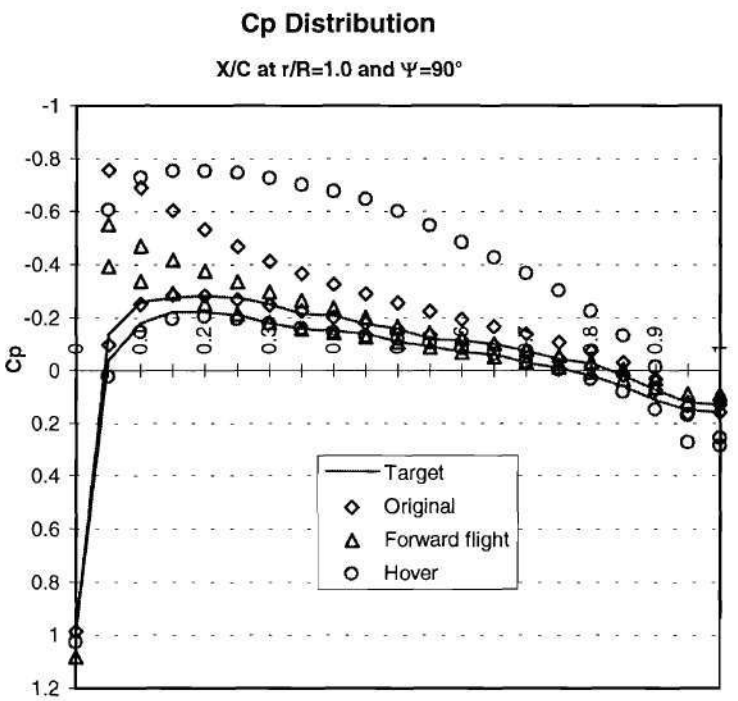

Figure 104. Comparison of pressure distributions in forward flight at r/R=1.0 and Ψ=90° for example on different flight conditions.

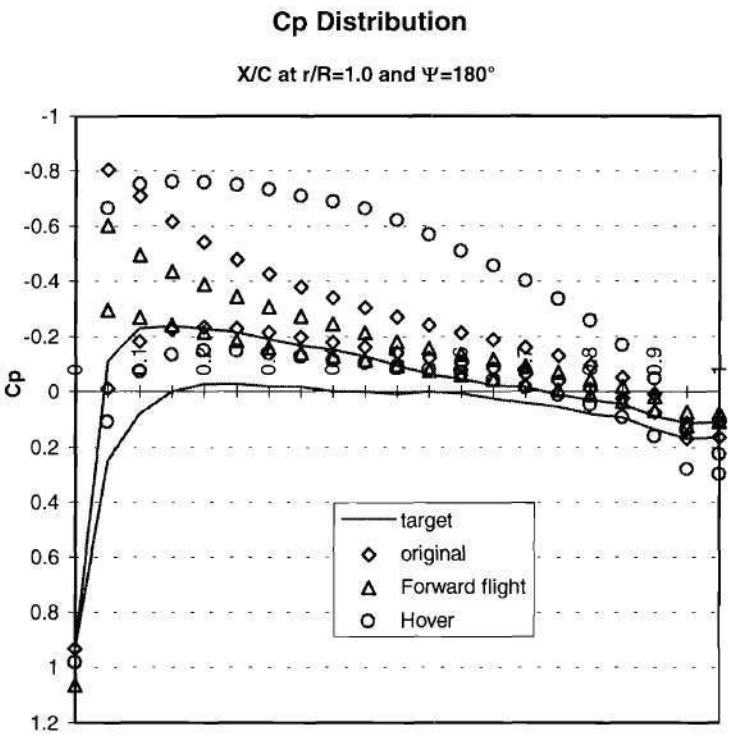

Figure 105. Comparison of pressure distributions in forward flight at r/R=1.0 and Ψ=180° for example on different flight conditions.

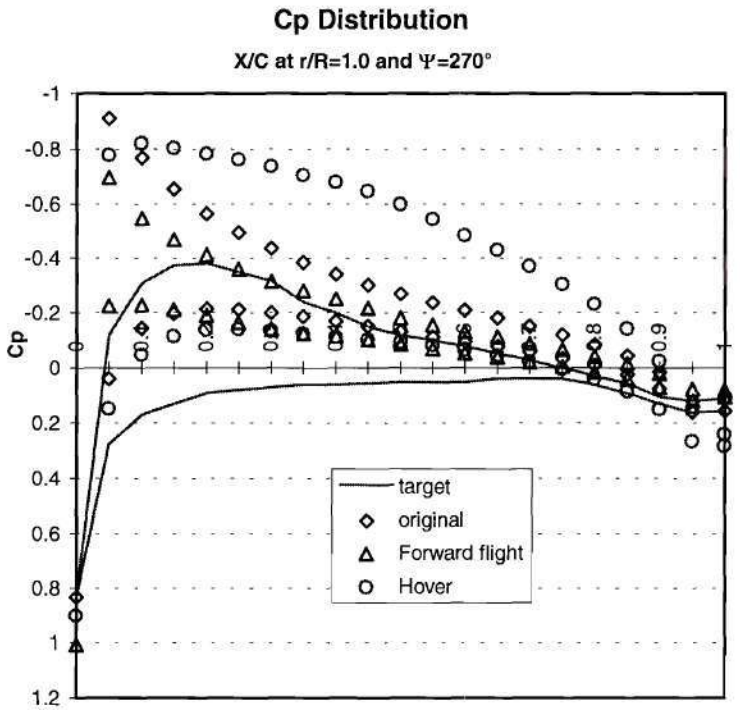

Figure 106. Comparison of pressure distributions in forward flight at r/R=1.0 and Ψ=270° for example on different flight conditions.

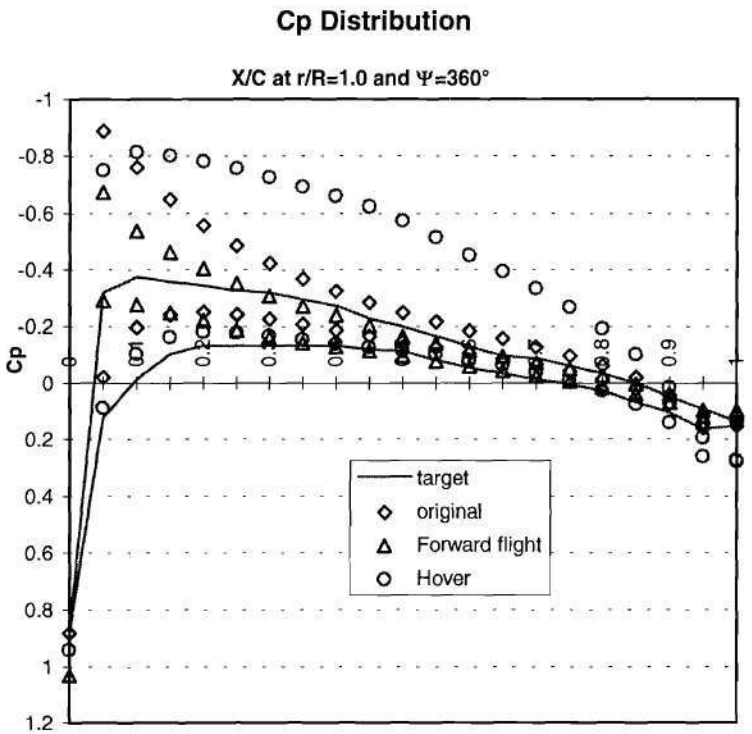

Figure 107. Comparison of pressure distributions in forward flight at r/R=1.0 and Ψ=360° for example on different flight conditions.

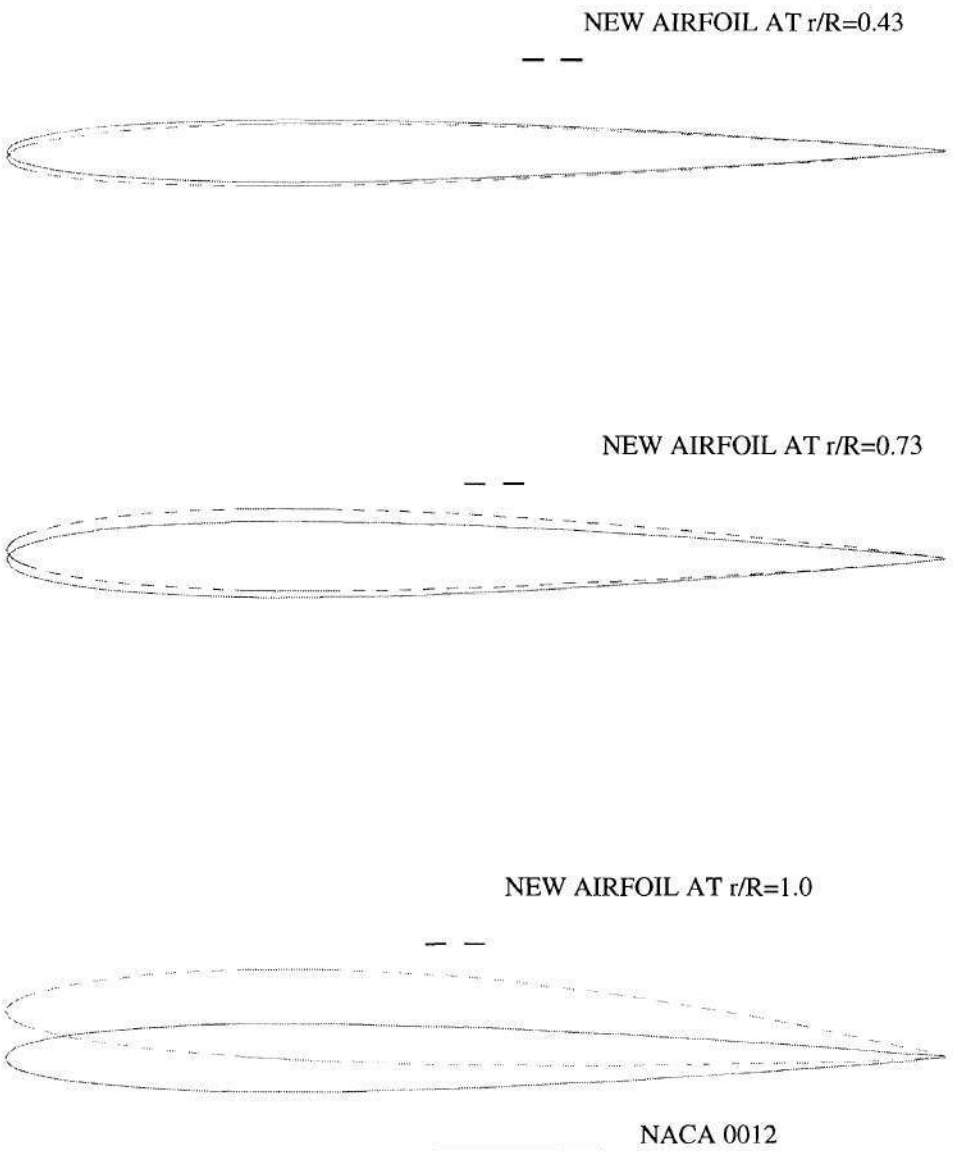

Figure 108. Airfoil comparison. Rotor designed for hover for example on different flight conditions.

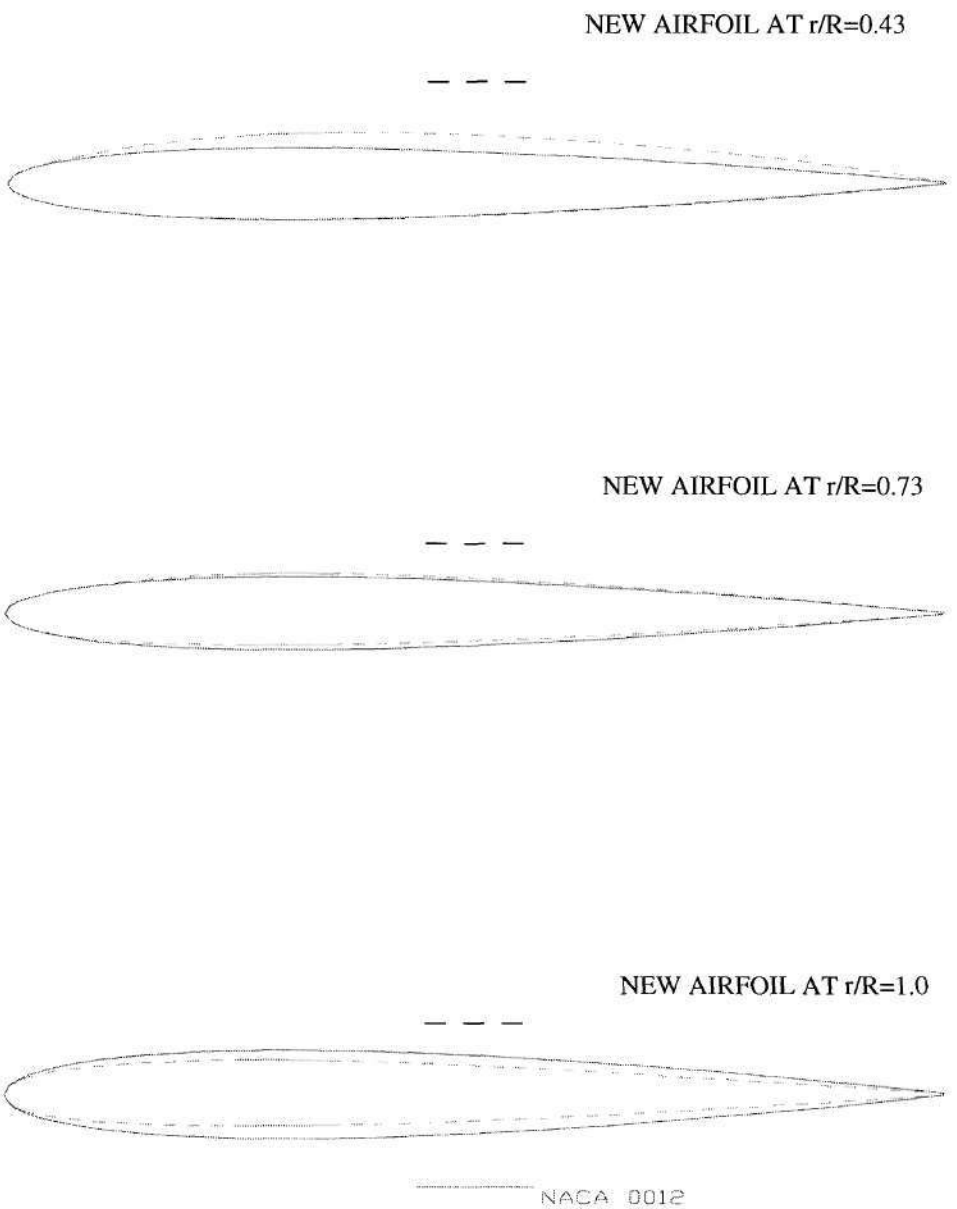

Figure 109. Airfoil comparison. Rotor designed for forward flight for example on different flight conditions.

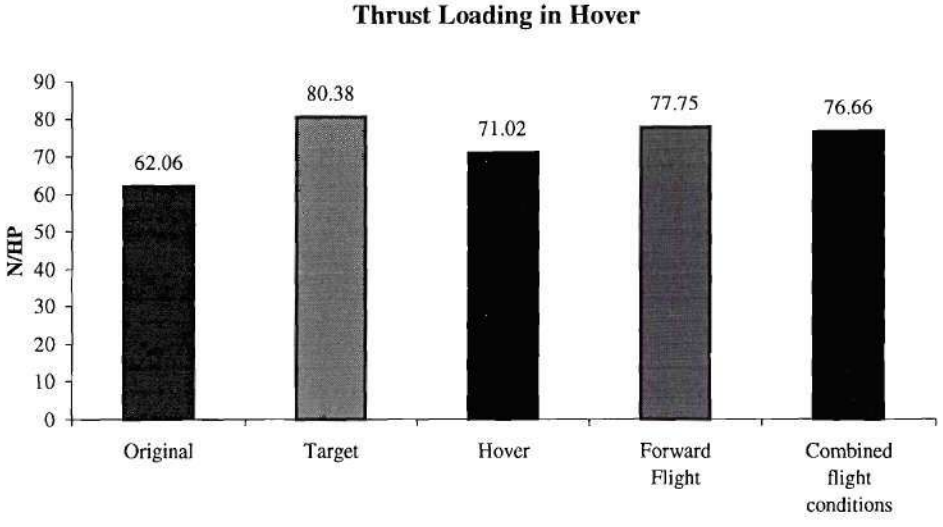

Figure 110. Performance comparison of different rotors in hover for example on combination of flight conditions.

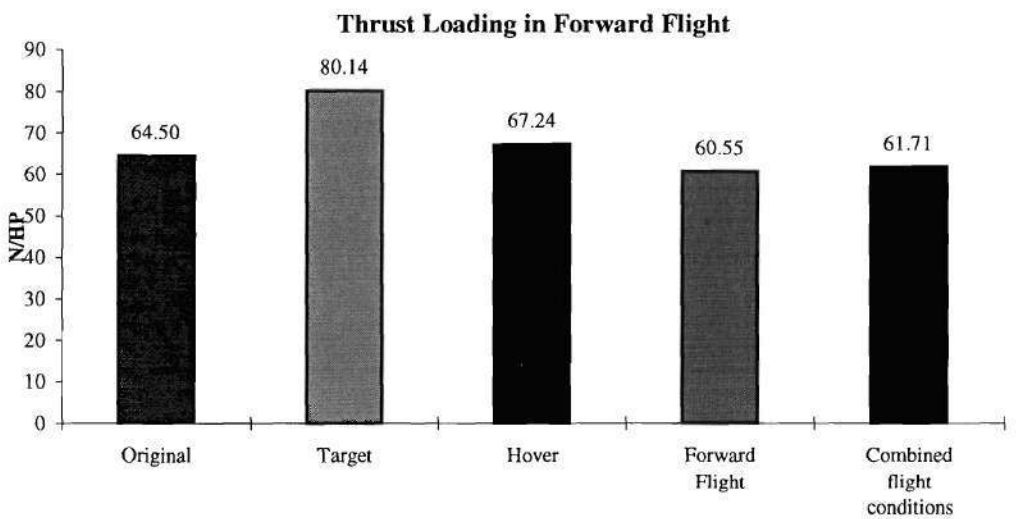

Figure 111. Performance comparison of different rotors in forward flight for example on combination of flight conditions.

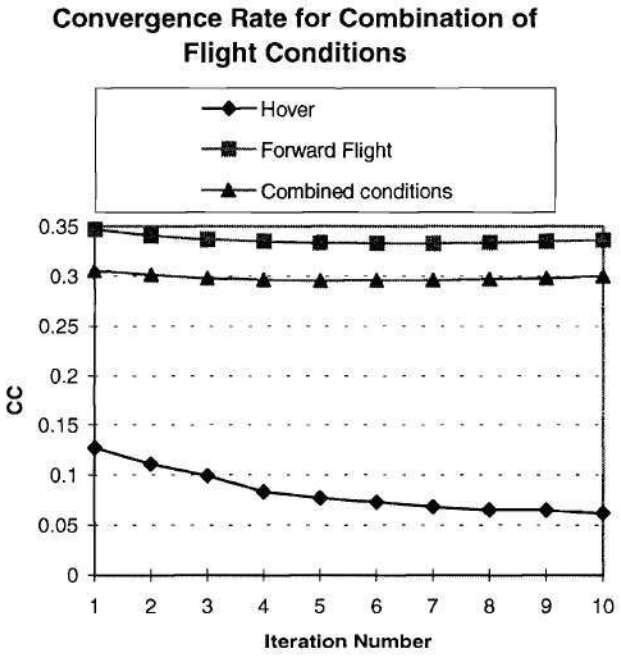

Figure 112. Convergence rate for example on combination of flight conditions.

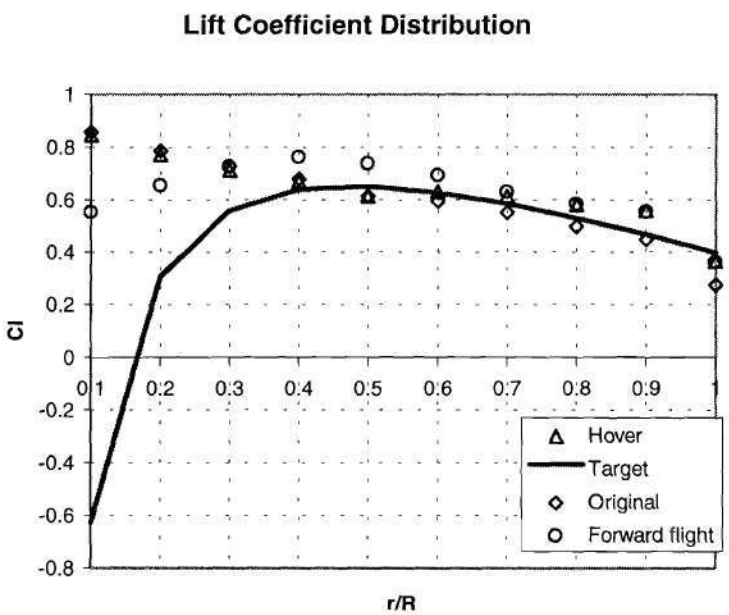

Figure 113. Lift coefficient distribution comparison in hover for example on combination of flight conditions.

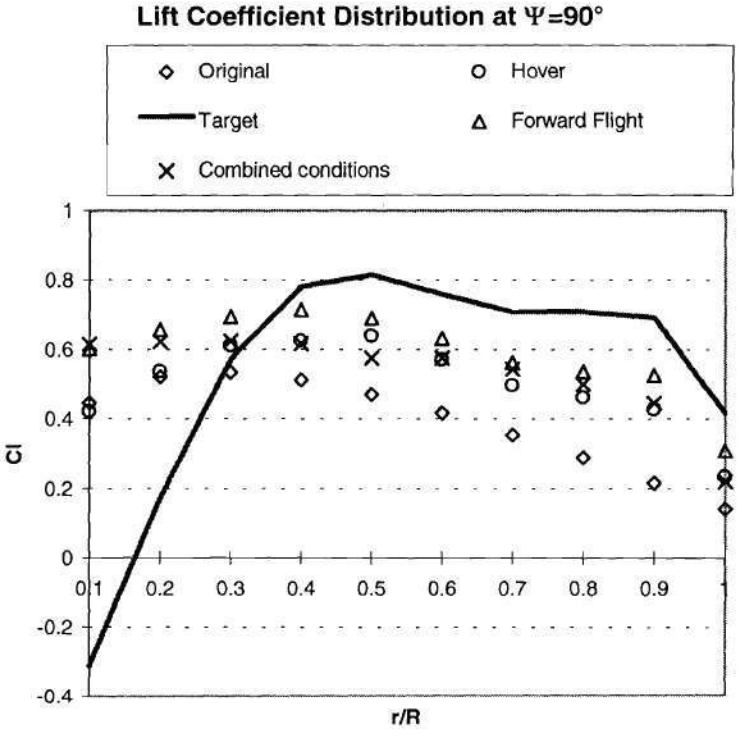

Figure 114. Lift coefficient distribution comparison in forward flight at Ψ=90° for example on combination of flight conditions.

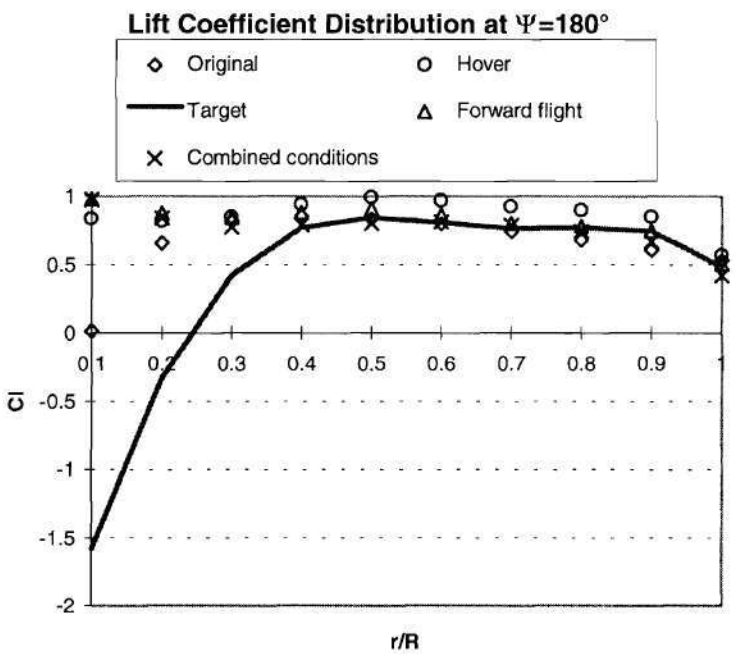

Figure 115. Lift coefficient distribution comparison in forward flight at Ψ=180° for example on combination of flight conditions.

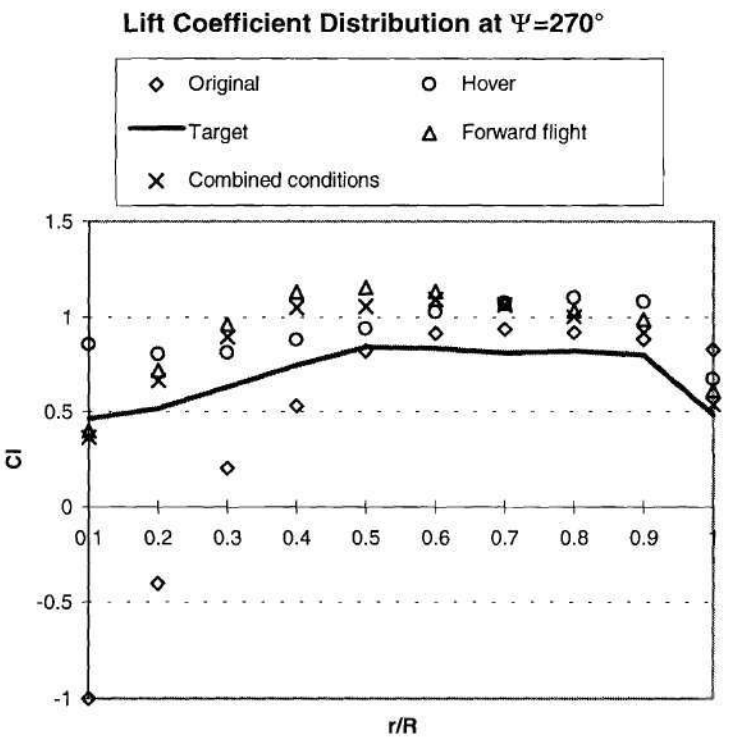

Figure 116. Lift coefficient distribution comparison in forward flight at Ψ=270° for example on combination of flight conditions.

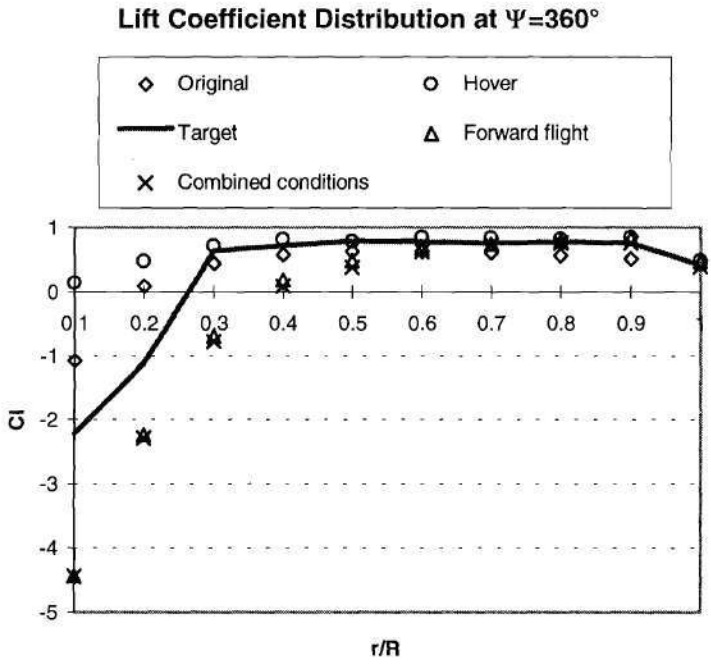

Figure 117. Lift coefficient distribution comparison in forward flight at Ψ=360° for example on combination of flight conditions.

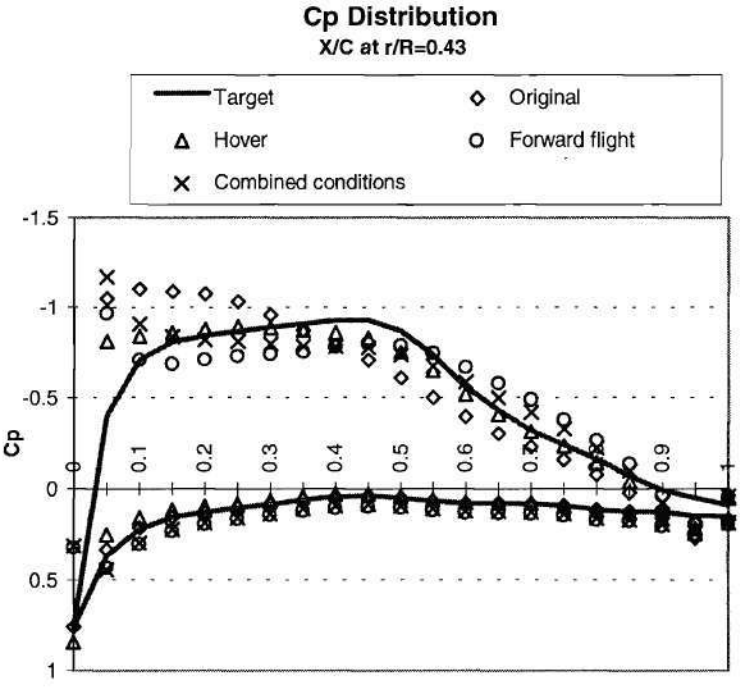

Figure 118. Pressure distribution comparison in hover at r/R=0.43 for example on combination of flight conditions.

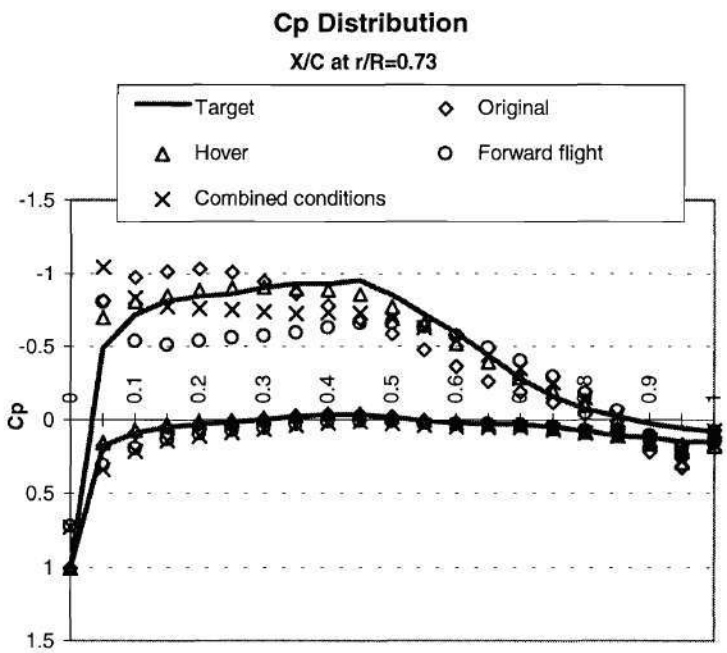

Figure 119. Pressure distribution comparison in hover at r/R=0.73 for example on combination of flight conditions.

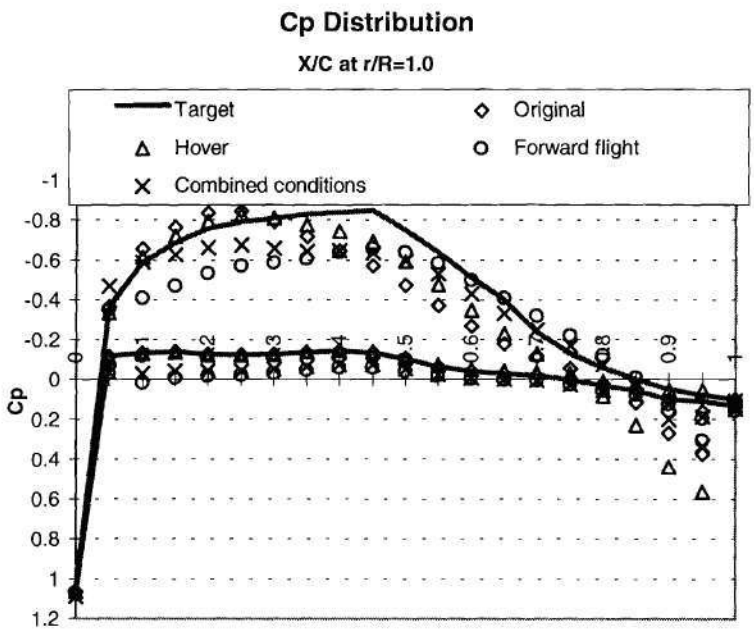

Figure 120. Pressure distribution comparison in hover at r/R=1.0 for example on combination of flight conditions.

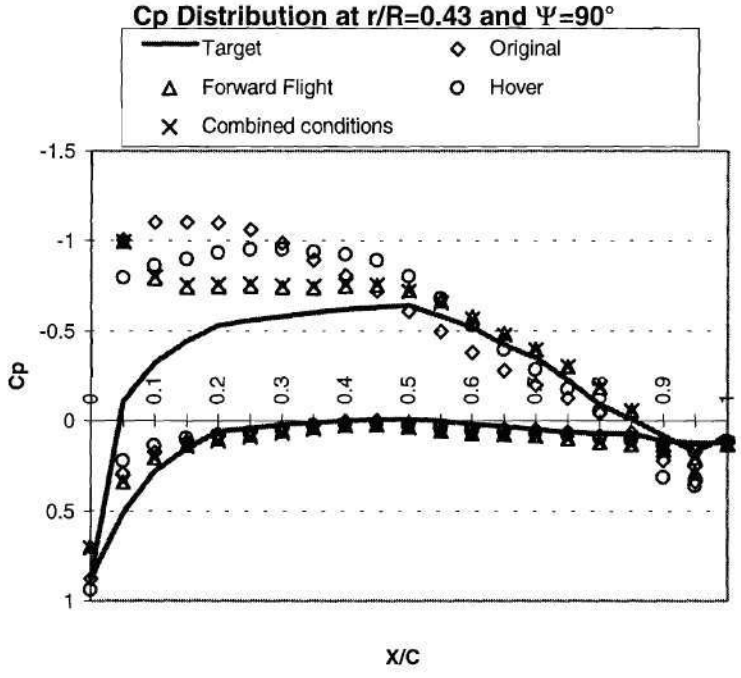

Figure 121. Pressure distribution comparison in forward flight at r/R=0.43 and Ψ=90° for example on combination of flight conditions.

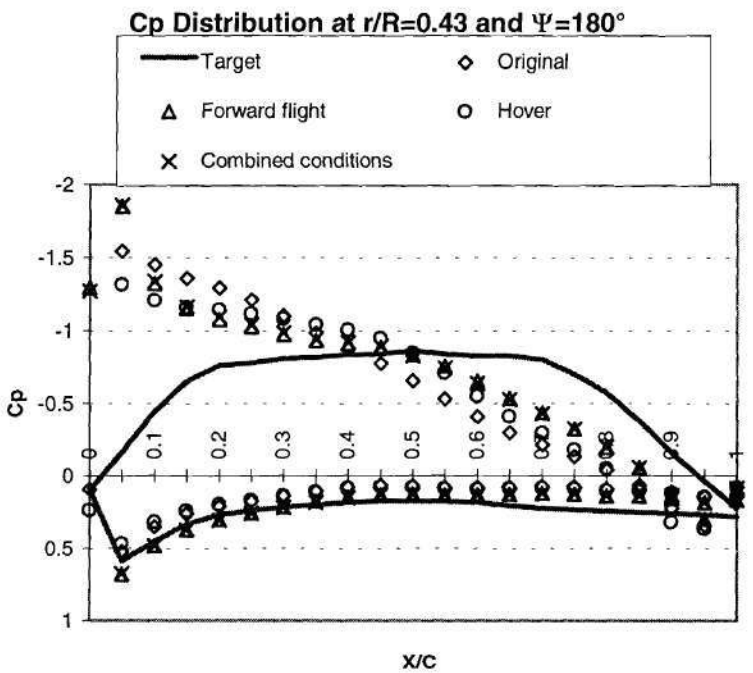

Figure 122. Pressure distribution comparison in forward flight at r/R=0.43 and Ψ=180° for example on combination of flight conditions.

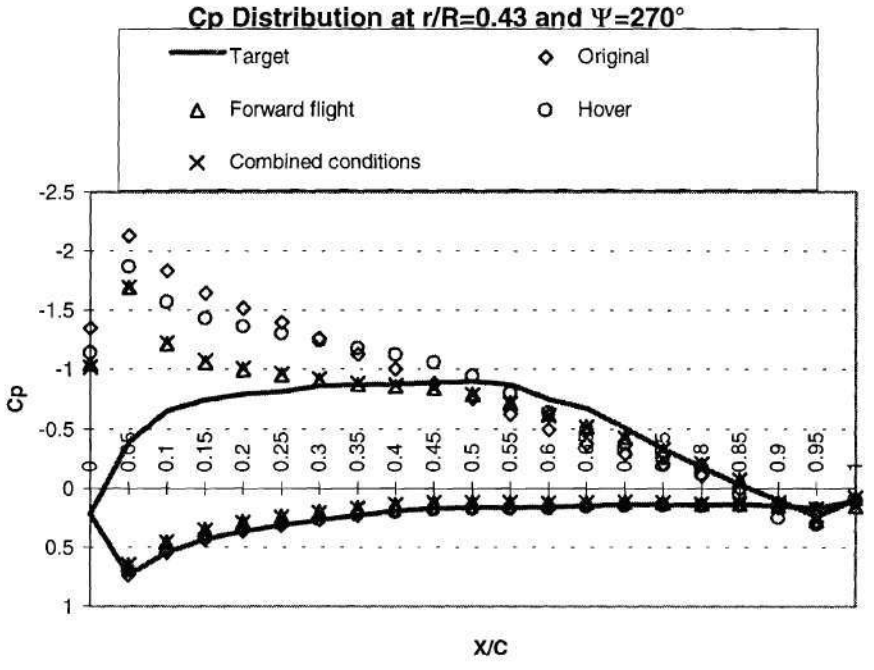

Figure 123. Pressure distribution comparison in forward flight at r/R=0.43 and Ψ=270° for example on combination of flight conditions.

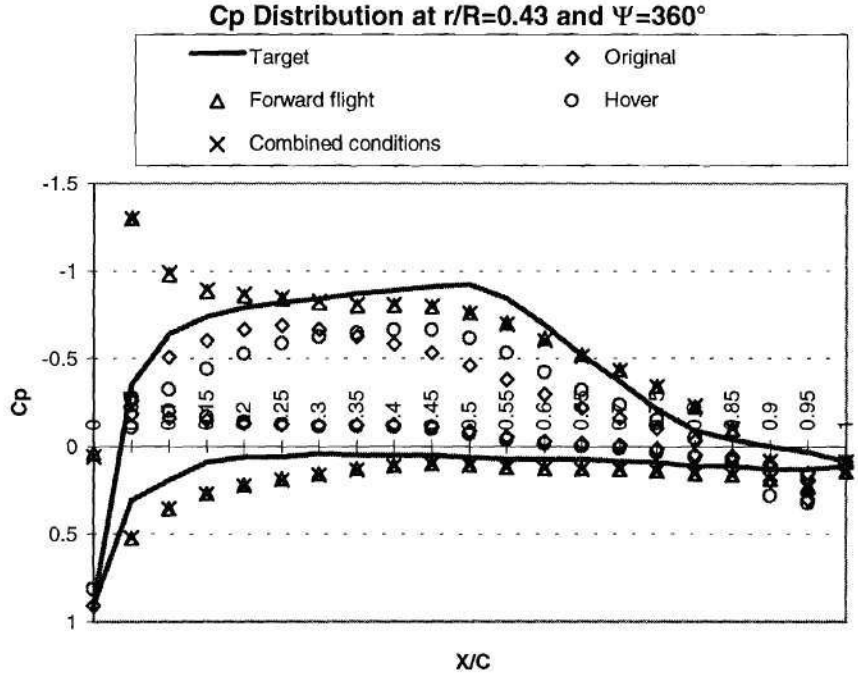

Figure 124. Pressure distribution comparison in forward flight at r/R=0.43 and Ψ=360° for example on combination of flight conditions.

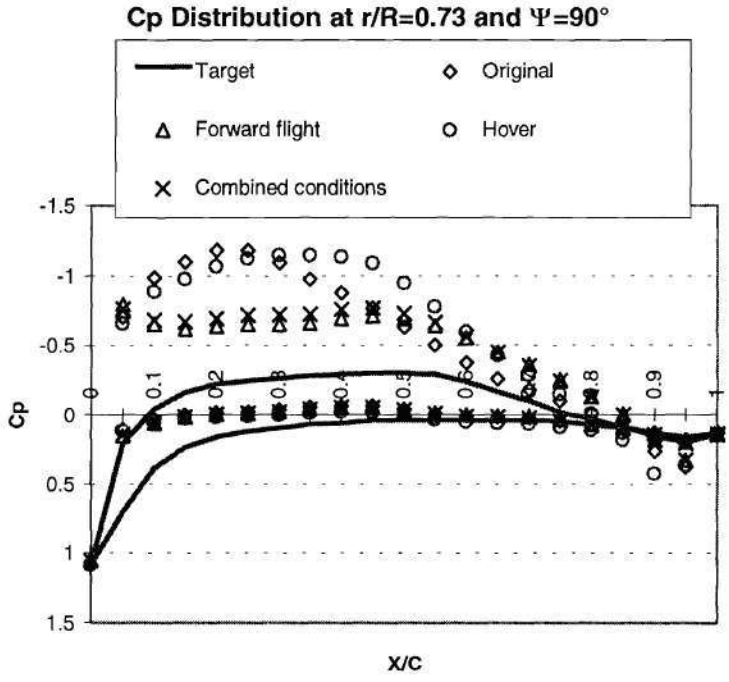

Figure 125. Pressure distribution comparison in forward flight at r/R=0.73 and Ψ=90° for example on combination of flight conditions.

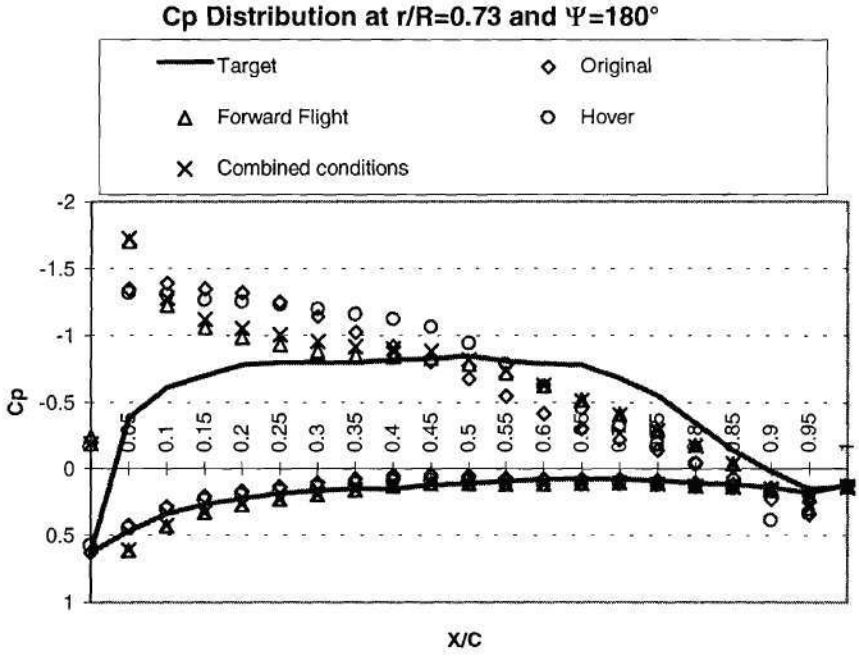

Figure 126. Pressure distribution comparison in forward flight at r/R=0.73 and Ψ=180° for example on combination of flight conditions.

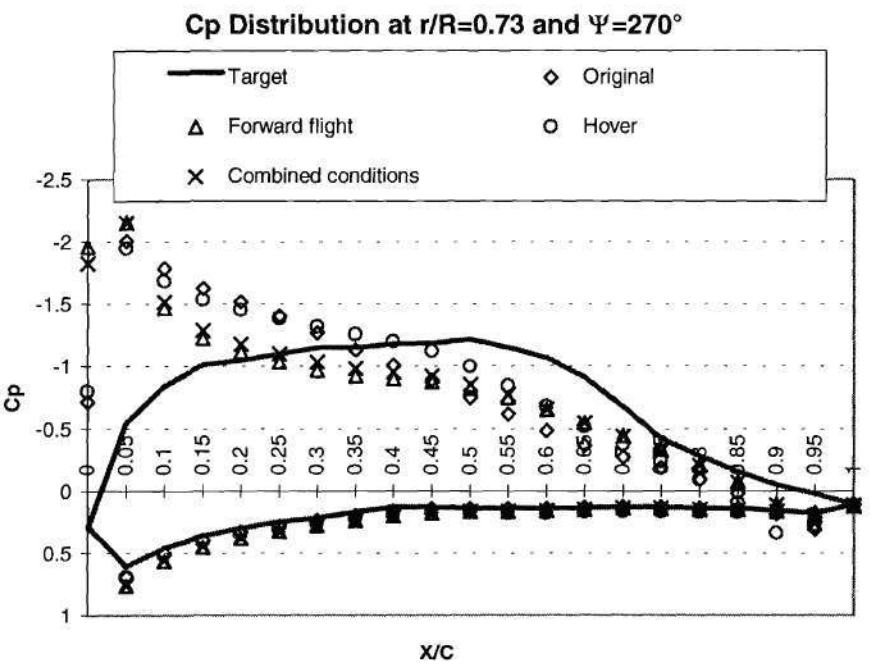

Figure 127. Pressure distribution comparison in forward flight at r/R=0.73 and Ψ=270° for example on combination of flight conditions.

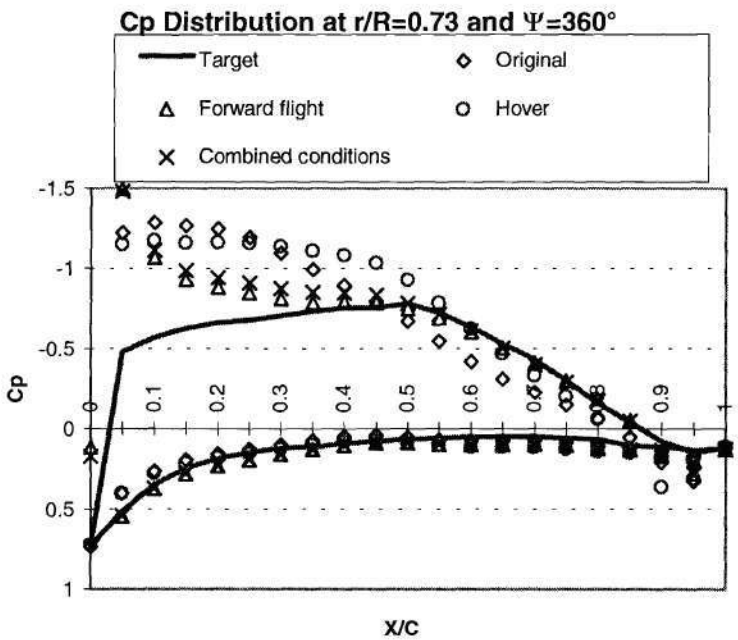

Figure 128. Pressure distribution comparison in forward flight at r/R=0.73 and Ψ=360° for example on combination of flight conditions.

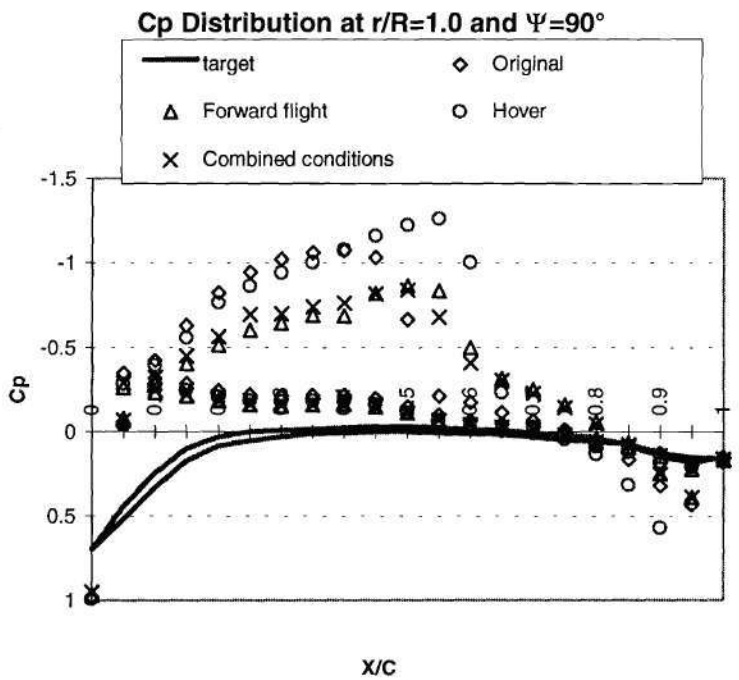

Figure 129. Pressure distribution comparison in forward flight at r/R=1.0 and Ψ=90° for example on combination of flight conditions.

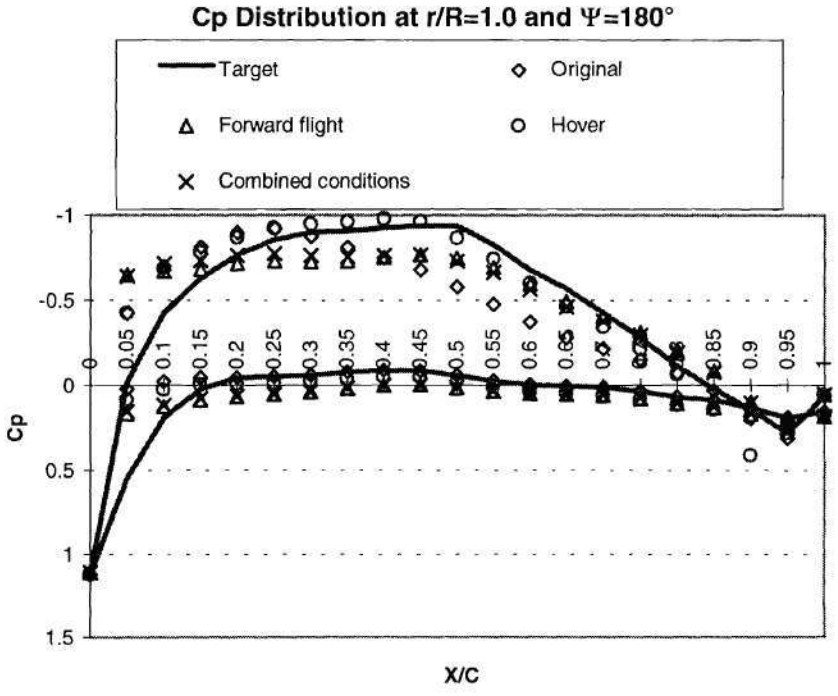

Figure 130. Pressure distribution comparison in forward flight at r/R=1.0 and Ψ=180° for example on combination of flight conditions.

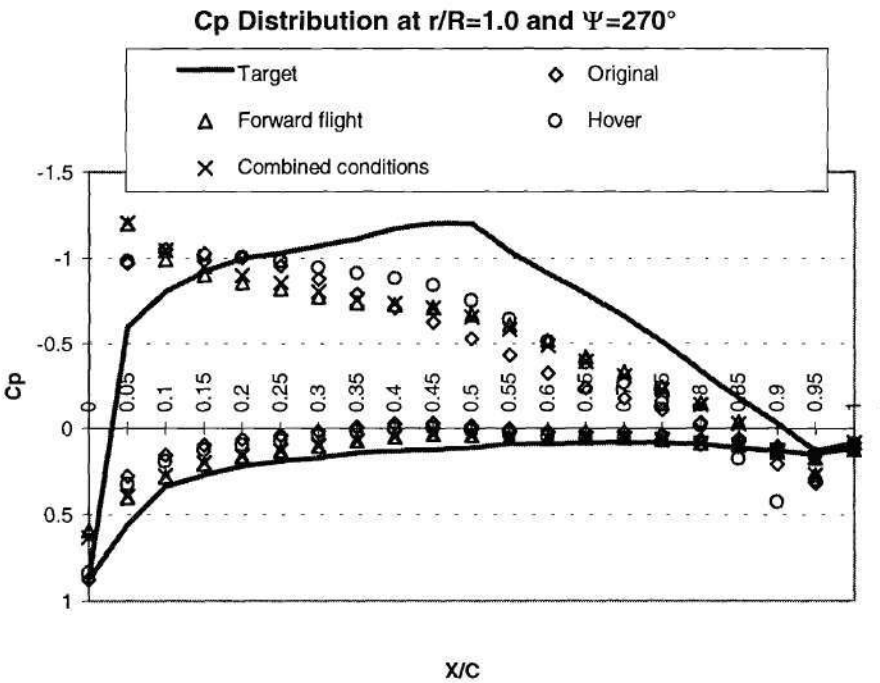

Figure 131. Pressure distribution comparison in forward flight at r/R=1.0 and Ψ=270° for example on combination of flight conditions.

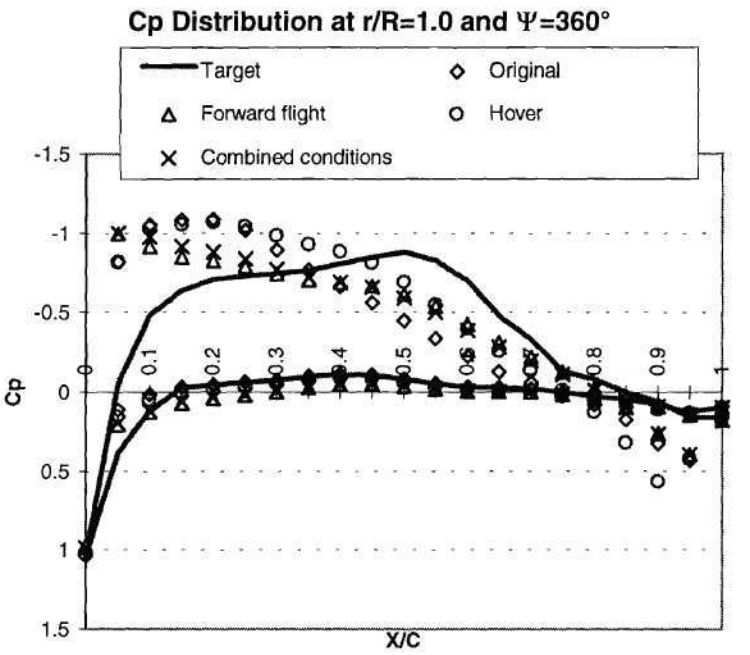

Figure 132. Pressure distribution comparison in forward flight at r/R=1.0 and Ψ=360° for example on combination of flight conditions.

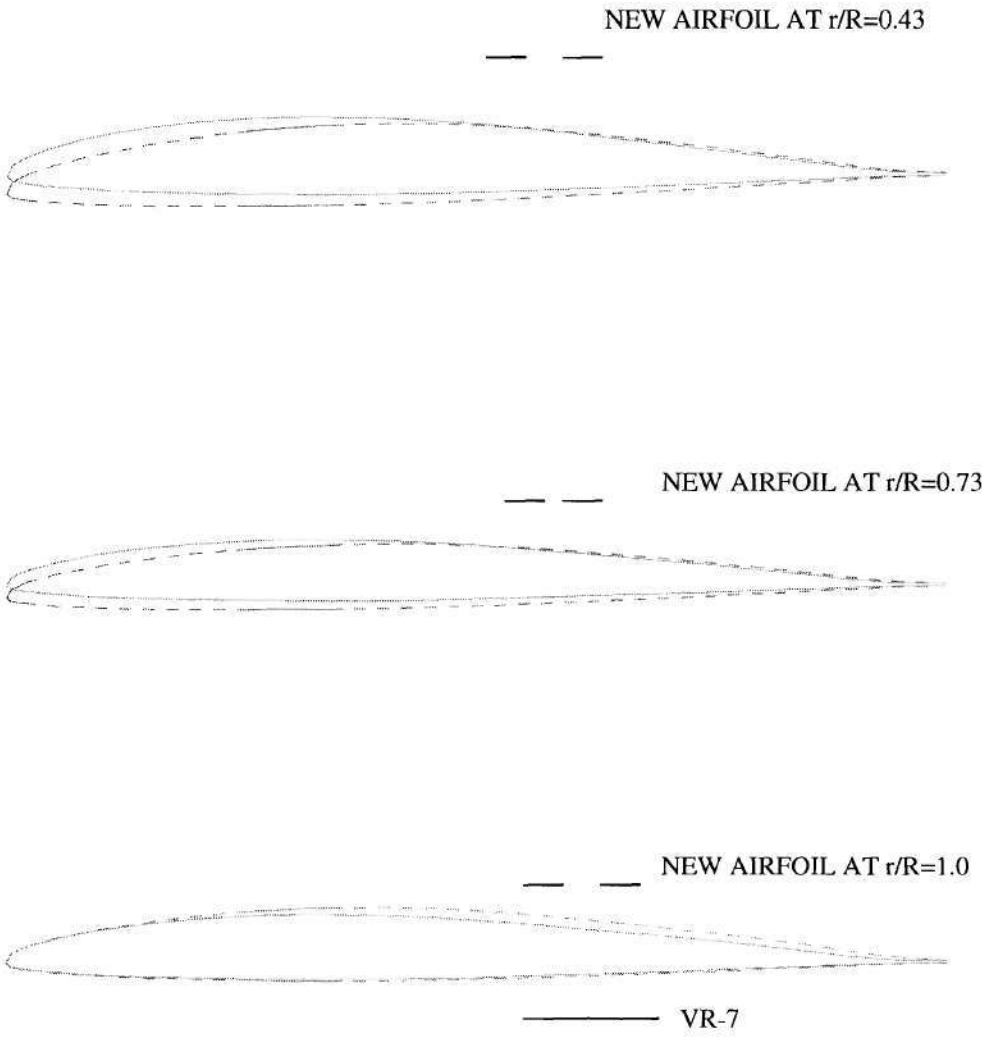

Figure 133. Airfoil comparison. Rotor designed for hover for example on combination of flight conditions.

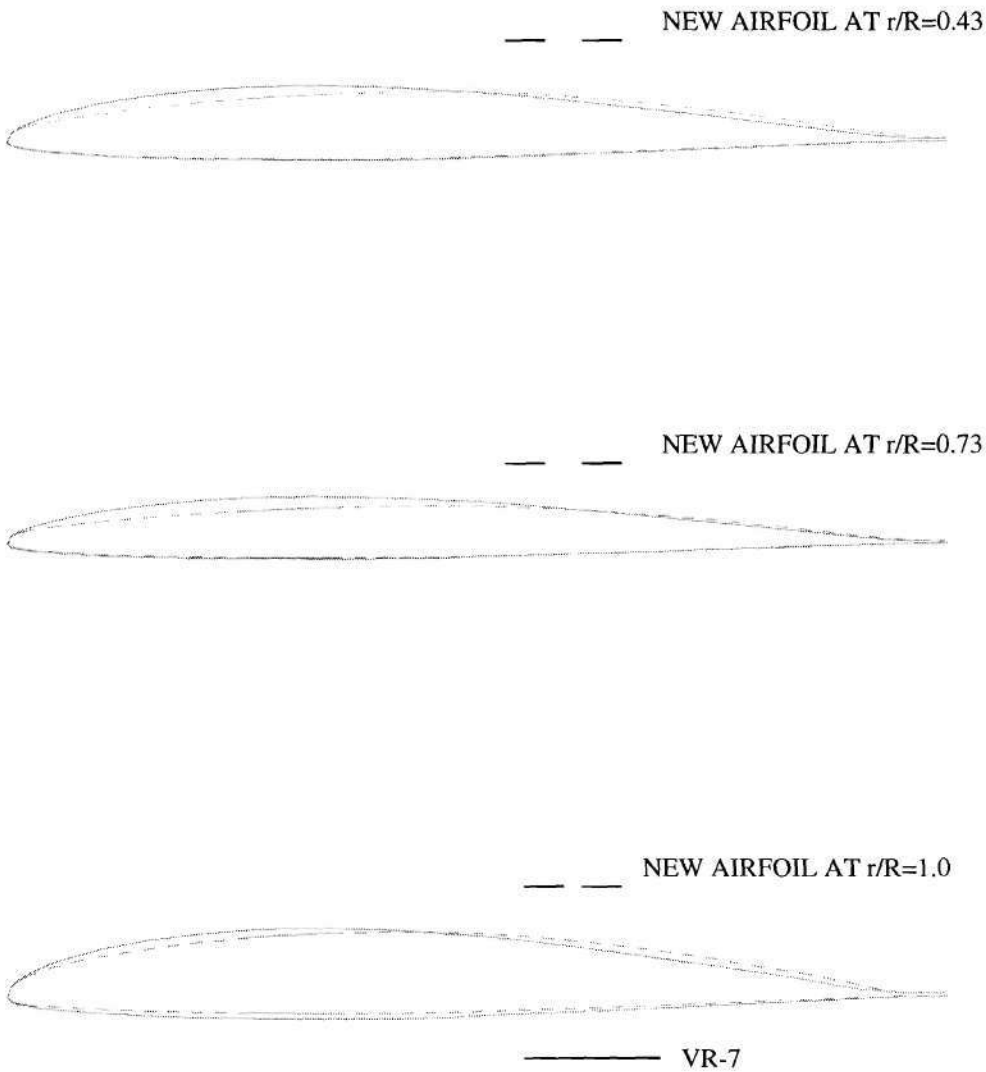

Figure 134. Airfoil comparison. Rotor designed for forward flight for example on combination of flight conditions.

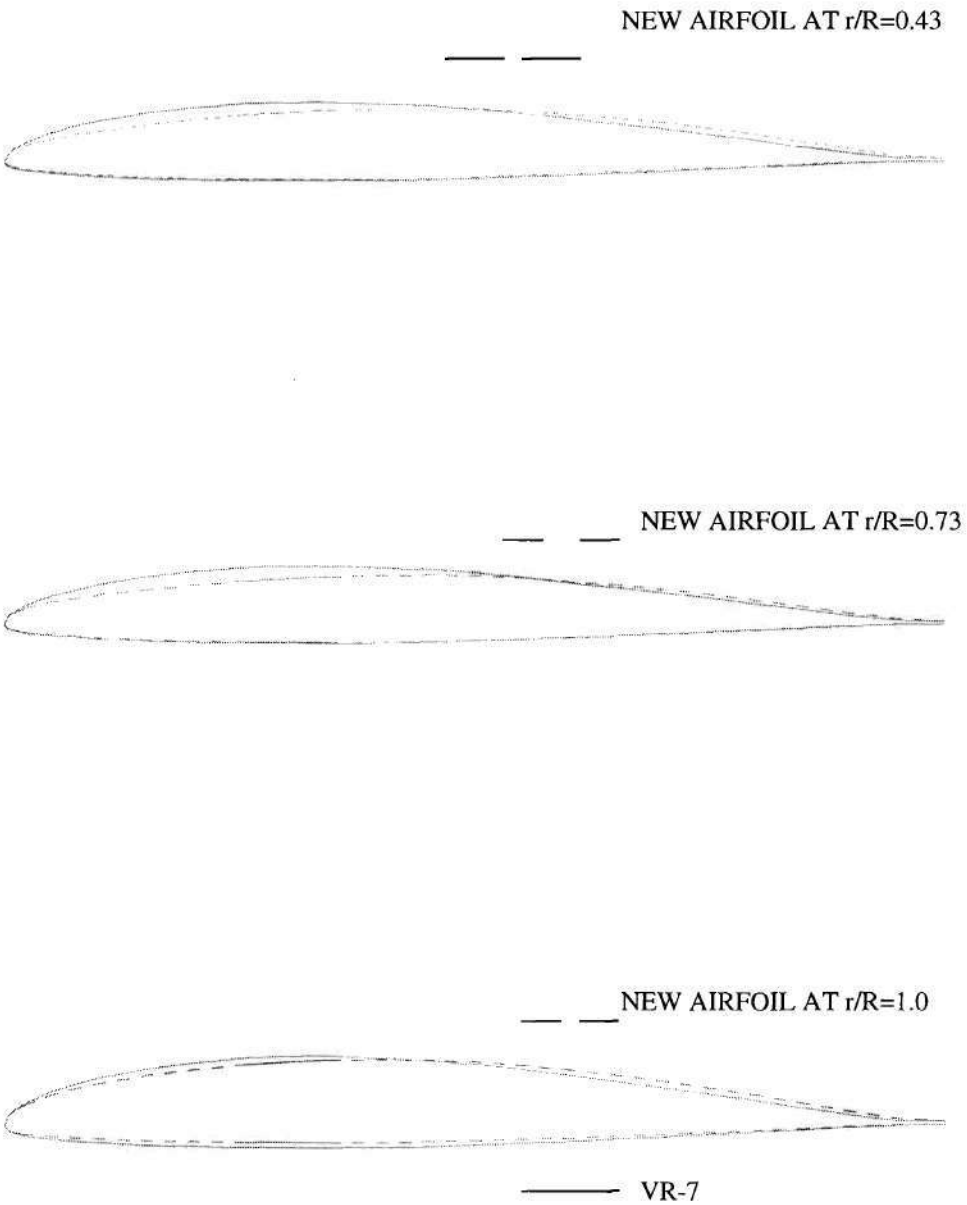

Figure 135. Airfoil comparison. Rotor designed for combination of flight conditions for example on combination of flight conditions.

CHAPTER V

CONCLUDING REMARKS

An efficient methodology for rotor blade design has been developed and presented. Using this methodology, rotor blades can be designed for any set of flight conditions. Lift distributions are optimized for these flight conditions and inflow angles associated with these lift distributions are computed. Target lift distributions are translated into a specific set of target pressure distributions so that a baseline rotor is modified sequentially toward the specified target performance. The design process is stopped when the convergence criteria is satisfied.

The methodology can make use of potential theory only, for faster and approximate results; but preferably, a boundary layer analysis should be added in the design process. The main advantage of designing blades by means of potential flow theory alone is the time saved at the beginning of the design process. The designer will not need to find a specific pressure distribution that will match a certain drag value in this case, but will have to consider only the lift required for the control stations selected, this means that the induced power is naturally selected as the objective function in this type of

analysis. On the other hand, by using the boundary layer analysis the designer can control the drag produced by the newly designed rotor blade, and thus, after integration, the profile drag can be minimized. Solid airfoils, which must be used to build the blade , are specified by subtracting the displacement thickness from the 'fluid' airfoil designed using only potential flow theory.

Pressure distributions can be tailored with several priorities. Most important of all is matching the required lift coefficient at the specific control station. Moment coefficient will be matched as well if it is specified. Drag coefficient is minimized analyzing different pressure distributions with the inclusion of the boundary layer code. Final specification of target pressure distribution should follow the helicopter airfoil design objectives presented in chapter two.

Separation and weakening of shocks are other aspects that can be considered when the target pressure distributions are being implemented. All of these are aerodynamic constraints but structural requirements and acoustic considerations can also be considered. After considering these and other factors, there is still an infinite number of pressure distributions that will match all these requirements. Since there is no such thing as the 'best pressure distribution', and thus no such thing as the 'best airfoil', the target pressure distributions have to be developed independently for every case. Even though several automated methodologies to develop the target pressure distributions had been considered -such as Startford's recovery pressure profile, or the ADAM methodology- there is a need

for a pressure distribution optimizer for helicopter rotor flow conditions which will consider all these aspects and will be able to specify the target pressure distributions by varying a few parameters.

Laminar flow offers many advantages in most applications, and blade design is not the exception; the main advantage is the drastic reduction in viscous drag as opposed to turbulent flow. Although it is very unlikely that laminar flow will be present around the helicopter rotor, it can be specified as the target for the design methodology. The related work presented in this thesis proved a strong dependence between the flow regime over the designed blade and the MGM coefficients that were used to generate this airfoil. Local modification of the coefficients proved some success but this dependency should be studied further.

Minimization of power is very often the objective of a design case. In helicopters this can be achieved by lowering the induced or profile power. The mathematical problem of minimizing the induced power can be posted as this:

Minimize:

$$Q_i = \frac{b}{2\pi}\int_0^R\int_0^{2\pi}\frac{1}{2}\rho U_t^{\,2} c_l c r\phi d\psi dr$$

while keeping the thrust constant:

$$T = \frac{b}{2\pi} \int_0^{2\pi} \int_0^R \frac{1}{2} \rho a \left(\theta U_T^2 + U_p U_T \right) c dr$$

This variational problem should be studied further to get the global optimum lift distribution. In this work, this problem was solved numerically and no proof of optimality was given; any reduction of the induced torque at constant thrust was considered a candidate target lift distribution. Although the actual design process is driven by the specified target pressure distributions, these pressure distributions are tailored to match lift requirements and thus the specification of the target lift distribution is a step that must be emphasized, since the performance of the final rotor will be greatly influenced by this lift distribution selection.

Inclusion of viscous effects in the design process proved to be very useful. Actual solid airfoils can be now specified for the hover case by subtracting the displacement thickness from the 'fluid' airfoil designed using potential theory. This displacement thickness is induced by the unique pressure distribution present at a certain radial station. The methodology to do the equivalent in forward flight has to be developed yet, since only one 'fluid' airfoil is defined producing different pressure distributions along the blade revolution. And thus producing different values for the displacement thickness. This means that they cannot only be subtracted from the 'fluid' airfoil, because this process will yield several different 'solid' airfoils. Viscous effects inclusion proved its usefulness for profile power reduction by means of controlling the local drag coefficient. Minimization

of the drag produced by the target pressure distributions can be enforced so that when integrated the profile power will be reduced.

Design methods for any discipline traditionally search for the best components to select from. In the case the blade design, the traditional approaches will select a set of candidate airfoils, and after analyzing them in different flight conditions the designer will decide which ones of them will be selected for the present application. The methodology developed here does not use that concept anymore; the main idea is that the designer can specify a custom rotor for every new application, which will consider aspects decided as early as the mission specification, where the most important flight conditions will be highlighted so that the designer can specify the new rotor with these conditions in mind. The major concept posted here is the proposal of designing a new airfoil for each application, not to force the designer to select the known airfoil that will fit better into the application.

REFERENCES

1. AMPC 706-201, '*Engineering Design Handbook, Helicopter Engineering, Part One, Preliminary Design,*' Headquarters, U. S. Army Materiel Command, Aug. 1974.

2. Prouty, R. W., '*Helicopter Performance, Stability and Control,*' PWS Engineering, Boston, 1986.

3. Gessow, A. and Myers, G. C., '*Aerodynamics of the Helicopter,*' College Park Press, 1985.

4. Bingham, G. J., 'The Aerodynamic Effect of Rotor Blade Airfoils, Twist, Taper and Solidity in Hover and Forward Flight Performances', American Helicopter Society 37th Annual Forum, pp. 37-50, 1981.

5. Kemp, L. D., 'An Analytical Study for the Design of Advanced Airfoils,' American Helicopter Society 29th Annual Forum, 1973.

6. Dadone, L. U., 'Design and Analytical Study of a Rotor Airfoil,' NASA CR-2988, 1978.

7. Blackwell, J. B. and Hinson, B. L., 'The Aerodynamic Design of an Advanced Rotor Airfoil', American Helicopter Society 34th Annual Forum, 1978.

8. Dadone, L. U. and Fukushima, T., 'A Review of Design Objectives for Advanced Helicopter Airfoils,' American Helicopter Society Symposium on Helicopter Aerodynamic Efficiency, Hartford, CT, March 6-7, 1975.

9. Schrage, D. P. and O'Malley, J. A., 'Performance and Aerolastic Tradeoffs in Recent Rotor Blade Designs,' Presented at the American Helicopter Society National Specialists Meeting, Rotor System Design, October, 1980.

10. Nakadate, M. and Obukata, M., 'Design of New Generation Rotor Blade Airfoils Using Navier-Stokes,' Fuji Heavy Industries, Japan, 1994.

11. Cheeseman, I. C., 'Developments in Rotary Wing Aerodynamics,' Vertica, Vol. 6, pp. 181-202, 1982.
12. Davenport, F. J. and Front, J. V., 'Airfoil Sections for Helicopter Rotors -A Reconsideration,' American Helicopter Society 22nd Annual Forum, pp.29-44, 1966.

13. Helicopter Design DATCOM, US Army, Volume I - Airfoils, Prepared by the Boeing Company, Sept. 1976.

14. Wortmann, F. X. and Drees, J. M., 'Design of Airfoils for Rotors,' 1969.

15. Daripa, P., 'An Exact Inverse Method for Subsonic Flows,' Quarterly of Applied Mathematics, Vol. XLVI, #3, Sept. 1988, pp. 505-526.

16. Davis, W. H., 'Technique for Developing Design Tools from the Analysis Methods of Computational Aerodynamics,' AIAA Journal, Vol. 18, pp. 1080-1087, Sept. 1980.

17. Beatty, T. D. and Narramore, J. C., 'Inverse Method for the Design of Multi-Element High Lift Systems,' Journal of Aircraft, Vol. 13, #6, 1976.

18. Labrujere, Th. E. and Sloof, J. W., 'Computational Methods for the Aerodynamic Design of Aircraft Components,' Annual Review of Fluid Mechanics, 1993.

19. Ormsbee, A. I. and Chen, A. W., 'Multiple Element Airfoils Optimized for Maximum Lift Coefficients', AIAA Journal, Vol. 10, #2, 1972.

20. Malone, J. B., Vadyak, J. and Sankar, L. N., 'Inverse Aerodynamic Design Method for Aircraft Components,' Journal of Aircraft, Vol. 24, #1, Jan. 1987.

21. Silva, D. M. and Sankar, L. N., 'An Inverse Method for the Design of Transonic Wings,' AIAA Paper 92-1025.

22. Whyte, P. H., 'Use of CFD in Helicopter Aerodynamic Design,' Canadian Aeronautics and Space Journal, Vol. 34, #2, pp. 92-101, Jun. 1988.

23. Liebeck, R. H., 'Design of Subsonic Airfoils for High Lift,' Journal of Aircraft, Vol. 15, #9, Sept. 1978.

24. Narramore, J. C. and Yeary, R. D., 'Airfoil Design and Analysis Using an Information System Approach,' 1980.

25. Malone, J. B., Narramore, J. C. and Sankar, L. N., 'Airfoil Design Using the Navier-Stokes Equations,' Journal of Aircraft, Vol. 28, #3, pp. 216-224, March 1991.

26. Stratford, B. S., 'The Prediction of Separation of the Turbulent Boundary Layer,' Journal of Fluid Mechanics, Vol. 5, Part 1, pp. 1-16, Jan. 1959.

27. Narramore, J. C., Malone, J. B. and Vermeland, R., 'Application of a New Navier-Stokes inverse Method to the Design of Advanced Airfoils,' American Helicopter Society 46th Annual Forum, pp. 1089-1098, 1990.

28. Lyrintzys, A. S. and Farmer, J. D., 'On the Design for Maximum Lift Airfoils,' FED-Vol. 129, Multidisciplinary Applications of CFD, ASME 1991.

29. Owen, S. J., 'Design and Experimental Verification of a Family of High-Speed Tilt Rotor Airfoils,' American Helicopter Society 51st Annual Forum, pp. 93-100, 1995.

30. Banerjee, D. and Shanthakumaran, P., 'Application of Numerical Optimization Methods in Helicopter Industry,' Vertica, Vol. 13, #1, pp. 17-42, 1989.

31. Vanderplaats, G. N., 'Efficient Algorithm for Numerical Airfoil Optimization,' Journal of Aircraft, Vol. 16, # 12, Dec. 1979.

32. Bezard, H., 'Rotor Blade Airfoil Design by Numerical Optimization and Unsteady Calculations,' American Helicopter Society, 48th Annual Forum, pp.1283-1294, 1992.

33. Vuillet, A., 'Rotor and Blade Aerodynamic Design,' AGARD, Special Course on Aerodynamics of Rotorcraft, 1990.

34. Narramore, J. C., 'Airfoil Design, Test and Evaluation for the V-22 Tilt Rotor Vehicle,' American Helicopter Society 43rd Annual Forum, Vol. 1, pp.49-60, 1987.

35. Liu, J., Paisley, D. J. and Hirsh, J., 'Tilt-Rotor Aerodynamic Blade Design by Numerical Optimization Method,' American Helicopter Society 46th Annual Forum, pp. 557-567, 1990.

36. Santos, L. C. and Sankar, L. N., 'An Efficient Design Technique for Helicopter Blade Airfoils,' 1993.

37. Hassan, A. A. and Charles, B. D., 'Airfoil Design for Helicopter Rotor Blades -A Three-Dimensional Approach,' American Helicopter Society 50th Annual Forum, 1994.

38. Tapia, F., Sankar, L. N. and Schrage, D. P., 'An Inverse Aerodynamic Design Method for Rotor Blades in Forward Flight,' American Helicopter Society 51st Annual Forum, Vol. 2, 1995.

39. Garabedian, P. and McFadden. G., 'Design of Supercritical Swept Wings,' AIAA Journal, Vol. 20, pp. 289-291, March 1982.

40. Prichard, D., 'Development of a Full Potential Solver for Rotor Aerodynamics Analysis,' Ph. D. Thesis, Georgia Institute of Technology, 1990.

41. Johnson, W., CAMRAD/JA, *A Comprehensive Analytical Model of Rotorcraft Aerodynamics and Dynamics,* Johnson Aeronautics, Palo Alto, Calif., 1988.

42. Drees, J. M., 'A Theory of Airflow Through Rotors and its Application to Some Helicopter Problems,' Journal of the Helicopter Society of Great Britain, Vol. 3, (2), 1949.

43. Scully, M. P., *Computation of Helicopter Rotor Wake Geometry and its Influence of Rotor Harmonic Airloads,* Massachusetts Institute of Technology, ASRLTR 178-1, March 1975.

44. Cebeci, T., Mosinskis, G. J. and Smith, A. M. O., 'Calculation of Separation Points in Incompressible Turbulent Flows,' Journal of Aircraft, Vol. #9, 1972.

45. Eppler, R. and Sommers, D. M., 'A Computer Program for the Design and Analysis of Low Speed Airfoils,' NASA TM 80210, 1980.

46. Wortmann, F. X., 'A Contribution to the Design of Laminar Profiles for Gliders and Helicopters,' German Ministry of Aviation Translations TIL/T4903, Sept. 1960.

VITA

Fidencio Tapia Rodríguez was born on June 8, 1964, in Guadalajara, Mexico. He received a B. S. degree from the Autonomous Metropolitan University in Mexico City after completion of the thesis research untitled 'Ultralight Helicopter Design' in 1990.

He worked for a research institute in Mexico City for about one year and joined the design lab at the School of Aerospace Engineering in the Georgia Institute of Technology in 1991, after being granted a CONACYT-Fulbright scholarship for Ph. D. studies.

He received his M. S. degree in Dec. 1992 and continued his research focusing in helicopter aerodynamics and rotor design which resulted in this thesis.